INVESTIGATIONS ON THE PERFORMANCE UPGRADATION OF PERCHLORATE CELLS AND RTD MODELLING STUDIES

A Thesis

Submitted by

by

SANANTH H MENON

for the award of the degree
of

DOCTOR OF PHILOSOPHY

Under the faculty of Engineering

SCHOOL OF ENGINEERING
COCHIN UNIVERSITY OF SCIENCE AND TECHNOLOGY, KOCHI

JUNE 2019

THESIS CERTIFICATE

This is to certify that the thesis entitled “**INVESTIGATIONS ON THE PERFORMANCE UPGRADATION OF PERCHLORATE CELLS AND RTD MODELLING STUDIES**” submitted by **Sananth. H. Menon** to the Cochin University of Science and Technology, Kochi for the award of the degree of Doctor of Philosophy is a bonafide record of research work carried out by him under my supervision and guidance at School of Engineering, Cochin University of Science and Technology. The contents of this thesis, in full or in parts, have not been submitted to any other University or Institute for the award of any degree or diploma.

I further certify that the corrections and modifications suggested by the audience during the pre-synopsis seminar and recommended by the doctoral committee are incorporated in the thesis.

Prof. (Dr.) G. Madhu *(Research Guide)*
Professor & Head,
Division of Chemical Engineering,
School of Engineering,
Cochin University of Science and Technology
Kochi-682 022, Kerala, India

Place : Kalamassery
Date

DECLARATION

I hereby declare that the work presented in the thesis entitled "**INVESTIGATIONS ON THE PERFORMANCE UPGRADATION OF PERCHLORATE CELLS AND RTD MODELLING STUDIES**" is based on the original research work carried out by me under the supervision of Prof. (Dr) G. Madhu, Professor, Division of Chemical Engineering, School of Engineering, Cochin University of Science and Technology. I further declare that the contents of this thesis in full or in parts have not been submitted to any other University of Institute for the award of any degree or diploma.

Place : Kochi **Sananth. H. Menon**

Date:

Dedicated to ***My parents and My family***

ACKNOWLEDGEMENTS

I wish to bow my head before Almighty God for giving me strength and courage for completing my thesis report.

First and foremost, I express my profound gratitude to Prof. (Dr.) G.Madhu, my guide for giving me an esteemed opportunity for doing research under his supervision and guidance. His timely advice and valuable suggestions given to me at various stages of this work are gratefully acknowledged. His extreme patience in listening to me during various stages of work and proposing various improvements helped me to progress my work in a smooth and uninterrupted manner.

I express my deep sense of gratitude and sincere thanks to Director VSSC and Dy. Director VSSC (SPRE) for granting me the permission, to carry out research. My heart goes to Shri Jojo Mathew, GM APEP/SPRE/VSSC for providing me all the necessary facilities for doing this research project smoothly and successfully at Ammonium Perchlorate Experimental Plant (APEP). His abundant love and caring especially in my tougher times are profoundly acknowledged gratefully.

I profusely thank Dr Shaneeth M, Dy. Division Head, ESD/ PCM/VSSC for teaching me basics of electrochemistry by deciphering it in chemical engineering language.

I also express my gratitude to Smt Jitha P Thomas, Dy. Manager Electrolysis and Strontium Perchlorate Plant, APEP, Shri Samjith M.G, Sci/Eng SC, APEP, Shri Anil Kumar P.S, Technician G, APEP and all other staff and contract staff of Electrolysis and Strontium Perchlorate Production facility, APEP for cooperating and assisting me in the course of this study.

I express my sincere love and thanks to my loving parents for their advices and prayers which has been a constant source of inspiration for me. Last but not the least, I thank my beloved wife Divya, my daughters Mayukha and Meghana for their prayers, love and support during the course of this research work.

Sananth. H. Menon

ABSTRACT

Ammonium perchlorate (AP) is the oxidiser for all solid propellants used in launch vehicle technology. Sodium perchlorate is one of the major raw materials used in the manufacture of AP, which is produced by the electrolytic oxidation of sodium chlorate aqueous solution using TSLA (Titanium Substrate Lead dioxide Anodes) and SS 316L cathodes.

Occasional peeling of lead dioxide crystals due to the difference in thermal expansion coefficients during electrolysis is a serious problem faced by allied electrochemical industries. Moreover, decisive removal of lead dioxide particles from the conductive substrate (after definite lapse of service life) and recoating with fresh lead dioxide crystals, for want of higher energy efficiencies, is a common procedure adopted in many similar electrochemical industries.

Major portion of this work focuses on the effective utilization of discarded lead dioxide particles as particulate electrodes in a carefully designed packed/compact bed electrolyser. The above electrolyser was used for studying its effectiveness in the electrochemical oxidation of sodium chlorate to sodium perchlorate. Yet more attractive take-away of this module is the total exclusion of costly inert conductive support and mixed metal oxide (Ru ,Pd ,Ti) conductive coating essential for conventional flat plate configuration. A demonstration of continuous electrosynthesis of sodium perchlorate by arranging similar dual bed compact electrochemical cells was made and a higher average current efficiency could be achieved when compared with conventional parallel plate electrode system. A Modified Dispersion Plug Flow Model (MDPFM) was developed to predict the residence time distribution function under electrolyzing conditions

Another area of research under this broad topic was the influence of certain additives in the lead dioxide coating electrolyte for modifying the morphological, electrochemical and mass transfer features of lead dioxide deposits for conventional parallel plate configuration. An extensive study was carried out with the modified and unmodified lead dioxide anode samples. Scanning Electron Microscope (SEM) and X-Ray Diffraction (XRD) studies were carried out to understand the morphological/ structural characteristics. Electrochemical Impedence Spectroscopy (EIS) and Potentio Dynamic Response (PDR) studies were carried out to understand the electrochemical, kinetic and mass transfer characteristics. Finally, validation of above modification in a higher capacity electrochemical cell was also derived.

Keywords: lead dioxide; packed bed electrolyser; particulate electrodes; perchlorate reaction; scrap lead dioxide; hazardous solid waste; effluent treatment of organics; solid propellants; electrolytic oxidation;lead dioxide; perchlorate cells; TSLA;RTD; tracer; MDPFM.

CONTENTS

ACKNOWLEDGEMENTS i

ABSTRACT iii

TABLE OF CONTENTS v

LIST OF TABLES viii

LIST OF FIGURES ix

ABBREVIATIONS xii

CHAPTER 1 INTRODUCTION 1

1.1 Development of a compact/packed bed electrochemical reactor (PBER) 1

1.2 Development of a dual PBER for continuous electrosynthesis application 3

1.2.1 Penetration issue 3

1.3 Modelling residence time distribution (RTD) behaviour in a PBER 5

1.4 Impact of modified lead dioxide anodes in conventional cells 7

1.5 Quantification of interfacial adsorptive characteristics 9

CHAPTER 2 LITERATURE REVIEW 10

2.1 Design of packed bed reactors 10

2.2 Interfacial current distribution in packed bed reactors 13

2.3 Potential distribution in packed bed reactors 14

2.4 Mass transfer behaviour in packed bed reactors 15

2.5 Different applications of packed bed reactors 17

2.6 Effect of foreign ions in lead dioxide electrode performance 18

2.7 Summary 21

CHAPTER 3 MATERIALS AND METHODS

3.1 Development of a compact/packed bed electrochemical reactor 22
3.2 Residence time distribution in PBER 27
3.3 Effect of foreign ions in Lead dioxide electrode performance 28
3.3.1 Preparation of working electrode 28
3.4 Quantification of interfacial adsorptive characteristics over PbO_2 anode 31
3.4.1 Preparation of working electrode 32
34

CHAPTER 4 RESULTS AND DISCUSSION

4.1 Development of a compact/packed bed electrochemical reactor 34
4.1.1 Optimization of design configuration 34
4.1.1.1 Calculation of current efficiency 34
4.1.2 Influence of Current density 37
4.1.3 Influence of electrolyte flow rate 39
4.1.4 Influence of temperature 41
4.1.5 Influence of bed height 43
4.1.6 Concentration- Time model 44
4.1.6.1 Theoretical Model development 44
4.2 Development of a system for continuous electrosynthesis of sodium perchlorate using single bed PBER's 46
4.2.1 Configuration of cells 46
4.2.2 Trial results 50
4.3 Development of a dual bed packed/ compact bed electrochemical reactor 52

4.4 Development of a system for continuous electrosynthesis of sodium perchlorate using dual bed PBER's 54
4.4.1 Modifications/ Improvements carried out 56
4.5 Modelling residence time distribution (RTD) behaviour in a compact/packed bed electrochemical reactor (PBER) 58
4.5.1 Theory 58
4.5.2 RTD curves at various flow rates 60
4.5.3 Modelling RTD behaviour 62
4.5.4 RTD curves under electrolyzing conditions 67
4.5.5 Modified Dispersed Plug Flow Model (MDPFM) under electrolyzing conditions 69
4.5.6 Validation of MDPFM 71
4.6 Effect of modified lead dioxide anodes in conventional perchlorate cells 73
4.6.1 SEM characterization 73
4.6.2 X-ray Diffraction 76
4.6.2.1 Evaluation of % α-PbO_2 in β-PbO_2 samples 78
4.6.3 EIS results 80
4.6.4 PDR results 82
4.6.5 Validation in a perchlorate cell 84
4.7 Quantification of interfacial adsorptive characteristics over lead dioxide electrodes 85
4.7.1 Theory 85
4.7.1.1 Plotting of Electrocapillary curves of electrodes 86
4.7.1.2 Differential double layer capacity 87
4.7.2 Determination of charge density of electrode samples 87

4.7.3 Electrocapillary curves 93
4.7.4 Determination of differential double layer capacity 95
96

CHAPTER 5 SUMMARY AND CONCLUSIONS

5.1 Studies related with single bed PBER 96
5.2 Studies related with dual bed PBER 96
5.3 Flow modelling using RTD studies 97
5.4 Effect of modified lead dioxide anodes in conventional perchlorate cells 98
5.5 Quantification of interfacial adsorptive characteristics 98
5.6 Scope of future research 99
REFERNCES 100
APPENDICES 109
LIST OF PUBLICATIONS 111
CURRICULUM VITAE 112

LIST OF TABLES

Table No	Title	Page No
Table 3.1	Particle size distribution	25
Table 3.2	Image analysis of PbO_2 particles	25
Table 3.3	Coating conditions	29
Table 3.4	Experimental Conditions for Validation	31
Table 3.5	Experimental conditions for Potentiostatic studies	32
Table 4.1	Moments at various flow rates	61
Table 4.2	Difference between space time and observed mean	62
Table 4.3	Calculated values of D/u.L	66
Table 4.4	Moments at various flow rates	69
Table 4.5	Parameters from X-ray Diffractogram	79
Table 4.6	Fraction of calculated α-PbO_2 in prepared β-PbO_2 sample	79
Table 4.7	EIS Experimental Conditions	81
Table 4.8	Calculated values of $(q_M)_\theta$	92
Table 4.9	Electrocapillary maximum for various anode samples	94

LIST OF FIGURES

Figure	**Title**	**Page No**
Fig. 3.1	Schematic setup of PBER	23
Fig. 3.2	Components of PBER	24
Fig. 3.3	Actual experimental setup	24
Fig. 3.4	Isothermal System in Overflow tank	25
Fig. 3.5	Schematic setup for dual bed PBER	26
Fig. 3.6	Actual experimental setup for dual bed PBER	26
Fig. 3.7	Schematic setup for RTD studies	27
Fig. 3.8	Experimental setup for RTD studies	28
Fig. 3.9	Lead dioxide Coating Setup	30
Fig. 3.10	Prepared lead dioxide samples	30
Fig. 3.11	Three electrode cell setup	32
Fig. 4.1	Various configuration of PBER	36
Fig. 4.2	Comparison of average current efficiencies	36
Fig. 4.3	Effect of current on performance of electrolyser	38
Fig. 4.4	Effect of current on initial current efficiency	38
Fig. 4.5	Effect of concentration of $NaClO_3$ on current efficiency	39
Fig. 4.6	Effect of flow rate on performance of electrolyser	40
Fig. 4.7	Effect of electrolyte flow rate on initial current efficiency	40

Fig. 4.8 Effect of electrolyte temperature on current efficiency 42

Fig. 4.9 Effect of electrolyte temperature on initial current efficiency 42

Fig. 4.10 Effect of bed height on current efficiency 43

Fig. 4.11 Comparison between prediction and actual behavior at limited conditions 45

Fig. 4.12 Major components fabricated for arrangement of single bed PBER’s 47

Fig. 4.13 Electrolyte cooler 47

Fig. 4.14 Schematic sketch for cont. electrosynthesis of SPC 48

Fig. 4.15 Arrangement of cells for continuous electro synthesis of SPC using single bed PBER’s 48

Fig. 4.16 Temperature distribution at various locations of arrangements for cont. electrosynthesis of PBER 49

Fig. 4.17 Provision of tapped recirculation line to individual cells for cot. Electrosynthesis of SPC 49

Fig. 4.18 Improved temperature distributions across cells after providing recirculation tapping across each cell 50

Fig. 4.19 Transient behavior in $NaClO_3$ conc. in product SPC during course of electroysis 51

Fig. 4.20 Modification in entry of fresh feed to electroysers arranged in series 52

Fig. 4.21 Transient behavior in $NaClO_3$ conc. before and after modification (in entry feed) 52

Fig. 4.22 Voltage variation with current in single bed PBER 53
Fig. 4.23 Voltage variation with current in single and dual bed PBER 53
Fig. 4.24 Major components fabricated for arrangement of dual bed PBER's for cont. electrolysis 54
Fig. 4.25 Arrangement of cells for continuous electro synthesis of SPC using dual bed PBER's 55
Fig. 4.26 Transient behavior in $NaClO_3$ conc. in product SPC during course of electrolysis 55
Fig. 4.27 Line condensers inserted between cells 57
Fig. 4.28 Modified orientation of 4th cell ("Polishing cell") 57
Fig. 4.29 Transient behavior in $NaClO_3$ conc. in product SPC during cont. electroysis 58
Fig. 4.30 RTD behavior under various electrolyte flow rates 61
Fig. 4.31 Modelling RTD behavior under various electrolyte flow rates 65
Fig. 4.32 Plot of D/u.L for various flow rates 66
Fig. 4.33 RTD behavior under various electrolyte flow rates 68
Fig. 4.34 MDPFM conceptual block diagram 70
Fig. 4.35 Prediction of $E(\theta)$ using MDPFM 73
Fig. 4.36 SEM images of anodes modified using surfactants 75
Fig. 4.37 SEM images of Modified Anodes with combination 75
Fig. 4.38 XRD of anodes modified using surfactants 77

Fig. 4.39	XRD of anodes modified using combinations of surfactants and additives	78
Fig. 4.40	EIS plots of anodes modified with surfactants	81
Fig. 4.41	EIS plots of anodes modified withcombination of surfactants& additives	82
Fig. 4.42	PDR plots of anodes modified with surfactants and additives	83
Fig. 4.43	Exchange current density (i_0) values	84
Fig. 4.44	Calculated current efficiencies for perchlorate formation	84
Fig. 4.45	Current transients for various samples	88
Fig. 4.46	Charge transients for various samples	90
Fig. 4.47	Modified current transients for various samples	92
Fig. 4.48	Variation of $(q_M)_\theta$ with potential	93
Fig. 4.49	Electrocapillary curves for various samples	93
Fig. 4.50	Variation of differential capacity(C) for various samples	95

LIST OF ABBREVIATIONS/ SYMBOLS USED

Abbreviations used

AP - Ammonium Perchlorate
TSLA - Titanium Substrate Lead dioxide Anode
PBER - Packed Bed Electrochemical Reactor
RTD - Residence Time Distribution
SEM - Scanning Electron Microscope
XRD - X-Ray Diffraction
EIS - Electrochemical Impedance Spectroscopy
CV - Cyclic Voltammetry
PDR - Potentio Dynamic Response
CTAB - Cetyl Tri methyl Ammonium Bromide
LA - Lead dioxide
MMO - Mixed Metal Oxide
CE - Counter Electrode, Current Efficiency
WE - Working Electrode
RE - Reference Electrode
LPM - Lit/min
MDPFM - Modified Dispersed Plug Flow Model

Mathematical symbols used

e - electronic charge
k_s - surface reaction rate
η - overpotential
α - surface area per unit volume
k_m, K - mass transfer coefficient

n	- no: of electrons
F	- Faraday’s constant
C_0	- Concentration of radicals, Outlet concentration.
I_L	- Limiting current
Q, Q_R	– Volumetric Flow rate
C_i, C_i^0	- Initial concentration
A	- Area
L	- Length of bed
t, Θ	- Time elapsed
τ	- Residence time, Space time
$C_i(t)$	- Conc. after elapsing time ‘t’
D	- Diffusion / Dispersion Coefficient
u	- velocity of electrolyte,
z	- position
F_T	-Mass flow rate of tracer
C_T	-Concentration of tracer
U	- Superficial velocity
$E(\theta)$ or E_θ or $E(t)$	- Residence time distribution function
C_d	- Concentration of pulse
n_T	–no: of tanks in series
Pe	- Peclet no
T_R	– Tank residence time
V_R	- Volume of tank/reactor
σ^2	- Variance
σ^2_θ	- Variance (dimensionless)
q	- Tracer quantity
$\delta(t)$	- Dirac delta function,
α	– Fraction of back flow

C_1' – Concentration immediately after the dispersed plug flow region

C_1 – Final output concentration

j_{α}, j_{β} - Intensity of prominent diffraction lines for α and β PbO_2 respectively

Z' & Z_r - Real part of Impedance

Z'' & Z_j - Imaginary part of Impedance

i_0 - Exchange current density

q_M - Charge density of the electrode

γ - Interfacial tension

dV - Change in voltage

j - Particular species involved at non polarizable interface

r_i –Surface excess of species ‘i’ of interest; here Chlorate ions

μ –Chemical potential.

C - Double Layer Capacitance/ Differential Capacitance

E - Voltage

α_A - Anodic Transfer Coefficient

α_C - Cathodic Transfer Coefficient

CHAPTER 1

INTRODUCTION

Ammonium Perchlorate (AP) is the oxidiser for all solid propellants used in launch vehicle technology. Sodium perchlorate is one of the major raw materials used in the manufacture of AP , which is produced by the electrolytic oxidation of sodium chlorate aqueous solution using TSLA (Titanium Substrate Lead dioxide Anodes) and SS 316L Cathodes.

1.1 DEVELOPMENT OF A COMPACT/PACKED BED ELECTRO-CHEMICAL REACTOR (PBER)

Lead dioxide is used as one of the insoluble anodes in the electrochemical industries due to their significant stability, better electronic conductivity and inherently low cost (Xiaohong, 2011). However, their relatively weak mechanical strength necessitates the use of conductive support such as expensive titanium metals. The use of conductive supports, leads to a problem of adhesion between the metal substrate and lead dioxide coating due to the formation of insulating oxides. This calls for the need of a careful under coating of highly expensive noble metal oxides over the valve metal for making the surface conductive. In spite of this, occasional peeling of lead dioxide crystals due to the difference in thermal expansion coefficients during electrolysis is a serious problem faced by allied electrochemical industries. Moreover, decisive removal of lead dioxide particles from the conductive substrate(after definite lapse of service life) and recoating with fresh lead dioxide crystals, for want of higher energy efficiencies, is a common procedure adopted in many similar electrochemical industries.

Generally, lead dioxide anodes coated over conductive titanium substrates are commercially manufactured through electrodeposition techniques from lead containing salts like nitrates, acetates, methane sulphonates, etc. Long term stability is always a critical issue when lead dioxide anodes are considered because corrosion of the coating must lead to contamination of the product/effluent with toxic lead (II) (Carr, 1972). In a typical perchlorate manufacturing unit, these electrodes are dipped in electrolytes like sodium chlorate solution, which will be subsequently electrochemically oxidized to sodium perchlorate, a major intermediate for any type of perchlorate manufacture. Though these electrodes are sufficiently inert and falls in the class of DSA (Dimensionally Stable Anodes) under these oxidizing environments, PbO_2 slowly loses its adherence from its substrate resulting in its peeling out after completing a definite period of its service life. Consequently, the performance of these electrolysers comes down necessitating the removal of such substrates for want of another layer of coating. Above detached PbO_2 particles, generally seems to be ‘relently useless’, still retains all its chemical features other than loss of its adherence from the parent substrate. Moreover, such lead dioxide flakes which are removed from the substrate metal, becomes a solid hazardous waste, if allowed to accumulate.

Its known from the literatures that lead compounds interfere with a variety of body processes and is toxic to many organs and tissues including the heart, bones, intestines, kidneys, and reproductive and nervous systems. It interferes with the development of the nervous system and is therefore particularly toxic to children, causing potentially permanent learning and behaviour disorders. Symptoms include abdominal pain, confusion, headache, anemia, irritability, and in severe cases seizures, coma, and death. Hence safe disposal of discarded lead compounds is one of the major challenges in the recent era (Onwughara, 2013).

The present work focuses on the effective utilization of above generated discarded or peeled off Lead dioxide particles as particulate electrodes in a carefully designed packed bed electrolyser. It is known that particulate electrodes provide a large electrode area in proportion to conventional flat electrode configuration (Newman, 1962; Volkman, 1978; Doherty, 1996; Kaminari, 2005). Consequently, this packed bed electrolyser, will be exceptionally useful when dealing with low reactant concentrations or slow reactions. This “substrateless” design entirely avoids the necessity of expensive valve metals as substrates and associated noble metal oxide undercoating. Additionally, the service life of such electrodes is also found to be remarkably higher. In the present study, an optimized design of a packed bed electrolyser setup using peeled off electro deposited lead dioxide particles was carried out for proper current and voltage distribution. The above electrolyser was used for studying its effectiveness in the electrochemical oxidation of sodium chlorate to sodium perchlorate, which is the starting raw material for the manufacture of rocket propellant oxidisers. Effect of critical cell parameters such as current load, electrolyte flow rate and temperature was also carried out in the present study. An attempt for corroborating above results in a known concentration - time model as explained in 1.1.1 was also carried out.

1.1.1 Concetration-time model

Inorder to assess the theoretical behavior of the above PBER at limiting conditions, imminence with already established concentration- time (C-t) model by Walter and Wagg (1977) was checked. For ideal plug flow assumption at limiting current conditions in a recirculation system, C-t relationship is reproduced as follows.

$$C_{\mathrm{i}}(\mathrm{t}) = C_{\mathrm{i}}^{0}.\, e^{\left(-\frac{t}{\tau}\right)[1-e^{\left(-\frac{KAaL}{Q}\right)}} \tag{1.1}$$

where $C_i(t)$ - Concentration of reactant ions in the electrolyte (here Sodium Chlorate) C_i^0 –initial concentration of reactant ions. All other terms are conventional and have usual meanings.

1.2 DEVELOPMENT OF A DUAL COMPACT/PACKED BED ELECTROCHEMICAL REACTOR FOR CONTINUOUS ELECTROSYNTHESIS APPLICATION

1.2.1 Penetration issue

For a flow-through porous electrode, with electrolyte velocity parallel to the direction of current flow indicate that few portion of the porous electrode is operating under mass transport limiting conditions if the electrode thickness is considerably larger than a certain value called as “Penetration depth”. This issue is referred as Penetration issue. This calls for the limitation in increasing the depth of bed beyond a certain value. Theoretical treatment of this behaviour is well established and shows that the penetration depth (p) of the limiting current density (assuming that the electrode is fully conducting) is given by (Doherty, Sunderland, Roberts and Pickett, 1996).

$$\sqrt{\frac{2ek_s\Delta\eta}{ak_m nFC_0}} \tag{1.2}$$

Authors have presented the simulation results for high surface area graphite felt. Some of their findings are as follows.

- For thin electrodes the limiting current plateau is clearly evident and the total current increases approximately linearly with thickness for large cathodic potentials. For thick electrodes most of the electrode is operating under electron transfer control. In this region the total current decreases with electrode thickness due to the potential drop within the electrode material.

- Simulation profiles show that the normalized concentration (C/C0) plotted for thinner bed electrodes over the length of bed is indistinguishable between exponential profile and simulated value. While as the electrode bed thickness is increased, both results diverged. Hence, the assumption that the electrode is operating entirely under mass transport limiting conditions is no longer valid and the reduction in concentration is significantly over predicted by the established theory.

- For thicker electrodes the divergence from the established models becomes increasingly significant. The two approaches show widely different profiles as the electrode is much thicker than the penetration depth ‘p’. Most of the electrode is, therefore, operating under electron transfer control.

- Optimum thickness of the electrode is thus explicitly a design requirement.

In this context, the development of a dual bed PBER by repeating one more bed of electrode particles and its assessment, beckons a significant role. These electrolysers were stacked in series for demonstrating continuous electro-synthesis of sodium perchlorate.

1.3 MODELING RESIDENCE TIME DISTRIBUTION (RTD) BEHAVIOUR IN A PACKED BED ELECTROCHEMICAL REACTOR (PBER)

Flow behavior of electrolyte through these reactors via RTD studies has been one of the key components in understanding its vessel hydrodynamics. In an experimental study of residence time distribution, flow elements are tagged by a tracer (coloured, radioactive, etc.) and the variation of tracer concentration in the exit stream with time is measured. The injection of tracer into the flow stream is frequently done in such a manner that it can be well approximated by a delta function or a thin finite width pulse. The tracer concentration distribution at the exit (called also the tracer output signal) has a characteristic shape depending upon the relative strength of dispersion, and on the location of tracer injection and detection. Developing a suitable theoretical model justifying RTD behavior has been an onus among the engineers for quite a long period of time. Not surprisingly, various studies were reported exhibiting peculiar flow behaviours in variety of systems.

Saravanathamizhan (2008) provided a three parameter model to describe the electrolyte flow in continuous stirred tank electrochemical reactor (CSTER) consisting bypass, active and dead zones with exchange flow between active and dead zones. Authors validated the model for the effluent color removal inside a typical CSTER. Atmakidis (2015) conducted a numerical analysis of dispersion in packed beds and developed a RTD model using CFD modeling. Zou *et al.* (2017) performed simulations of the RTD of a bubbling fluidized bed reactor using CFD based on the modified structure-based drag model. A general comparison of the computed RTD with the experimental data was also shown for validation. Ouassila Benhabiles *et al.* (2012) conducted the experimental study of photo catalytic degradation of an aqueous solution of linuron in a tubular type reactor and used RTD data for investigating the malfunction of the photo reactor. Martin (2000) shown that ETIS (Extension to tanks in series) model in tandem with the reactor network structure is a versatile method of describing the characteristics of a small but diverse group of reactors.

Earlier studies had shown that conventional models like open dispersion models, small dispersion models and Tanks in Series models can explain with lot of clarity, the behavior of electrolyte inside a typical packed bed reactor under non electrolyzing conditions. However, not many studies were reported in literature regarding the applicability of a suitable model in a packed bed reactor operating under electrolyzing conditions. Many of these models fail to explain the recirculation flow expected inside such reactor due to obvious gas evolution around the particulate electrodes. In the initial phase of present study, a detailed interpretation of electrolyte flow inside a packed bed electrochemical bed reactor was made under non electrolyzing conditions using an experimental RTD analysis. Applicability of available theoretical models was also carried out to strengthen the experimental findings. At a later part of the study, similar RTD studies were repeated at analogous flow conditions but operated under electrolyzing environment, for getting comparative flow behaviors with and without electrolyzing environment. A Modified Dispersed Plug Flow Model (MDPFM) was developed to validate the variation in such flow circumstances.

1.4 IMPACT OF MODIFIED LEAD DIOXIDE ANODES IN CONVENTIONAL PERCHLORATE CELLS

Conventional perchlorate cells are “parallel plate cells” employing lead dioxide coated over titanium substrate and stainless Steel (SS 316 L preferably) as the electrodes and chlorate solution (here sodium chlorate) as electrolyte. Electrolytic oxidation of sodium chlorate occurs at high positive potential. This makes it necessary that the anode materials used in the cell have high electrode potential and oxygen over voltage. Current efficiency for perchlorate formation is always less than unity because of simultaneous oxygen evolution reactions (Munichandraiah, 1987).

$$H_2O \rightarrow (OH)_{ad} + H^+ + e^-$$
$$(OH)_{ad} + ClO_3^- \leftrightarrow ClO_4^- + H^+ + e^-$$

OR

$$ClO_3^- \rightarrow (ClO_3)_{ad} + e^-$$
$$H_2O \rightarrow (OH)_{ad} + H^+ + e^-$$
$$(OH)_{ad} + (ClO_3)_{ad} \leftrightarrow ClO_4^- + H^+ \qquad (1.3)$$

In other words, charge not utilized for conversion is inevitably used for liberation of oxygen from aqueous solution of sodium chlorate as per the following reaction.

$$2\,H_2O \rightarrow O_2 + 4\,H^+ + 4\,e^-$$

The above equation (1.2) suggests that the mechanism of anodic oxidation of chlorate to perchlorate on β- PbO_2 (Ti) anode involves the anodic oxidation of water in a one electron transfer step to give adsorbed (OH) radical as the rate determining step. Perchlorate ion is produced by a subsequent fast oxidation of chlorate ion or adsorbed chlorate radical and the adsorbed (OH) radical. A “highly active surface” of lead dioxide is therefore necessary for the purpose. Extensive characterization of lead dioxide electrode for its coated surface area, porosity and electrochemical performance assumes major significance in this context.

Presence of surfactants like t-octyl phenoxy polyethoxyethanol (Triton X-100), sodium sec- alkyl sulphates (Teepol), cetyl trimethyl ammonium bromide (CTAB)and few additives like sodium fluoride, cerium nitrate, etc. in the lead dioxide coating bath is known to modify the morphological, electrochemical and mass transfer features of lead dioxide deposits (Ghaemi, 2006). In the present work, combined effect of surfactants and additives on performance of perchlorate cell is studied. Inorder to examine the comparative performance, different samples of lead dioxide coated over titanium substrates were prepared by adding above referred additives and surfactants in the conventional nitrate bath for lead dioxide coating. Scanning electron microscope (SEM) (using CARL ZEISS EVO50 Instrument) and X-ray diffraction (XRD) (using PANALYTICAL-XPERT-PRO-MPD Instrument) studies were carried out to understand the morphological/ structural characteristics. Electrochemical impedence spectroscopy (EIS), and Potentio Dynamic Response (PDR) (all using SOLARTRON SI 1260/1287 instrument) studies were carried out to understand the electrochemical, kinetic and mass transfer characteristics. Various kinetic and mass transfer parameters were determined. Finally, samples of bigger dimensions were functionally tested in an actual perchlorate cell.

1.5 QUANTIFICATION OF INTERFACIAL ADSORPTIVE CHARACTERISTICS OVER LEAD DIOXIDE ELECTRODES

It is known that adsorption of chlorate and hydroxyl ions at the lead dioxide/ electrolyte interface primarily controls the kinetic facets of perchlorate formation reaction. Adsorption of species in the electrode-electrolyte interface needs a closer analysis. It is well known that, at the interface, separation of charges occur leading to anisotropic forces setting up there. Perturbations or departures from the bulk concentration take place. Perturbations or excess concentration are quantitative measures of the accumulation or depletion of species in the interface region which in turn quantifies the intensity of adsorption at the electrode – electrolyte interface. At present there are no techniques sensitive enough to experimentally determine the spatial variation in concentration of various species in the solution at the interface (Bockris, 2000).

Present work focuses on indirect quantification of adsorption features of conventional and modified lead dioxide anodes through analysis of electrocapillary characteristics. Since direct measurements of interfacial tension are not possible in solid electrodes, the same is determined indirectly by measuring current transients (current as a function of time). Lead dioxide anodes modified by addition of certain surfactants like CTAB and few additives like sodium fluoride and their combinations in the lead dioxide coating bath was investigated for their possible surface modifications using the above technique.

CHAPTER 2
LITERATURE REVIEW

2.1 DESIGN OF PACKED BED REACTORS

Packed-bed or porous electrodes, offering a high specific surface area, have been suggested as suitable means for carrying out electrochemical reactions with low current densities especially when the reaction rate is limited by mass-transfer (Bennion & Newman, 1972; Houghton & Kuhn, 1974; Newman & Tiedeman, 1975). These electrodes can be used for electrosynthesis of chemicals and electrochemical recovery of heavy metals from a variety of industrial and laboratory model solutions (Sioda, 1971; Bennion & Newman, 1972; Gaunand *et al.*,1977; Trainham & Newman, 1977; Matlosz & Newman, 1986; Doherty *et al.*, 1996; El-Deab *et al.*, 1999; Saleh, 2004). In several experimental works it was noted that when aqueous solutions are treated, water decomposition occurs within the porous electrode, along with the useful reaction. Alkire and Gould (1976) analysed multiple reaction sequences in packed-bed electrodes, but the practical aspects of parasitic reactions were studied by Volkman (1978). The theory of such electrodes was reviewed by Newman and Tiedeman (1975). More technical and practical aspects were summarized by Kreysa and Heitz (1976). Armstrong (1968), in his paper investigated out that the main drawback of porous electrodes is the excessive potential drop in the electrolyte. Assuming that voltage losses in the electrode matrix are negligible, the potential difference across the electrode-electrolyte interface increases as the potential of the solution decreases.

Sioda (1971) gave an analysis for a flow-through porous electrode operating below the limiting current for a reversible reaction described by the Nernst equation, which also includes treatment of the interfacial mass transfer resistance. Alkire and Gracon (1975) included a very general analysis of a single electrode reaction below the limiting current, including the effects of axial diffusion; results are given for an upstream counter electrode. Alkire and Gould (1976) have extended this work to multiple reaction sequences, which includes deposition of several metals, deposition of a metal in the presence of a redox system and results are given for a downstream counter electrode. Ateya (1977) gave an analysis similar to Sioda for a single electrode reaction described by the Nernst equation and studied the effects of axial diffusion and dispersion under conditions when the interfacial mass transfer resistance appears to be negligible. An optimal design of packed bed cells for high conversion is given by Kreysa & Reynan (1982). Kaminari *et al.* (2005) conducted work for the recovery of lead ion using a fluidized bed electrode to simulate an industrial effluent. The reactor's performance was evaluated based on dimensionless variables: voidage of the bed (ε), current density (i)/limiting currents density (I_{lim}), transport number of lead (t_{Pb}) and transport number of support electrolyte (t_{Na}), and their influence on current efficiency (CE) and power consumption. Due to the almost total absence of mathematical models that fit the system and also due to the complexity of such models, the choice fell upon a statistical technique, the central composite design (CCD), to obtain the desired responses as empirical functions. Response surfaces were then plotted to identify the behaviour of current efficiency and power consumption when the values of variables dimensionless were changed.

Computational fluid dynamics (CFD) is a tool that is becoming more realistic for use in the description of the detailed flow fields within fixed beds of low tube-to-particle diameter ratio (*N*). The motivation for the use of CFD is presented by reviewing the current state of fixed-bed reactor modelling, with an emphasis on the treatment of the description of fluid flow within the bed. Challenges in the use of CFD for fixed beds of particles are treated and potential uses of the simulation information in design models for fixed-bed reactors are discussed. An approach to fluid flows in low tube-to-particle diameter fixed beds is needed that is general enough to be applicable for reactor design purposes, but that retains the detailed flow features that contribute to transport of heat and mass which influence reaction kinetics. This approach provide a link to bed structure, so that, if a packing or packing characteristics are known, flow features, transport rates, and reactor performance can be rapidly assessed. Computational fluid dynamics simulations of flow through packed-bed structures can provide highly detailed and reliable information about the temperature and flow fields. The challenge for the future is to use the information that will be available to gain knowledge and understanding that will allow to develop reduced models which are detailed enough for design purposes, but still intuitively understandable and computationally tractable (Dixon, 2001).

Nava (2009) discusses the use of potential distribution analysis during the deposition of metal ions, at limiting current conditions and determines the optimum electrode thickness at which no hydrogen evolution occurs. The potential distribution studies were carried out on stainless-steel fibres of three different surface areas. The fibres were used as cathodic porous electrodes during the deposition of Ag(I) ions contained in 0.1 mol.dm^{-3} KNO_3 and 0.6 mol.dm^{-3} NH_4OH electrolyte. The comparison between the experimental and the theoretical potential distributions show good agreement at mean linear flow rates in the range of 0.24 and 0.94 cm s^{-1}.

2.2 INTERFACIAL CURRENT DISTRIBUTION IN PACKED BED REACTORS

Newman (1962) were the first to establish an analytic equation for current as a function of time, flow rate and bed length, when the reaction is mass transfer controlled. A two-dimensional treatment for a packed-bed electrode, in which the direction of solution flow is perpendicular to the direction of current was authored by Alkire (1974) with cylindrical coordinates for practical applications. Kreysa and Heitz (1975) established an empirical law which can be used to find the effective length of the electrode. Fedkiw and Newman (1979) introduced a periodically constricted model for mass transfer phenomena in a packed-bed electrode though the results were not significantly different from those obtained with homogeneous models. Lyke and Langer (1991) illustrated the effect of ohmic drop in a packed-bed electrode when Tafel kinetics is followed. Elanadoulli and Ateya (1992) studied the effect of gas bubbles formed in the three dimensional electrode for application of the electrode to hydrogen evolution reaction.

Newman & Tobias (1962) described general equations explaining the behavior of porous electrodes. These equations are used to determine the initial and the steady-state conditions in one-dimensional porous electrodes of uniform geometry and polarization parameters. In particular, it is shown that the current and reaction distributions in the depth of the electrode are strongly influenced by the type of activation polarization and by mass transport of the reacting ionic species, in addition to the effective conductivities of the two phases. It is found that a linear approximation to a Tafel curve leads to an inadequate description of actual behavior when the reaction is distributed non-uniformly in the depth of the electrode. Kusakabe (1986*)* has studied the current paths and electrolysis efficiency in bi-polar packed bed electrodes.

2.3 POTENTIAL DISTRIBUTION IN PACKED BED REACTORS

Sioda (1968,1975) investigated fixed beds of graphite granules and proposed a model of the system. These results were unfortunately influenced by wall effects. Coeuret (1976) has investigated the efficiency of fixed beds of highly conducting spherical particles. In these experiments wall effects and contact resistances between individual particles were avoided. In a further paper by Couret (1976), the theoretical and experimental study of metal- solution potential distributions was undertaken for fixed and fluidized beds of highly conducting particles. It has to be mentioned that studies of flow-through porous electrodes with no granular packing also concerned the limiting current conditions (Sioda 1968; Sioda 1971;Alkire & Gracon 1975).A few papers used an analytical solution for the solution potential distribution within the electrodes in their theoretical developments.

Gaunand *et al.*(1977) carried out a more complete study dealing with the experimental investigation of the metal-solution potential distribution within flow-through fixed electrodes under limiting current conditions and the overall metal-solutions potential drop in these electrodes. The effective operation of an electrochemical cell utilizing a porous electrode is critically dependent on the potential distribution within the electrode. In particular, the penetration depth of the current may be limited due to ohmic loss in the electrolyte. Theoretical treatment of this behavior is well established. Pickett (1977) showed that the penetration depth (p) of the limiting current density for metal deposition (assuming that the electrode is fully conducting) can be determined. In order to achieve a maximum conversion rate per unit cell volume, the electrode should be no thicker than ‘p’. Saleh (2004) introduced an effectiveness factor ϕ to explain the extent of utilization of bed length for conversion.

2.4 MASS TRANSFER BEHAVIOR IN PACKED BED REACTORS

Although the active specific area and the space time yield of these electrode materials are high, they suffer from the high pressure drop and tendency to clogging especially when used to remove heavy metals from industrial waste solutions. Besides, fixed bed electrodes made of small particles, metal felt and metal foam may entrap gas bubbles (H_2 or O_2) which are likely to evolve simultaneously with the main reactions from dilute solutions with a consequent increase in cell resistance and electrical energy consumption (Walsh 1993). Moreover, such low porosity electrodes are difficult to operate under gas sparging or two phase flow which is sometimes essential as in the case of H_2O_2 synthesis, flue gas desulphurization and alkene oxide production (Oloman1987; Scott 1993).

Walker and Wagg (1977) made a rigorous concentration – time modeling for the packed bed electro chemical reactors assuming different flow configurations. A specific work was carried out to examine the mass transfer behaviour of a flow-by fixed electrode built of relatively large Raschig rings, and cylinders under different flow conditions such as single phase flow, gas sparging and two phase flow. Although, large particles give less active specific area and lower space time yield than small packing material they are expected to suffer less from pressure drop, clogging and entrapment of gas bubbles in case of metal deposition from waste solutions. Rates of mass transfer were determined under different conditions by measuring the limiting current of the cathodic deposition of copper from acidified copper sulphate solution (Soltan *et al.*2003). An analysis of the influence of mass transfer on porous electrode performance using a domain polynomial method was studied by Yan *et al.*(2004).

Meticulous inspection of the literature has unveiled the weakness of several empirical methods for predicting the macroscopic mass and heat transfer characteristics relevant to gas-liquid cocurrent downflow and upflow packed-bed reactors (Delanghe *et al.* (1990), Lyke *et al.* (1991), Soltan *et al.* (2003), Saleh (2004), Scott *et al.* (2004)). In response, using a wide experimental database consisting of 5279 measurements for trickle beds (downflow) and 1974 measurements for packed bubble columns (upflow), a set of reliable correlations has been recommended for the prediction of the gas-liquid interfacial area, the volumetric liquid- and gas-side mass-transfer coefficients, the wall and bed liquid-solid mass-transfer coefficients, the wall heat-transfer coefficient, the bed effective radial thermal conductivity, and the particle-to-fluid heat-transfer coefficient. Some of these correlations are from the literature, and others have been developed by combining artificial neural networks and dimensional analysis. The accuracy of the proposed correlations surpasses by far the performances of the available methods sometimes by up to a 10-fold reduction in scatter. Notwithstanding the substantial reduction in scatter, these correlations have been thoroughly tested for phenomenological consistency and have been shown to restore the expected trends documented in the database (Faisal Larachi *etal.*2003).

2.5 DIFFERENT APPLICATIONS OF PACKED BED ELECTROCHEMICAL REACTORS

Camino Fernandez (2014) studied about the production of H2 using a packed bed reactor with polyurethane foam acting as support material. Yang (2018) studied regarding catalytic hydrogenation of *N*-4-nitrophenyl nicotinamide in a micro-packed bed reactor. Similarly Selvaraj (2018) studied regarding tannase production through solid state fermentation. Bennion & Newmann (1972) attempted for electrochemical removal of copper ions from very dilute solutions using packed bed system. A similar study was attempted by Chu *etal.*(1974) and

Katsuki *et al.*(1986). Pressure drop behavior in a three dimensional packed bed cell during copper deposition and hydrogen evolution was studied by Stankovic *etal.*(1995). A flow by packed bed electrode for removal of metal ions from waste waters was studied by Simonsson (1984). A Carbon particulate packed bed electrolysis flow cell for the production of Techtenium complexes was attempted by Mikelsons *et al.*(1986). Somsaluay Suwanprasop *etal.* (2005) developed a laboratory-scale and pilot-plant fixed-bed reactors for carrying out the wet air oxidation of phenol over a commercial active carbon catalyst at mild temperatures and oxygen partial pressures of 120-160 °C and 0.05-0.2 MPa, respectively. The performances of the fixed-bed reactors have been assessed and compared to each other for both up and downflow operation mode. Depending on the flow mode and reactor scale, distinct phenol destruction rates have been observed in the experiments. A series of batch experiments are carried out to obtain phenol removal kinetics, which are subsequently implemented in the modelling of the pilot-plant fixed bed reactor. A one-dimensional, non-isothermal piston dispersion model was developed to describe in detail the interplay of reaction kinetics, gas-liquid hydrodynamics, and heat and mass transfer in both flow directions. The model predicts reasonably well the experimental data, thus allowing for a thorough explanation of the observed pilot-plant reactor performance.

2.6 EFFECT OF FOREIGN IONS IN LEAD DIOXIDE ELECTRODE PERFORMANCE

Doping of PbO_2 by cations (Fe^{3+}, Co^{2+} and Ni^{2+}), by F^- and by cations and F^- simultaneously is discussed as a way of improving the stability and electrochemical activity in processes occurring at high potentials. Doping allows the control of the amount of structural water in an oxide. Radiotracer experiments showed that high electrodeposition current densities favour the segregation of incorporated tritium (protons) at the surface. On the other hand, fluorine doping results in a marked decrease in the amount of surface oxygen species. The influence of doping with metal cations strongly depends on the nature of the metal. Iron behaves like fluorine, while nickel causes an accumulation of surface oxygen species. Doped PbO_2 electrodes have quite good activities for the electrogeneration of ozone. In particular, Fe and Co doped PbO_2 showed a current efficiency of 15–20% for this process. (Velichenko *et al.,*2001).

Studies were done for examining the behaviour of fluorine modified β-PbO_2 electrodes in the processes of O_2 and O_3 evolution in sulphuric acid. The electrochemical kinetic analyses of these processes are based on quasi-steady-state polarisation and impedance data. The good agreement between the two sets of measurements allows some basic conclusions to be drawn. In particular, the O_2 evolution process is always inhibited at F-doped PbO_2 electrodes, and impedance results suggest possible changes in the mechanism, with electro-desorption of intermediates becoming more important as the concentration of the doping element increases. The interpretation of the data for the less positive potentials region invokes the specific adsorption of SO_4^{2-} as a factor influencing the kinetics of O_2 evolution. The current efficiency for O_3 formation as a function of the amount of NaF added to the PbO_2 growth solution reaches a maximum for a concentration of 0.01 mol dm^{-3}. A plausible cause for the decrease on the higher concentration side is the discharge of adsorbed SO_4^{2-} (or HSO_4^{-}) eventually yielding persulphate. This reaction is known to be favoured in the presence of a relatively high amount of fluoride in the electrolyte. An analysis of the results of modified neglect of diatomic differential overlap (MNDO) calculations on Pb cluster models and of X-ray photoelectron spectroscopy (XPS) data suggests that the coverage by weakly adsorbed oxygen species (OH and H_2O) is an important parameter that is influenced by F-doping (Velichenko et al., 1999).

The effect of F^- on the modified films of lead dioxide in morphology and structure was studied. The results obtained by cyclic voltammetry (CV), X-diffractometer (XRD) and scanning electron microscope (SEM) techniques indicated that F^- could change the magnitude of lead dioxide crystal grain and the preferred crystallizing orientation on the substrate surface, even though it didn't change the basic structure of PbO_2. When the modified electrode was applied as an analytical sensor to determine phenolic compounds, the linearity was in the range of $2\times10^{-5} - 1\times10^{-3}$ mol/L and the detection limit was 2.5×10^{-6} mol/L. It was all found that the stability and reproducibility of the oxide-modified electrodes were improved by additional F^- (Jin et al., 2001).

The effect of antimony on the reduction of the two allotropic forms of lead dioxide in sulphuric acid electrolyte has been studied. The effects of antimony doping of the lead dioxide lattice and the effects of antimony contamination of the electrolyte have been considered separately. In the first case, antimony increases the quantity of charge related to the reduction, and in the second it exerts a strong passivating influence on the lead dioxide electrodes (Penazzi *et al.*, 2000).

A moderate layer of PbO_2 onto stainless steel from nitric acid solutions in the presence and absence of Ce^{+3} and Ce^{+4} ions has been electrodeposited. The properties like stability and the ability to support anodic oxidations of organic molecules have been investigated. The activity of these anodes depends on the preparation and pre-treatment of the electrode. The investigations suggest that the stability and activity of the lead dioxide anode is influenced by the presence of Ce^{+3} / Ce^{+4} ions in the lead dioxide electrodeposits (Amjad et al., 2010).

A passive and roughened surface is produced on 416-SS by anodization in phosphate medium. The passivating layer is concluded to be conductive and the roughened surface allows for the strong adherence of electrodeposited PbO films. Anodes consisting of PbO on passivated 416-SS can be used in alkaline, neutral and slightly acidic media at large positive applied potenial values without apparent decomposition. The high catalytic activity is concluded tentatively to be the result of Fe(III), produced by anodic corrosion of the SS substrate simultaneously with deposition, which is incorporated into the PbO films. It was concluded that Fe (1 and/or 111) added to solutions of Pb(II) used for deposition of PbO films will result in a significant increase in catalytic activity for the doped films (Feng et al 2002).

2.7 SUMMARY

A detailed survey on the wider perspectives of packed bed electrochemical reactors touching its basic design comparisons, distribution of potential and mass transfer, its application as well as modifying the surface of PbO_2 electrodes by foreign ions is touched upon this chapter. It is specifically noted that researches on following areas are to still to be attempted in a rigorous way.

- Electrosynthesis of perchlorate using packed bed electrochemical reactor.
- Effective utilization of discarded lead dioxide particles as particulate anodes.
- Comprehensive studies exhibiting the influence of inevitable parameters over the performance of reactor.
- Multistage packed bed electrochemical reactor.
- Combination of a series of PBER (Packed Bed Electrochemical Reactor) for continuous electrosynthesis.

CHAPTER 3
MATERIALS AND METHODS

3.1 STUDIES FOR DEVELOPMENT OF PACKED/ COMPACT BEDELECTROCHEMICAL REACTOR

The cell was fabricated in cylindrical geometry using High Density Polyethylene (HDPE). Its overall dimensions were 17.78 cm (ID) × 30 cm (H). Scrapped lead dioxide particles (about 3.5 Kg) were thoroughly cleaned using deionized water and closely packed in the electrolyser upto 5 cm height having a porosity of 0.5. Perforated polypropylene supports (which also serves as distributor) with nylon mesh filter were used at both ends for ensuring rigid and leak proof packing. Schematic setup is shown in Fig.3.1 and actual experimental setup in Fig.3.2. Components of electrolyser are shown in Fig. 3.3. Particle size distribution of these particles obtained using sieve analysisand its image analysis using Zoom Stereoscopic Microscope are mentioned in Tables 3.1 and 3.2 respectively. Since particles collected were widely varying in size and shape, particles belonging to fine, medium and coarse were individually taken for image analysis. The hydraulic flow circuits consisted of centrifugal pump, valves and tanks for feeding and overflow electrolyte collection. Electrolyte was introduced to the cell through the inlet opening at the bottom, leaving the cell by overflows at the top, pumped to the feed tank and got returned to the cell by gravity. The tanks were filled with about 11.5 liters of sodium chlorate solution having an initial concentration of 669 gm/litre (gpl).A conductive (noble metal oxides containing Ti, Ru and Pd) coated titanium tube was used as a current feeder while the counter electrode was SS 316 L. A DC rectifier having 200 A, 60 V specifications was used for providing DC current to the electrolyser. Isothermal conditions were maintained in the overflow collection tank by providing it with a cooling water circulation system through cooling coils and an electric heater. Both electric heater as well as solenoid valve in the cooling water feeding line was interlocked with temperature sensor kept in the over flow tank as shown in Fig.3.4.A dual bed type cell was made in a single bed type for resolving the possible current penetration issues developed inside. Its construction is similar to the single bed type but by repeating one more bed of particles as shown in schematic sketch Fig. 3.5 and actual setup in Fig. 3.6. Concentration of sodium chlorate in the liquour was determined using iodometric titration.

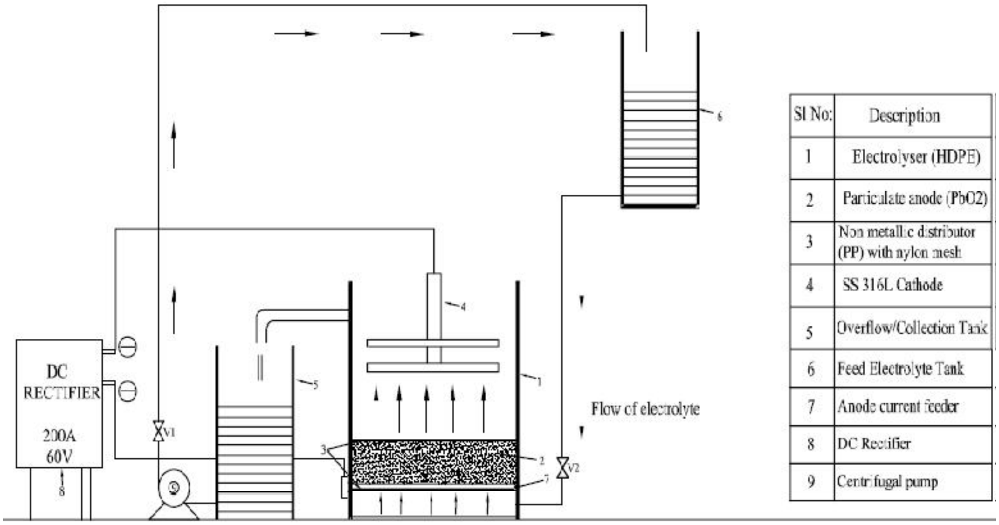

Sl No:	Description
1	Electrolyser (HDPE)
2	Particulate anode (PbO2)
3	Non metallic distributor (PP) with nylon mesh
4	SS 316L Cathode
5	Overflow/Collection Tank
6	Feed Electrolyte Tank
7	Anode current feeder
8	DC Rectifier
9	Centrifugal pump

Fig. 3.1 Schematic setup of PBER

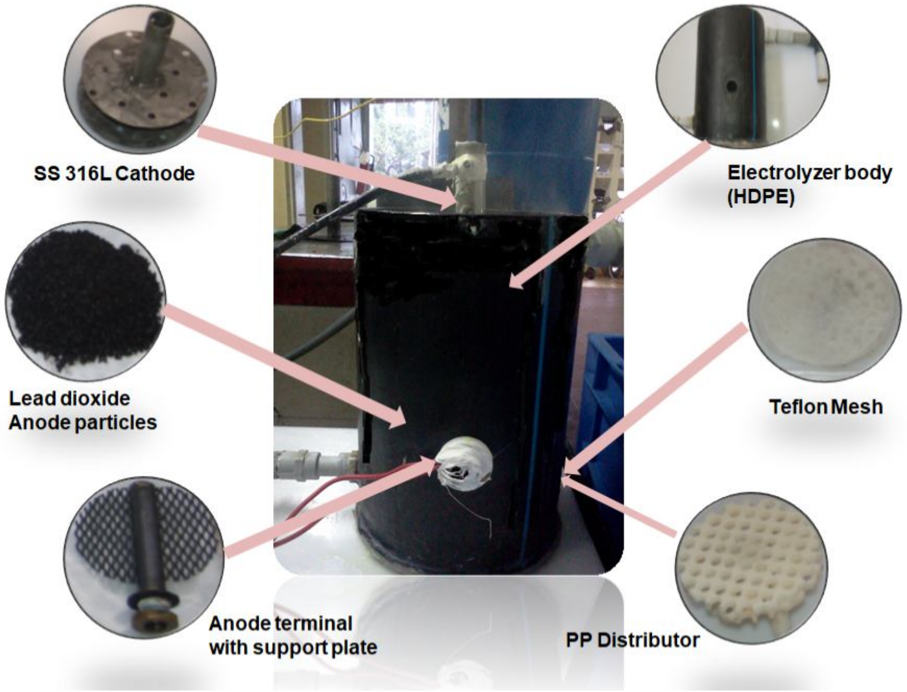
SS 316L Cathode
Electrolyzer body (HDPE)
Lead dioxide Anode particles
Teflon Mesh
Anode terminal with support plate
PP Distributor

Fig. 3.2 Components of PBER

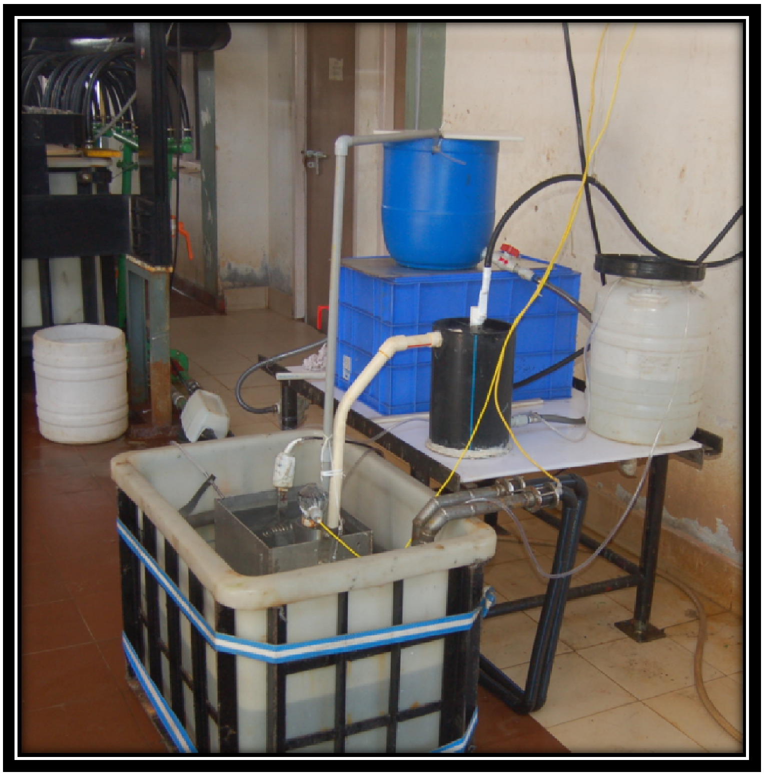

Fig. 3.3 Actual experimental setup

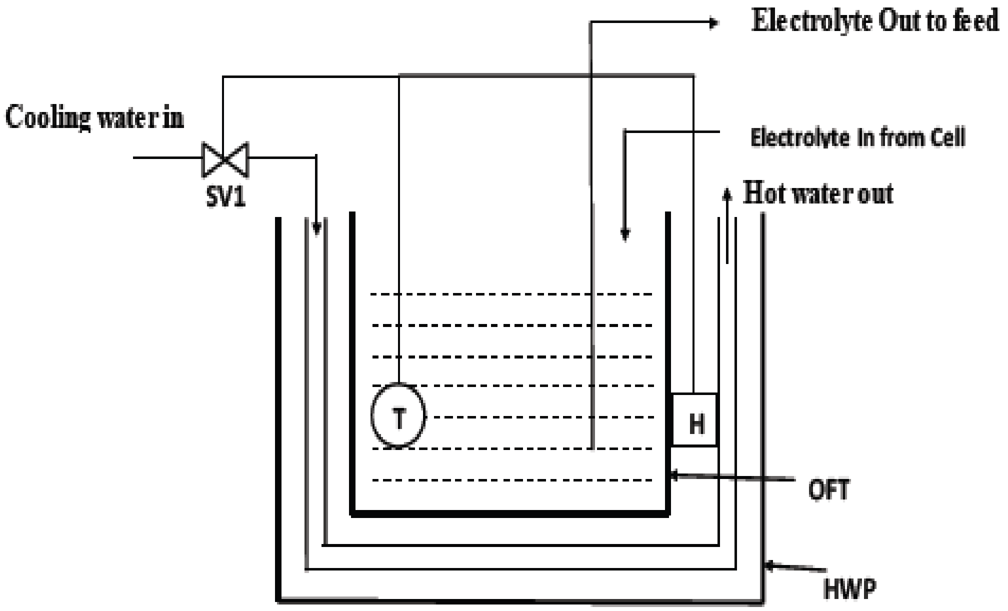
Electrolyte Out to feed
Cooling water in
SV1
Electrolyte In from Cell
Hot water out
T
H
OFT
HWP

Notations

T- RTD, H- Electric Heater, SV1- Solenoid Valve, OFT- Overflow collection tank, HWP – Hot water Pot

Fig.3.4 Isothermal System in Overflow tank

Table 3.1 Particle size distribution

Size Range	Weight %
> 710 µ	87.53
500-710 µ	9.46
355-500 µ	2.28
300-355 µ	0.27
<300 µ	0.46

Table 3.2 Image analysis of PbO_2 particles

Sl No:	**Sample Ref.**	**Size in Microns**	
		Min	**Max**
1	Fine PbO_2 -1	721.8	1756.6
2	Fine PbO_2 -2	485	837.4
3	Medium PbO_2 -2	1029.3	1245.4
4	Medium PbO_2 -2	1182.8	3285.7
5	Coarse PbO_2 -1	767.7	3341.9
6	Coarse PbO_2 -2	482.9	9439.4

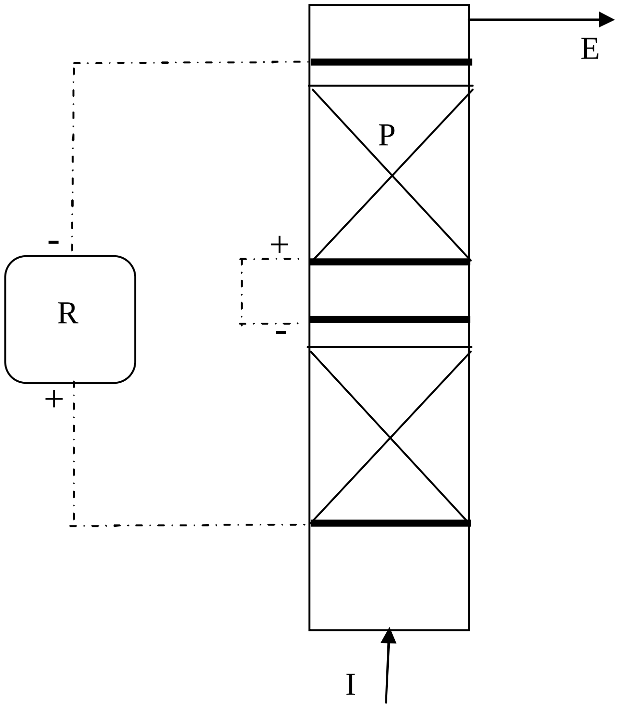

Fig.3.5 Schematic setup for dual bed PBER

(I- flow Inlet, P- packing, E-outlet, R- rectifier)

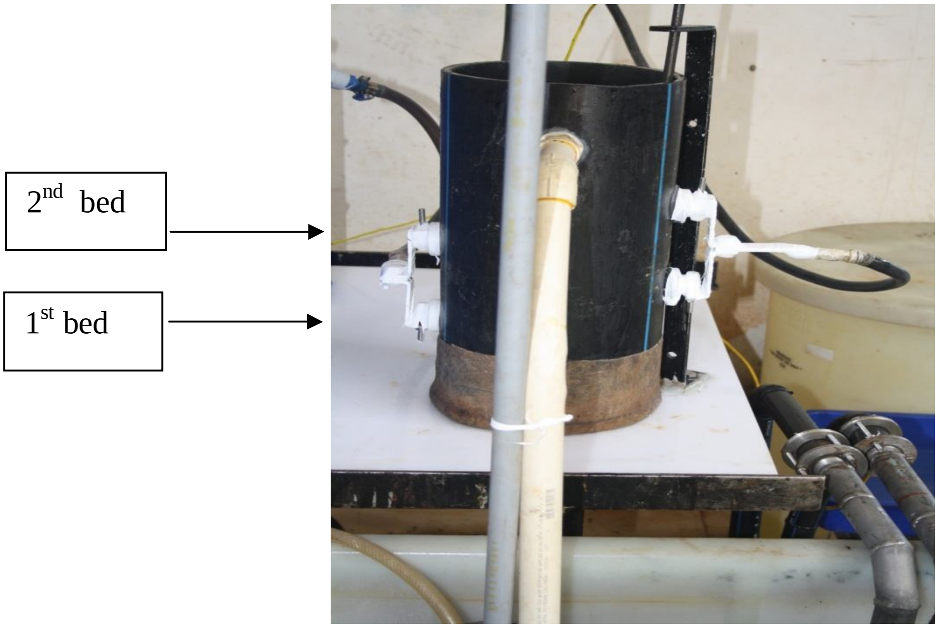

Fig.3.6 Actual experimental setup for dual bed PBER

3.2 RESIDENCE TIME DISTRIBUTION STUDIES IN PACKED/ COMPACT BED ELECTROCHEMICAL REACTOR

For carrying out RTD studies, methylene blue having concentration of 40/80 ppm was selected as tracer. Tracer was injected to cell closer to its inlet at about 2cm from HDPE body through a tee provided at the feed bottom. Flow medium used was water for conducting studies in non-electrolytic mode. On the contrary, sodium chlorate solution having 5 Kg/m^3 concentrations was chosen for studies in electrolytic mode. Flow rates of medium were varied from 3.33 $x10^{-5}$ m^3/sec to 1.33 $x10^{-4}m^3/sec$ for understanding the variation in RTD behaviour. A DC current of 15A was fed into the electrolyser (under electrolytic mode) using a rectifier having 200A, 60 V specification. A double beam UV spectrometer was used for estimating the transient variation in concentration of tracer in effluent, indirectly by measuring the colour intensity. Fig.3.7and3.8 shows the schematic and experimental setup respectively.

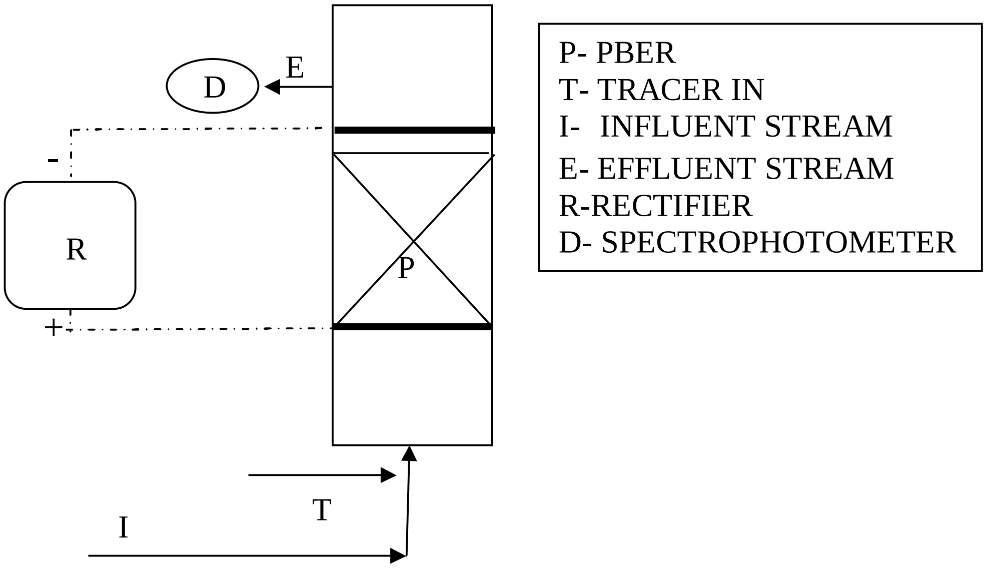
D
E
-
R
+
P
T
I
P- PBER
T- TRACER IN
I- INFLUENT STREAM
E- EFFLUENT STREAM
R-RECTIFIER
D- SPECTROPHOTOMETER

Fig. 3.7 Schematic setup for RTD studies

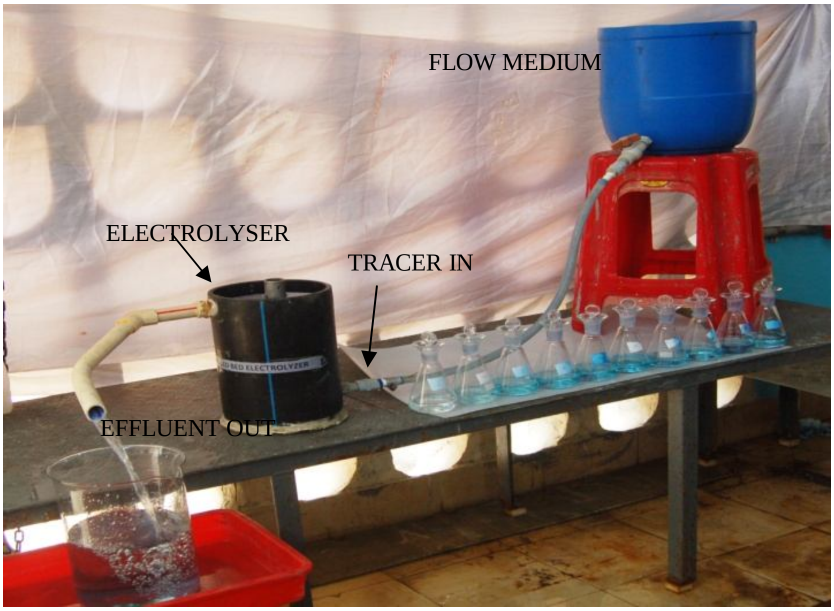
FLOW MEDIUM
ELECTROLYSER
TRACER IN
EFFLUENT OUT

Fig. 3.8 Experimental setup for RTD studies

3.3 STUDIES FOR UNDERSTANDING EFFECT OF FOREIGN IONS IN LEAD DIOXIDE COATING ELECTROLYTE FOR CONVENTIONAL PERCHLORATE CELLS

Lead dioxide coating electrolytic bath setup was made at 2 lit beaker scale. Titanium meshes used as anodes were given an undercoating of mixed metal oxides (MMO) consisting of Ru, Pd and Ti inorder to provide a conductive layer at lead dioxide – titanium interface. Surface preparation, MMO coating and Lead dioxide coating over titanium samples were done as follows.

3.3.1 Preparation of working electrode

Titanium mesh (5 cm x 3 cm) was first sandblasted for getting adequate roughness, followed by etching in dil. HCl for removing all impurities. Subsequently, sample is washed in demineralized water for removing excess acid adhering on its surface. Then, sample is dried and coated (3 layers) with prepared solution of MMO (Mixed Metal Oxide) solution for getting a conducting layer over the surface. Each layer of application is followed by baking in electric oven at a temperature of 450-5000C for about 10 minutes. Finally a conductive layer over the substrate is obtained. This is then followed by a electro deposition of Lead dioxide as mentioned in Table 3.3. Likewise samples were prepared with and without any surfactants and additives. Surfactants selected were Teepol, Triton X-100 and CTAB. Samples obtained were named as LA (or TSLA)/Teepol, LA (or TSLA)/TritonX and LA (or TSLA)/CTAB respectively. Unmodified sample was named as LA (or TSLA)/Normal (or Plain). Samples using both surfactants and additives like NaF and cerium nitrate were also prepared. Agitation of electrolyte was carried out by sparging oil free compressed air from bottom through an air distributor. Fig. 3.9 and Fig. 3.10 shows the actual experimental setup and prepared coated samples respectively. Scanning Electron Microscope (SEM) (using CARL ZEISS EVO50 Instrument) and X-Ray Diffraction (XRD) (using PANALYTICAL-XPERT-PRO-MPD Instrument) were used for analysis.

Table 3.3 Coating conditions

<table>
<tr><td colspan="2">Concentration of Electrolyte (Appx.)
$Pb(NO_3)_2$– 257 gpl,
$Cu(NO_3)_2$ - 16 gpl,
0.5gpl each of selected surfactants and additives were added separately to prepare different modified samples. Combined samples by adding surfactants and additives at above concentration each were also made.</td></tr>
<tr><td>Current density</td><td>5 A/dm^2</td></tr>
<tr><td>Voltage</td><td>3.8-4.0 V</td></tr>
<tr><td>Ampere hours</td><td>5 AH</td></tr>
<tr><td>pH</td><td>3-4</td></tr>
</table>

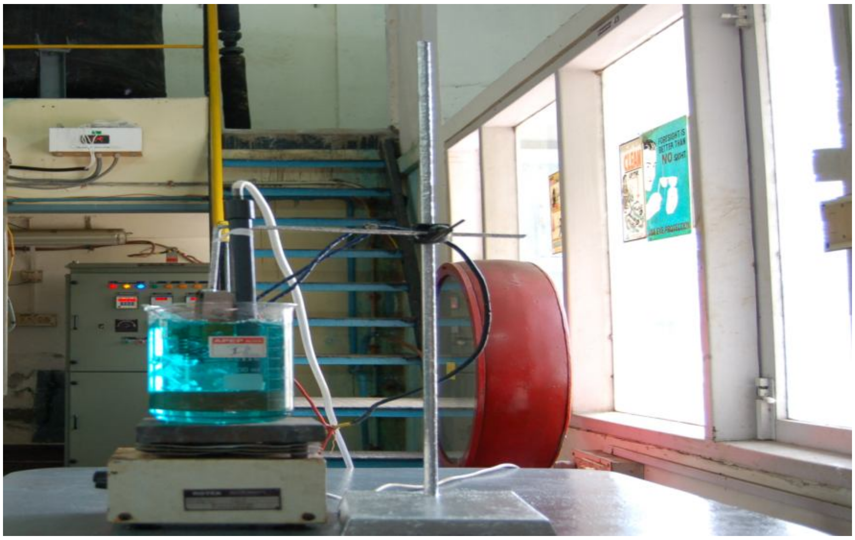

Fig.3.9 Lead dioxide Coating Setup

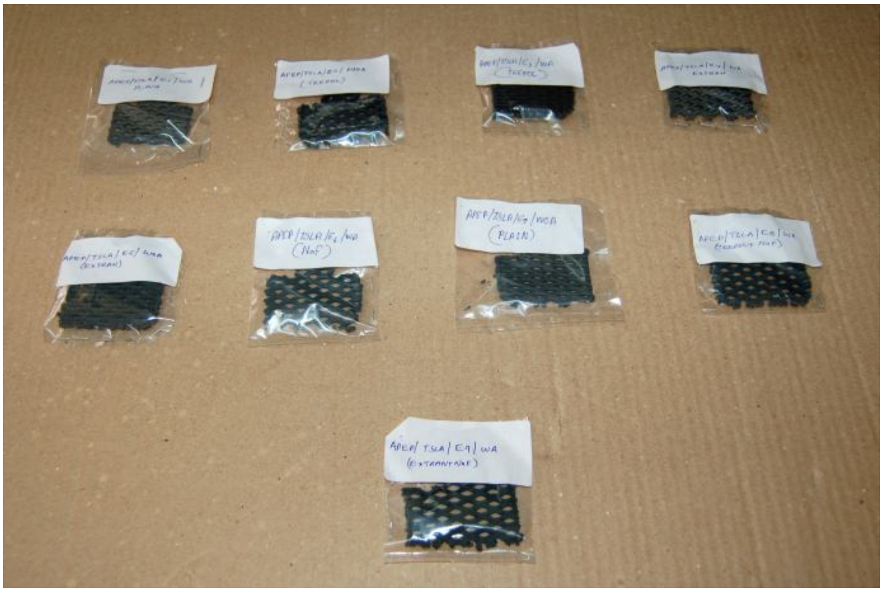

Fig.3.10 Prepared Lead dioxide Samples

Inorder to validate above results, 2 nos of 50 cm x 30 cm Titanium Substrate anodes were coated with lead dioxide from a bath containing 0.5 gpl of NaF and CTAB. Similarly another set of 2 nos of anodes (same dimensions) were also made with non-modified lead dioxide. These anodes were separately inserted in a 200 Lit perchlorate cell and experiments were carried out using sodium chlorate as electrolyte as per Table 3.4. Experiments were continued till sodium chlorate concentration reaches 100 gpl. Based on the difference in initial and final concentration of sodium chlorate in the electrolyte, current efficiency was calculated for perchlorate formation. Results are tabulated.

Table 3.4 Experimental Conditions for Validation

Anodes	Lead dioxide coated titanium
Cathodes	SS 316L
Electrolyte Volume	200 lit
Initial Concentration of Electrolyte $NaClO_3$– about 0.650 Kg/Lit	
Temperature	50-55^{o}C
Current density	22.5 A/dm^2
Voltage	4.0-4.2 V

3.4 STUDIES FOR QUANTIFICATION OF INTERFACIAL ADSORPTIVECHARACTERISTICS OVER LEAD DIOXIDE ELECTRODES

A 3- electrode mode setup was made. In three electrode mode, the reference electrode (R) is separated from the Counter (C) and connected to a third electrode. This electrode is most often positioned so that it is measuring a point very close to the working electrode (W/WS) (which has both Working and Working Sense leads attached). A diagram of a 3-electrode cell setup can be seen in Fig.3.11.

Table 3.5 shows the conditions and type of electrodes used for Potentiostatic studies. Model and Make of Potentiostat used was SOLARTRON SI 1260/1287.

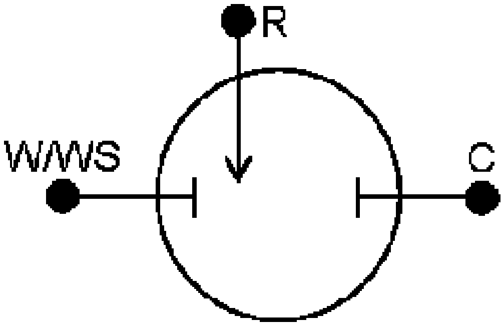

Figure 3.11 Three electrode cell setup

3.4.1 Preparation of working electrode

Titanium mesh (5 cm x 3 cm) was first sandblasted for getting adequate roughness, followed by etching in dil. HCl for removing all impurities. Subsequently, sample is washed in demineralized water for removing excess acid adhering on its surface. Then, sample is dried and coated (3 layers) with prepared solution of MMO (Mixed Metal Oxide) solution for getting a conducting layer over the surface. Each layer of application is followed by baking in electric oven at a temperature of 450-500^{0}C for about 10 minutes. Finally a conductive layer over the substrate is obtained. This is then followed by an electro deposition of Lead dioxide as mentioned in Table 3.3

Table 3.5 Experimental conditions for Potentiostatic studies.

Working electrode	Lead dioxide
Counter electrode	Platinum/Iridium mesh
Reference electrode	Calomel
Electrolyte	100gpl $NaClO_3$ solution
Various Potential difference (Vs Ref) maintained (in Volts)	0.01,0.1,0.5,0.9,1.3, 1.5,1.7,1.9,2.1

Three-electrode setups have a distinct experimental advantage over two electrode setups; they measure only one half of the cell. That is, the potential changes of the working electrode are measured independent of changes that may occur at the counter electrode. This isolation allows for a specific reaction to be studied with confidence and accuracy.

CHAPTER 4

RESULTS AND DISCUSSION

4.1 DEVELOPMENT OF A PACKED/ COMPACT BED ELECTROCHEMICAL REACTOR

4.1.1 Optimization of design configuration

Different design configurations in the mode of packing of particulate electrodes were attempted as shown in Fig.4.1 (a), 4.1 (b) and 4.1 (c).Central aim of this sub study was to conduct a broader screening while choosing the optimized packed bed electrolyser design configuration for perchlorate conversion study. Configuration I and II basically suits for a batch operation whereas configuration III allows a continuous mode of operation. Sodium chlorate solution of known concentration was filled in cell configuration I and II whereas same solution was allowed to over flow in configuration III as explained in Fig.4.1. All these cells were operated under similar conditions for about 3 days and average current efficiency (CE) for perchlorate formation was determined as shown in Fig.4.2. Method of calculation of current efficiency for perchlorate formation is as follows.

4.1.1.1 Calculation of Current efficiency

Let amount of $NaClO_3$ converted be ‘C’gms.

Theoretical Ampere hours required for converting ‘C’ gms, say T = C/106.5 x 2 x 26.8, where 2Faraday =2 x 26.8 Ampere hours

Let actual Ampere hours passed be ‘P’.

% Current efficiency for perchlorate formation, C.E = T/P x 100

From Fig.2, it is clear that annular design shown in Configuration I having PbO_2 particles filled in the inner cylinder, exhibited poor performance. Poor current distribution through the electrode bed owing to low resistance path between the cylinder regions had resulted in meager conversion. Significant improvement in current distribution and hence in CE was noticed in Configuration II when the anode feeder rod was inserted in to the bed of anode particulates. But the exact benefits from the inherent nature of Lead dioxide particulates were obtained in configuration III when there is a continuous circulation of electrolyte through the bed. Better current distribution coupled with uniform distribution of flow across the electrode bed had resulted in its improved CE. Resistance due to diffusion layer generated in the other two configurations was completely eliminated in configuration III owing to continuous regeneration of surface of electrode particles with fresh feed of unconverted chlorate ions. Configuration III was selected for further studies based on the above performance results.

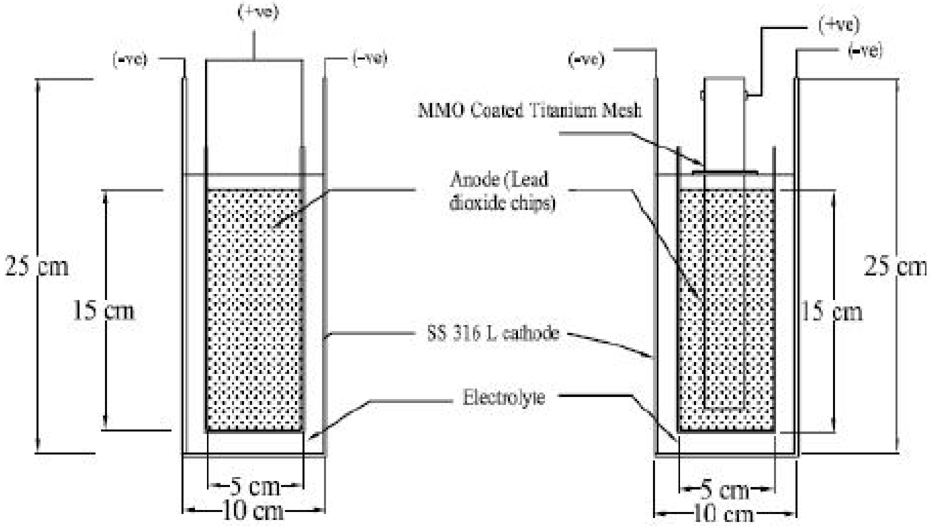
(+ve)
(-ve)
(-ve)
(-ve)
(+ve)
(-ve)
MMO Coated Titanium Mesh
Anode (Lead dioxide chips)
25 cm
15 cm
SS 316 L cathode
Electrolyte
25 cm
15 cm
5 cm
10 cm
5 cm
10 cm

Fig. 4.1 (a) Configuration I Fig. 4.1 (b) Configuration II

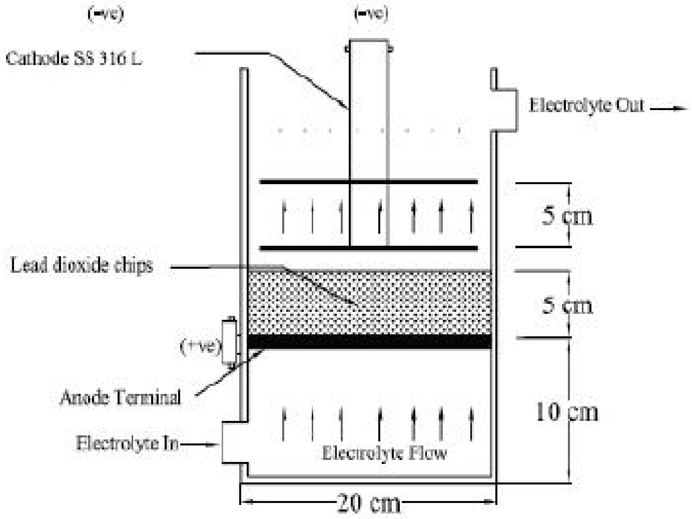
(-ve)
(-ve)
Cathode SS 316 L
Electrolyte Out
5 cm
Lead dioxide chips
5 cm
(+ve)
Anode Terminal
10 cm
Electrolyte In
Electrolyte Flow
20 cm

Fig. 4.1 (c) Configuration III

Fig. 4.1 Various configurations of PBER

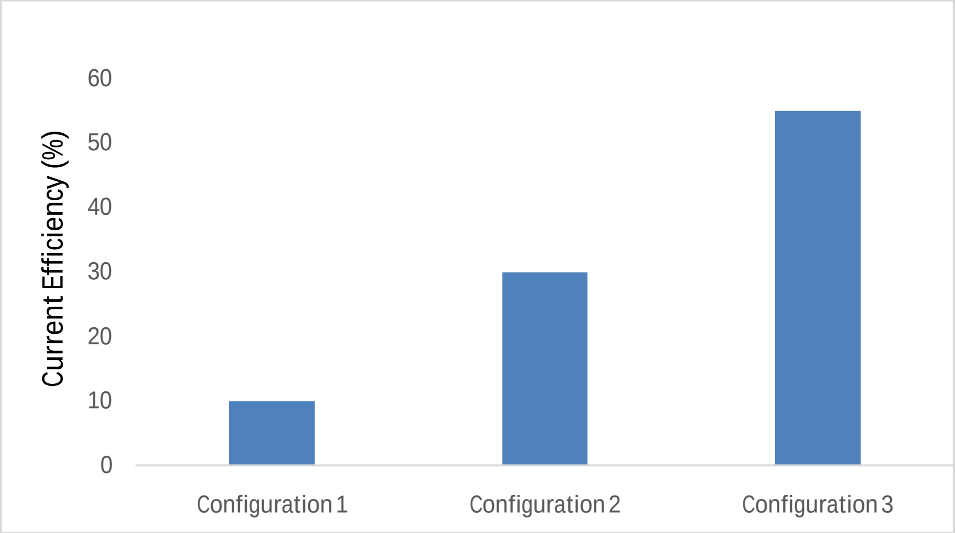

Fig.4.2 Comparison of average current efficiencies (Operating conditions: I=60A, Initial conc.of $NaClO_3$ = 669 gpl, Duration = 3 days)

4.1.2 Influence of Current density

Influence of current density on the performance of PBER was studied at various current load by keeping other parameters like temperature and flow rate constant. Fig.4.3 shows the variation of current efficiency for each current load. Fig.4.4 depicts the influence of current load on initial current efficiency. As expected, current efficiency increases steadily with current density in the electron transfer control regime where higher overpotential ensures better charge transfer reaction kinetics. A peak at 80A exhibits the limiting current region (I_L) where reaction rate reaches sufficiently high for given operating conditions where after mass transfer control region prevails. As the current load is still increased, reaction will be sufficiently mass transfer controlled resulting in slight drooping down of current efficiency owing to depletion of reactant radicals at the electrode surface. Another significant finding is the systematic reduction of current efficiency with the depletion in concentration of $NaClO_3$ as shown in Fig.4.5. This is due to the dependence of limiting current density on the concentration of reactant radicals as per following equation given by Walker and Wagg (1976).

$$I_L(t) = nFQC_i[1\text{-}e^{-KAaL/Q}]\{e^{\left(-\frac{t}{\tau}\right)[1-e^{\left(-\frac{KAaL}{Q}\right)}}\} \qquad (4.1)$$

As per above equation, limiting current value (I_L) also gets reduced as the concentration of Sodium Chlorate (Ci) decreases with time. Thus, maintaining electrolyser at I_L(optimized for higher Ci) during the lagging phase of electrolysis (lower Ci) clearly sets up a mass transfer control regime and thereby a progressive reduction in efficiency.

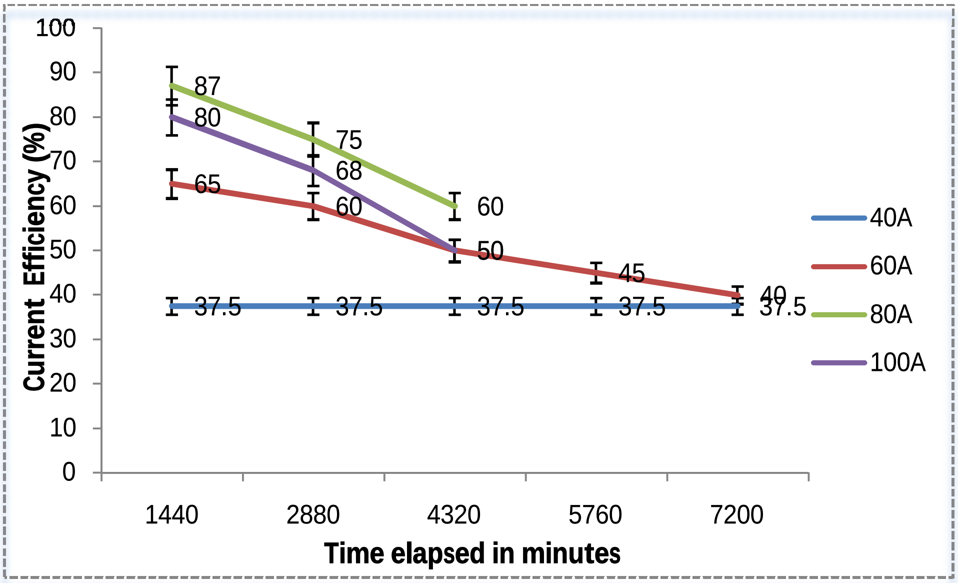

Fig.4.3 Effect of current on performance of electrolyser

(Operating conditions: Initial conc. of $NaClO_3$ = 669 gpl, Flow rate= 800 mL/min, Temperature = 60^0C, Bed height = 5 cm, Avg Particle Diameter = 690µ)

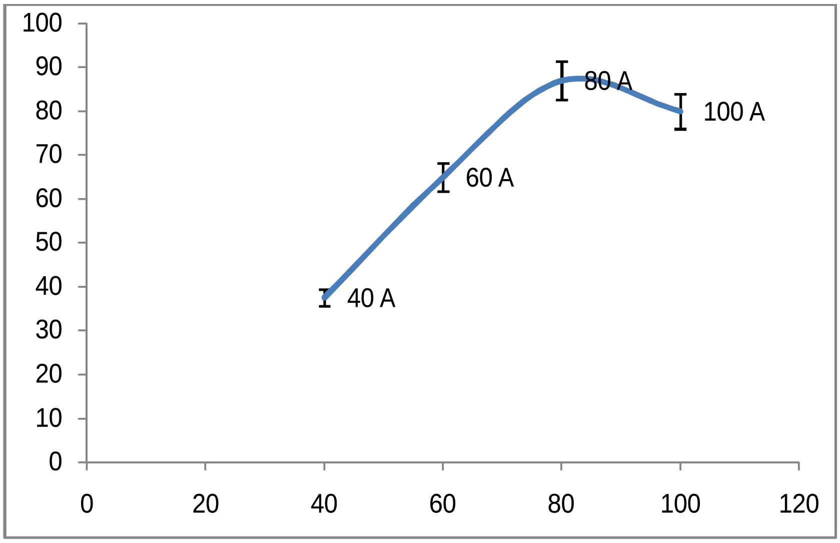

Fig.4.4 Effect of current on initial current efficiency

(Operating conditions: Initial conc. of $NaClO_3$ = 669 gpl, Flow rate= 800 mL/min, Temperature = 60^0C, Bed height = 5 cm, Avg Particle Diameter = 690µ)

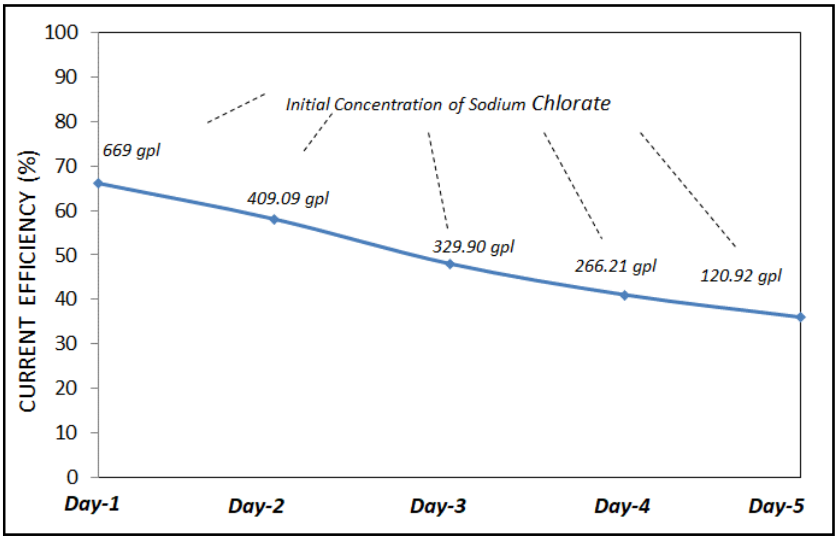

Fig. 4.5 Effect of Concentration of $NaClO_3$ on current efficiency

(Operating conditions: Initial conc. of $NaClO_3$ = 669 gpl, Current- 60A, Flow rate= 800 mL/min, Temperature = 60^0C, Bed height = 5 cm, Avg Particle Diameter = 690µ)

4.1.3 Influence of electrolyte flow rate

Fig.4.6 and 4.7 depicts the effect of electrolyte flow rate on the performance of electrolyser. Though not as influential as current density, an optimum flow rate of 800 mL/min was obtained when other parameters were kept unvaried. As the flow rate is significantly increased beyond this value, residence time distribution of the reacting radicals becomes poorer resulting in substantial reduction in current efficiency (CE). Another finding from the graph is that CE gets slightly improved towards the lagging phase of electrochemical oxidation for higher flow rates (1000 mL/min & 1500 mL/min). This can be due to better availability of unconverted radicals at the electrode surface at limiting current conditions thereby slightly overcoming the mass transfer resistance.

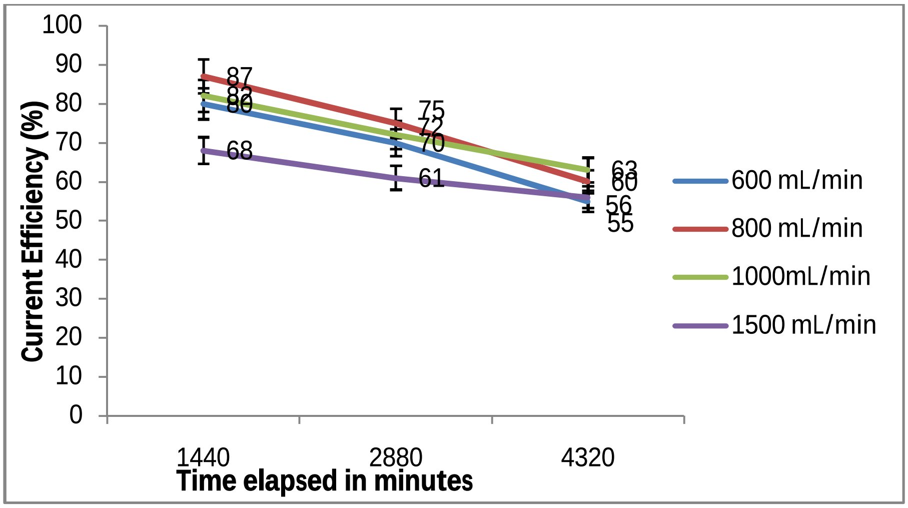

Fig. 4.6 Effect of flow rate on performance of electrolyser

(Operating conditions: Initial conc. of $NaClO_3$ = 669 gpl, Current load= 80A, Temperature = 60^0C, Bed height = 5 cm, Avg Particle Diameter = 690µ)

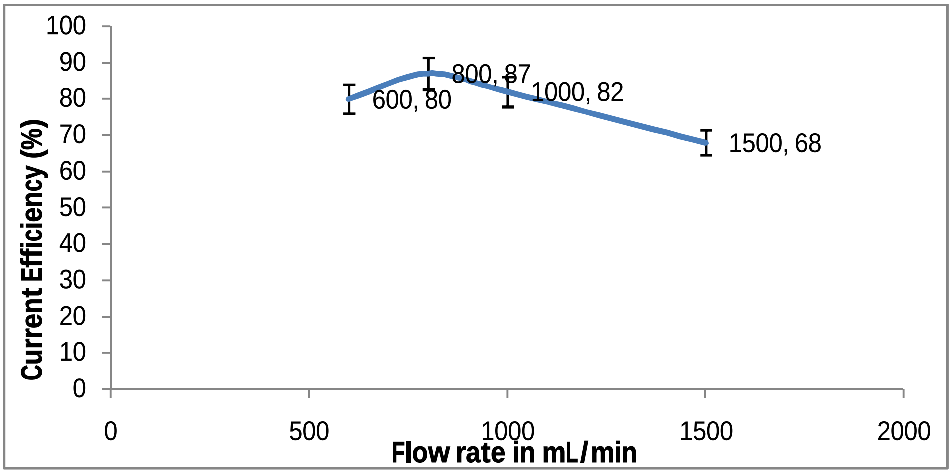

Fig. 4.7 Effect of electrolyte flow rate on initial current efficiency

(Operating conditions: Initial conc. of $NaClO_3$ = 669 gpl, Current load= 80A, Temperature = 60^0C, Bed height = 5 cm, Avg Particle Diameter = 690µ)

4.1.4 Influence of temperature

3 different electrolyte temperatures viz. 50^0C, 60^0C and 70^0C were selected to study its influence on the performance of electrolyser. Results are shown in Fig.4.8 & 4.9. In general, increase in temperature improves the rate of reaction. Surprisingly, a peak performance was observed at 60^0C, beyond which CE starts decreasing. This could be explained as follows. Basic electrochemical mechanism for Perchlorate formation is as follows.

$$\begin{aligned} ClO_3^- &\leftrightharpoons ClO_{3(ads)} + e^- \qquad (4.2) \\ H_2O &\rightarrow OH_{(ads)} + H^+ + e^- \\ ClO_{3(ads)} + OH_{(ads)} &\leftrightharpoons ClO_4^- + H^+ \end{aligned}$$

Perchlorate formation is a complex heterogeneous reaction proceeding through intermediate steps as shown above. Formation of hydroxyl ions by splitting of water molecule through one electron transfer step and its subsequent adsorption on lead dioxide surface forms the slowest among all. Charge transfer rate coupled with the net availability of hydroxyl ions on the electrode surface are the two complimentary requisites for the enhancement in net reaction rate and hence in CE. With temperature, though charge transfer rate could be improved due to the higher solution conductivity, there could be a reduction in net availability of hydroxyl ions on the electrode surface owing to higher desorption rate. This can be the most probable reason for above drop in CE at higher temperature.

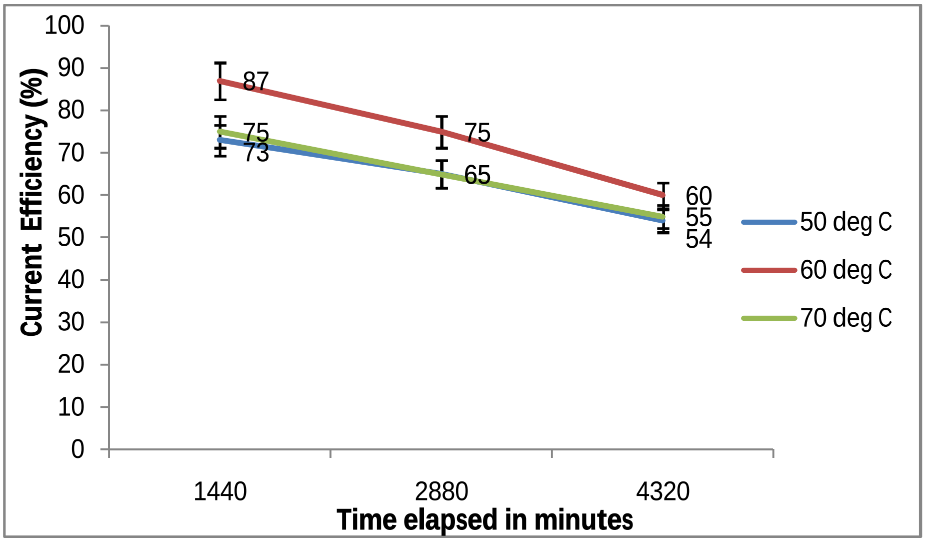

Fig.4.8 Effect of electrolyte temperature on current efficiency

(Operating conditions: Initial conc. of $NaClO_3$ = 669 gpl, Current load= 80A, Flow rate -800 mL/min, Bed height = 5 cm, Avg Particle Diameter = 690µ)

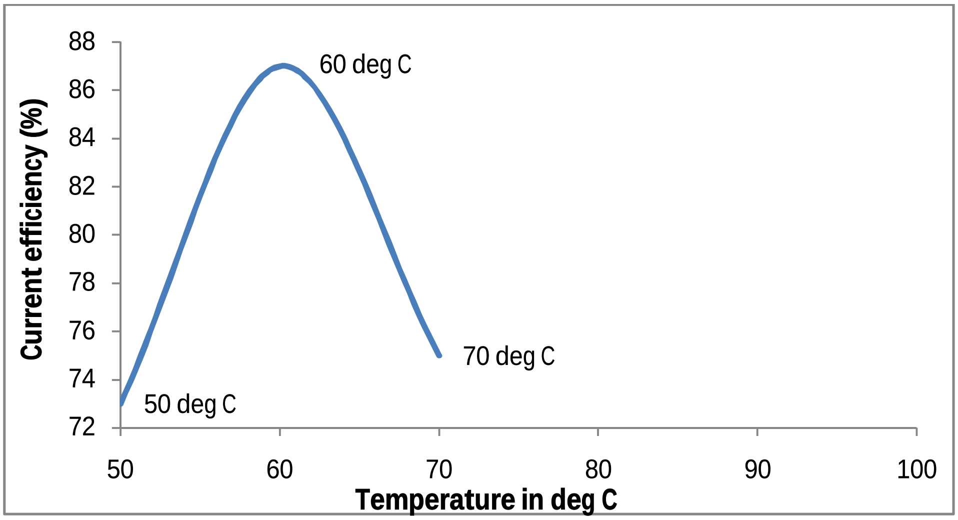

Fig.4.9 Effect of electrolyte temperature on initial current efficiency (Operating conditions: Initial conc. of $NaClO_3$ = 669 gpl, Current load= 80A, Flow rate -800 mL/min, Bed height = 5 cm, Avg Particle Diameter = 690µ)

4.1.5 Influence of bed height

Various bed thicknesses ranging from 3 cm to 6.5 cm were selected to capture its influence in the performance of the electrolyser. Performance gets better as the thickness increases denoting the availability of more specific surface area for undergoing desired reaction. However, beyond 5 cm, a dip in the performance is noticed which is due to the complimentary reverse effect of ‘current penetration problem imposed by the poor distribution of potential along the bed height. Fig. 4.10 shows the behavior. Details regarding current penetration are mentioned in sl no: 1.2.

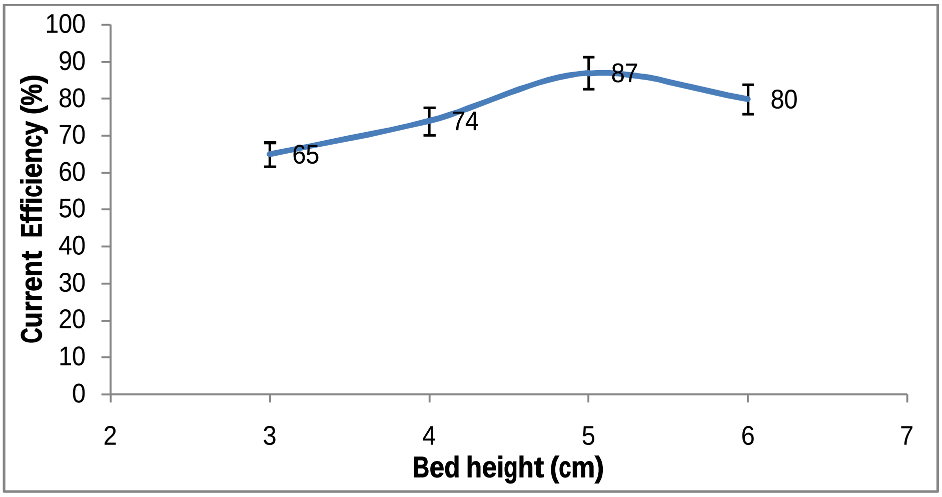

Fig.4.10 Effect of bed height on current efficiency

(Operating conditions: Initial conc. of $NaClO_3$ = 669 gpl, Current load= 80A, Flow rate -800 mL/min, Temperature- 60^0C, Avg Particle Diameter = 690µ)

4.1.6 Concentration- Time model

Inorder to assess the theoretical behavior of the above PBER at limiting conditions, imminence with already established concentration- time (C-t) model by Walter and Wagg (1977) was checked. For ideal plug flow assumption at limiting current conditions in a recirculation system, C-t relationship is reproduced as follows.

$$C_{\mathrm{i}}(\mathrm{t}) = C_{\mathrm{i}}{}^{0}.e^{\left(-\frac{t}{\tau}\right)[1-e^{\left(-\frac{KAaL}{Q}\right)}} \qquad (4.3)$$

where $C_i(t)$ - Concentration of reactant ions in the electrolyte (here Sodium Chlorate) C_i^0 –initial concentration of reactant ions. All other terms are conventional and have usual meanings. Parameters considered in the model were obtained as follows.

4.1.6.1 Theoretical Model development

Volume of Reservoir = 10.27 L

Vol. Flow rate = 0.8 L/ min

Space Time, T = Volume/ Vol. Flow rate= 10.27/0.8 = 12.5 min

Cross sectional area of reactor, A = π. $(7 \times 2.54)^2/4$ = 248.16 cm^2

Length of bed, L = 5 cm

Specific surface area, a = $6.\lambda/\rho_P.\ \Sigma\ \Delta Ø/D_P$

$\lambda = 1/\ 0.05 = 20$

a = 6x 20/4.72 x [(0.8753/710)+(0.0946/605)+(0.0228/427.5)+(0.0027/327.5)+ (0.0046/300)] x $(1/10^{-4})$] = 368.83 cm2/g

Mass Transfer Coefficient = I/ z.F A C

= 80 / (2 x 96500 x 248.16 x C)

= 6.44 x 10^{-5} / C

Thus, $$\boldsymbol{C_t = 669\ x\ e^{-\frac{t}{12.5}[1-e^{(-2.54/C_t)}]}} \tag{4.4}$$

Fig. 4.11 gives the comparison between the actual behavior and theoretical model. Slight deviation between the predicted and actual behavior can be attributed to the erroneous and non-uniform velocity distribution of electrolyte through the bed of non-spherical and irregular lead dioxide particles. Another reason can be the inadequacy of ideal plug flow assumption in the development of the above model.

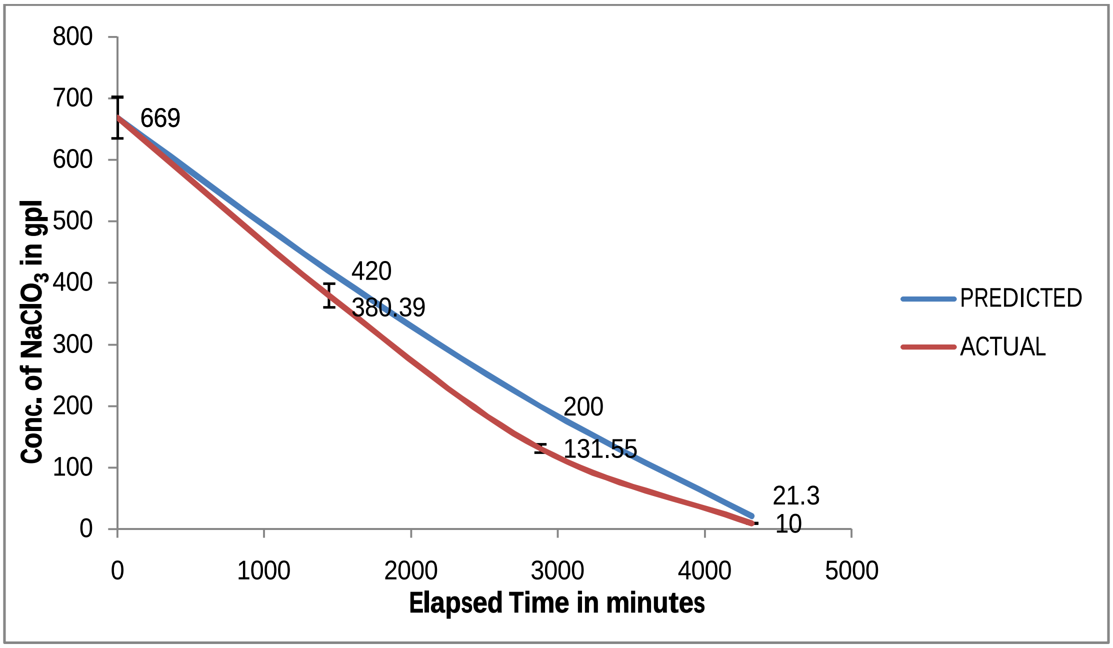

Fig. 4.11 Comparison between prediction and actual behavior at limited conditions

4.2 DEVELOPMENT OF A SYSTEM FOR CONTINUOUS ELECTROSYNTHESIS OF SODIUM PERCHLORATE USING SINGLE BED PBER'S

4.2.1 Configuration of cells

Industrial manufacture at higher scale of production always demands continuous mode of operation for keeping consistency in quality and to minimize space requirements. Four PBER's/compact electrochemical cells were arranged in series by properly designing hydraulic circuits so as to transfer adequate flow of electrolyte to the subsequent cells as well as for providing sufficient recirculation. Cooling of electrolytes was ensured by providing a jacketed product cooler capable of removing heat from the system by circulation of water through its jacket. A definite proportion of electrolyte from the cooler was taken as the final product and the remaining portion was recycled back to the system. Fig. 4.12 and 4.13 represents major components fabricated for above. Fig. 4.14 provides a sketch of arrangement.

As the feed electrolyte enters and flows upwards through the electrically charged bed, incremental conversion to sodium perchlorate (SPC) occurs at each stage and would overflow to the adjacent cell. In this way, output from the product cooler was analysed transiently for getting the concentration of $NaClO_3$ in product SPC. This procedure signifies the extent of conversion of sodium chlorate to sodium perchlorate inside these cells. Fig. 4.15 shows the configuration of cells.

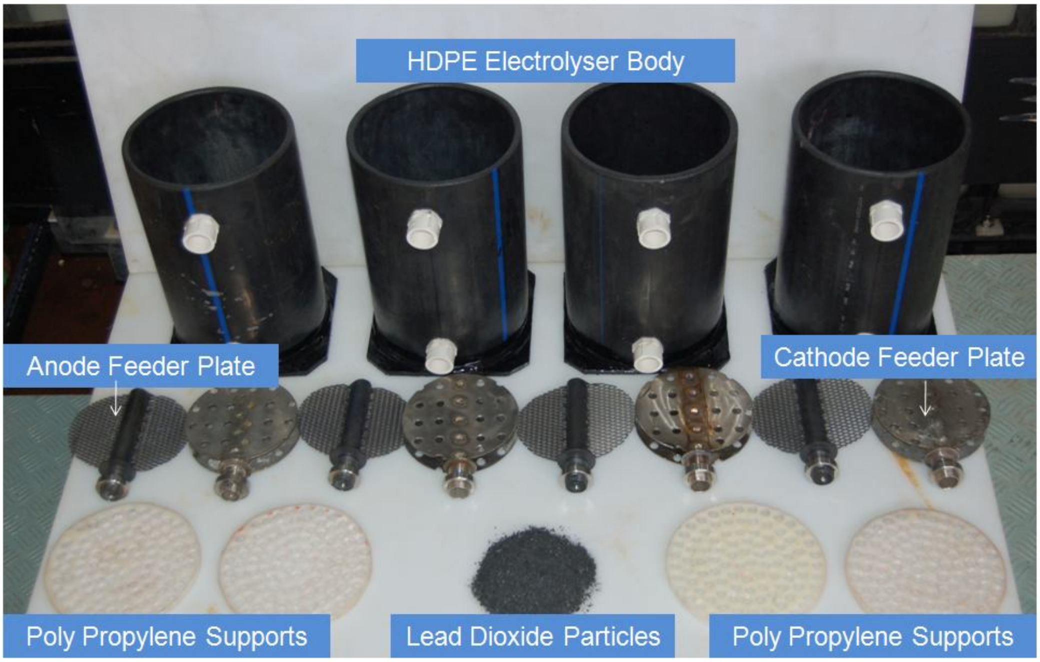
HDPE Electrolyser Body
Anode Feeder Plate
Cathode Feeder Plate
Poly Propylene Supports
Lead Dioxide Particles
Poly Propylene Supports

Fig.4.12 Major components fabricated for arrangement of single bed PBER’s

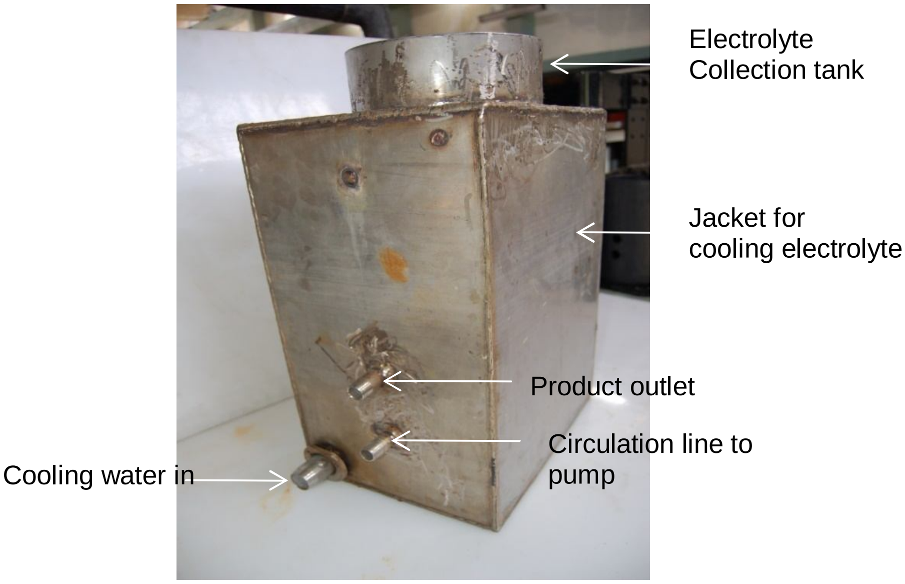
Electrolyte
Collection tank
Jacket for
cooling electrolyte
Product outlet
Circulation line to
pump
Cooling water in

Fig.4.13 Electrolyte Cooler

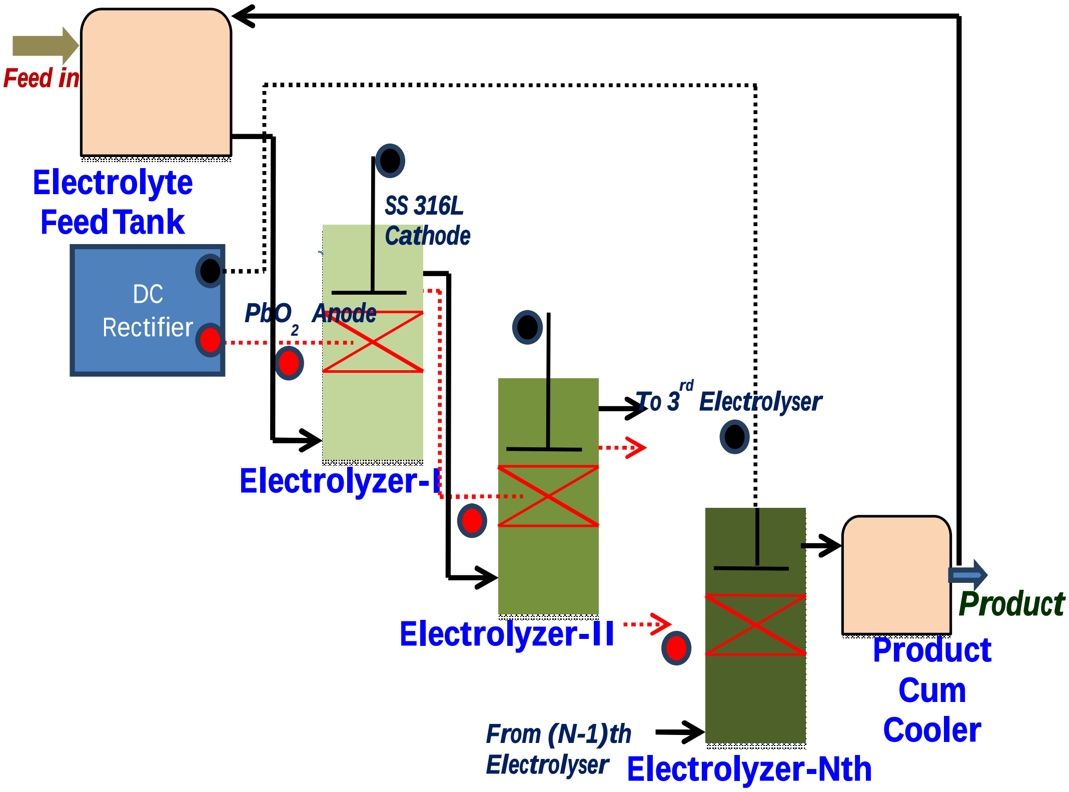
Feed in
Electrolyte
Feed Tank
DC
Rectifier
SS 316L
Cathode
PbO2 Anode
Electrolyzer-I
Electrolyzer-II
To 3rd Electrolyser
From (N-1)th
Electrolyser
Electrolyzer-Nth
Product
Product
Cum
Cooler

Fig.4.14 Schematic sketch for continuous electrosynthesis of SPC

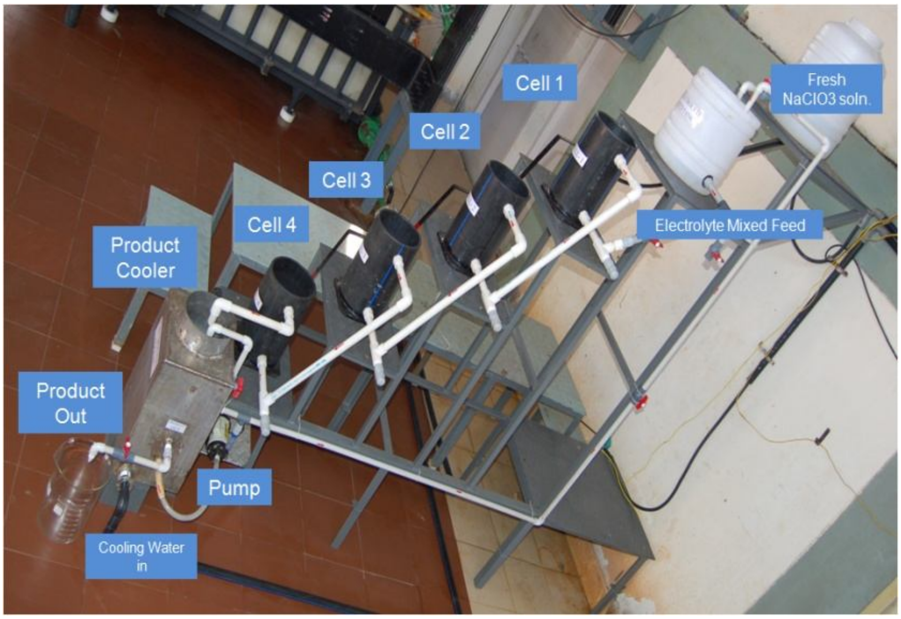
Cell 1
Cell 2
Cell 3
Cell 4
Fresh NaClO3 soln.
Electrolyte Mixed Feed
Product Cooler
Product Out
Pump
Cooling Water in

Fig.4.15 Arrangement of cells for continuous electro synthesis of SPC using single bed PBER's

Few teething troubles faced during the free running trials of electrolysis. One of the critical issues was the non-uniform temperature distribution inside various cells as can be seen in Fig.4.16. Higher temperature only worsens the situation as this leads to a reduction in net availability of hydroxyl ions at the surface of particles leading to a drop in current efficiency.

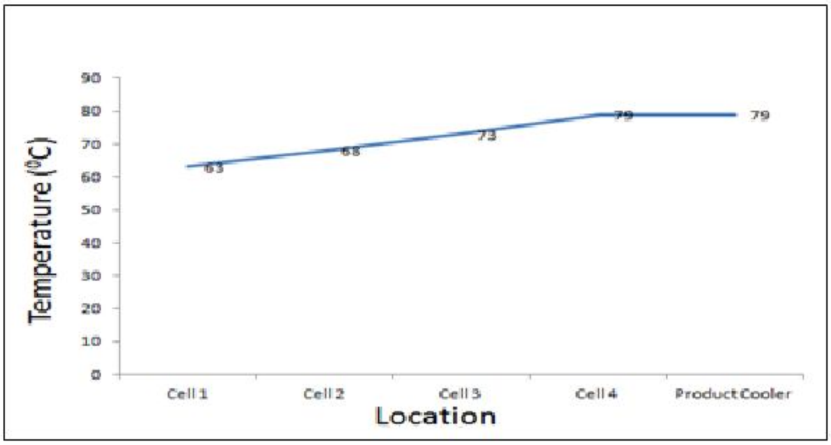

Fig.4.16 Temperature distribution at various locations of arrangement for continuous electrosynthesis of PBER

This issue was resolved by tapping a recirculation line to individual cells for systematic temperature control inside. Fig.4.17 shows a typical arrangement. Fig. 4.18 demonstrates the benefits.

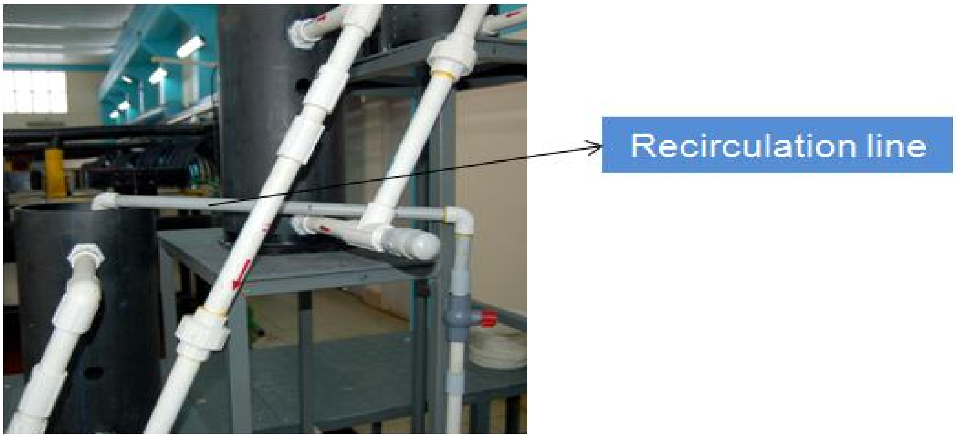

Fig. 4.17 Provision of tapped recirculation line to individual cells for continuous electrosynthesis

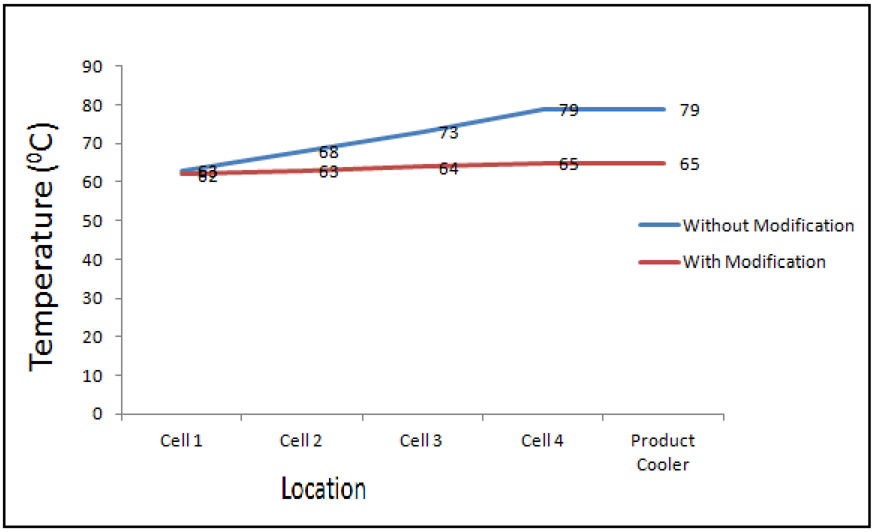

Fig.4.18 Improved temperature distributions across cells after providing recirculation tapping across each cells

4.2.2 Trial results

Initially, cells were charged in recirculation mode without feeding the fresh $NaClO_3$ solution. This period is termed as “stabilization period” where the initially filled sodium chlorate solution is converted completely to SPC solution having desired concentration. Beyond this, “continuous flow period” starts where the fresh feed is fed in at a define flow rate and the product is withdrawn at the same rate. As mentioned earlier, a definite proportion of output electrolyte is fed back to the system for maintaining adequate recirculation for cooling purpose. System was operated at initial concentration of Sodium Chlorate solution as 670 gpl, a recirculation flow rate of 800 mL/min, amperage of 80A and a product flow rate of 12mL/min during “continuous flow period”. Fig. 4.19 depicts the transient behavior in concentration of $NaClO_3$ in the collected product. From the above graph, its clear that there is a significant rise in concentration of $NaClO_3$ in the product solution after elapsing definite time period, in comparison with the predicted one. It can be seen that concentration of sodium chlorate in product SPC during continuous flow period kept on rising from desired value of 30 gpl. This emphasizes the incompletion of reaction even after traversing through all the cells arranged in series.

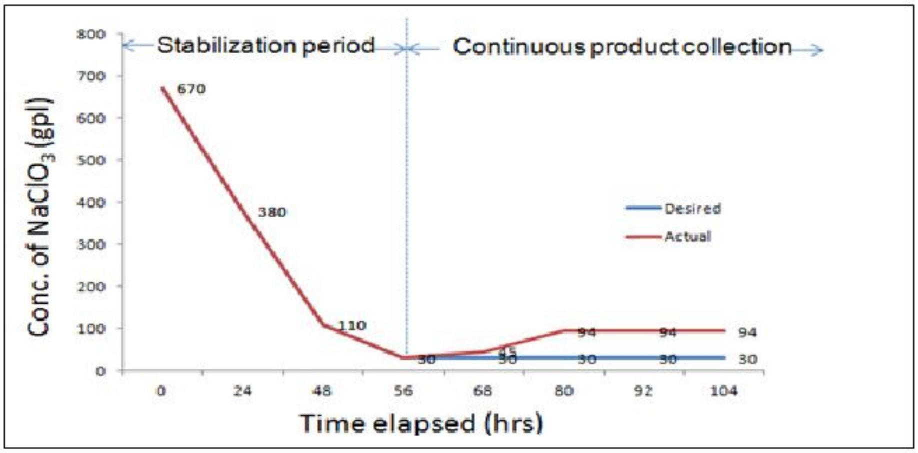

Fig.4.19 Transient behavior in $NaClO_3$ conc. in product SPC during course of electroysis

On preliminary analysis, it was felt that when the fresh electrolyte at a higher concentration (about 670 gpl) is getting mixed with the electrolyte feed tank where the recirculation flow (partially converted) arrives at a higher flow rate, sudden “churning” of solution results. This amplifies the flow disturbances and hence resulting in poor conversion. In order to resolve the issue, entry of fresh feed into the system was modified by inserting across the outlet of electrolyte feed tank as shown in Fig. 4.20

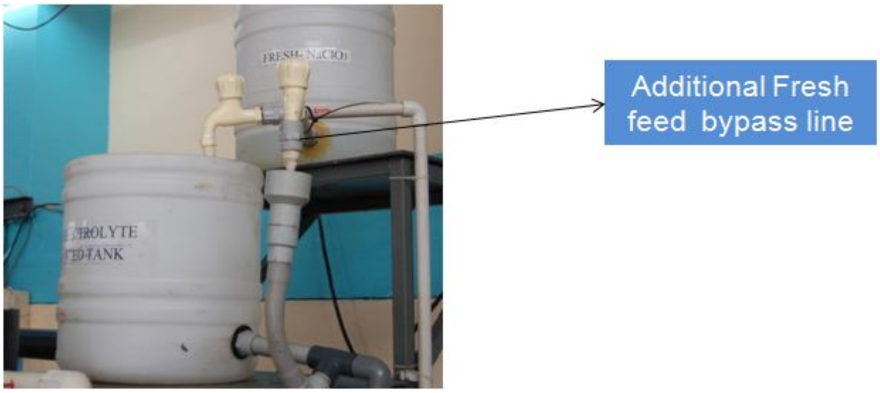

Fig.4.20 Modification in entry of fresh feed to electroysers arranged in series

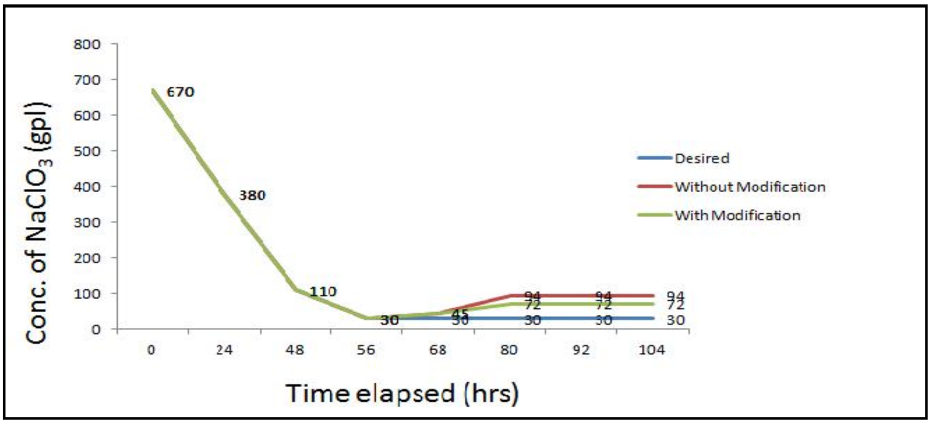

Fig. 4.21 Transient behavior in $NaClO_3$ conc. before and after modification (in entry feed)

From Fig. 4.21, it is clear that though there was an improvement in conversion, it is still far from the desired value.

4.3 DEVELOPMENT OF A DUAL BED PACKED/ COMPACT BED ELECTROCHEMICAL REACTOR

A dual bed electrochemical reactor was fabricated as mentioned in section 3.1. One of the serious issue with respect to single bed PBER in addition to “current penetration depth” is the sharp increase in voltage drop in the cell with increase in current load as shown in Fig. 4.22.

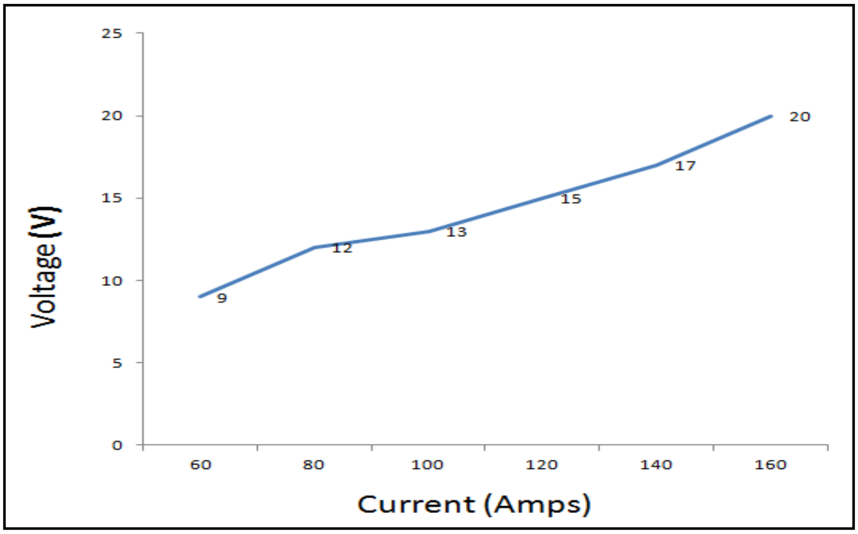

Fig.4.22 Voltage variation with current in single bed PBER

A typical graph was plotted for dual bed PBER for a better comparison. Fig.4.23 depicts the comparison.

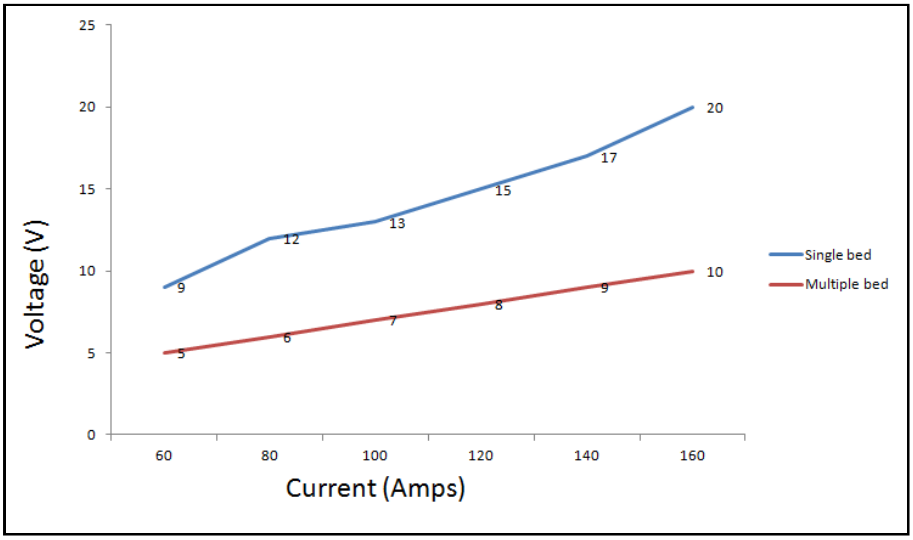

Fig.4.23 Voltage variation with current in single and dual bed PBER

It is seen that voltage drop across the cell could be brought down by converting to dual bed type. In multiple bed design, given volume of electrolyte passes through 2 similar electrode bed accommodated inside same electrolyser body. Higher electrode surface inside the same electrolyser body coupled with closer electrode gap provide a favourable environment for effective charge transfer. This could have brought down required potential for passing same amount of current.

4.4 DEVELOPMENT OF A SYSTEM FOR CONTINUOUS ELECTROSYNTHESIS OFSODIUM PERCHLORATE USING DUAL BED PBER'S

Four dual bed compact electrochemical cells were arranged in series as done for single bed type by properly designing hydraulic circuits so as to transfer adequate flow of electrolyte to the subsequent cells as well as for providing sufficient recirculation. Cooling of electrolytes was ensured by providing a jacketed product cooler capable of removing heat from the system by circulation of water through its jacket. Hydrogen liberated from the system was exhausted out through a HDPE line. A definite proportion of electrolyte from the cooler was taken as the final product and the remaining portion was recycled back to the system. Major components fabricated for such arrangement is shown in Fig.4.24 and arrangement of the system is shown in Fig. 4.25.

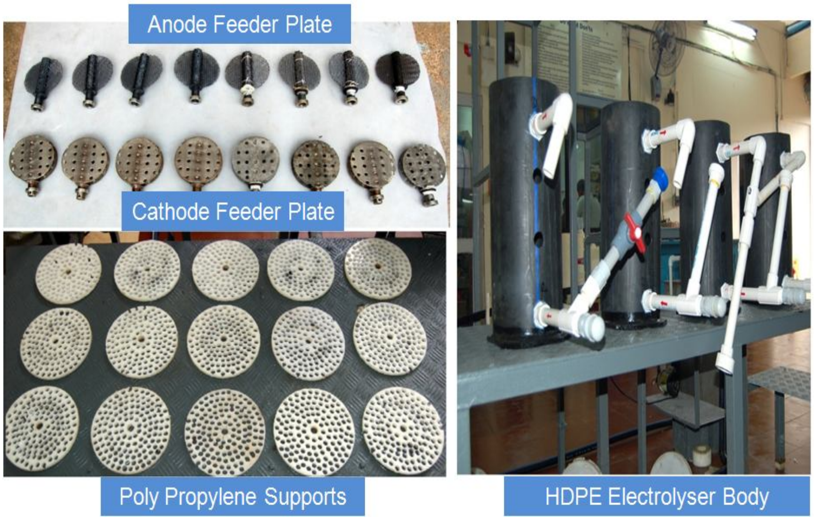
Anode Feeder Plate
Cathode Feeder Plate
Poly Propylene Supports
HDPE Electrolyser Body

Fig.4.24 Major components fabricated for arrangement of dual bed PBER’s for continuous electrolysis

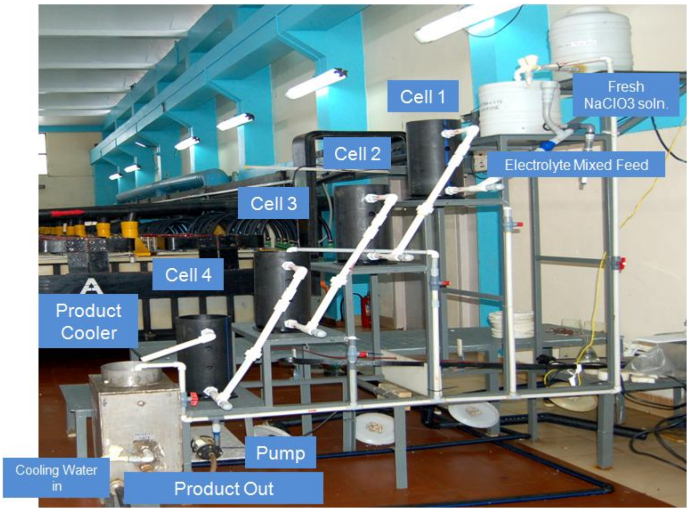
Cell 1
Fresh NaClO3 soln.
Cell 2
Electrolyte Mixed Feed
Cell 3
Cell 4
Product Cooler
Pump
Cooling Water in
Product Out

Fig.4.25 Arrangement of cells for continuous electro synthesis of SPC using dual bed PBER’s

System was operated at initial concentration of Sodium Chlorate solution as 670 gpl, a recirculation flow rate of 800 mL/min, amperage of 160A and a product flow rate of 19-24 mL/min during “continuous flow period”. Fig. 4.26 depicts the transient behavior in concentration of $NaClO_3$ in the collected product.

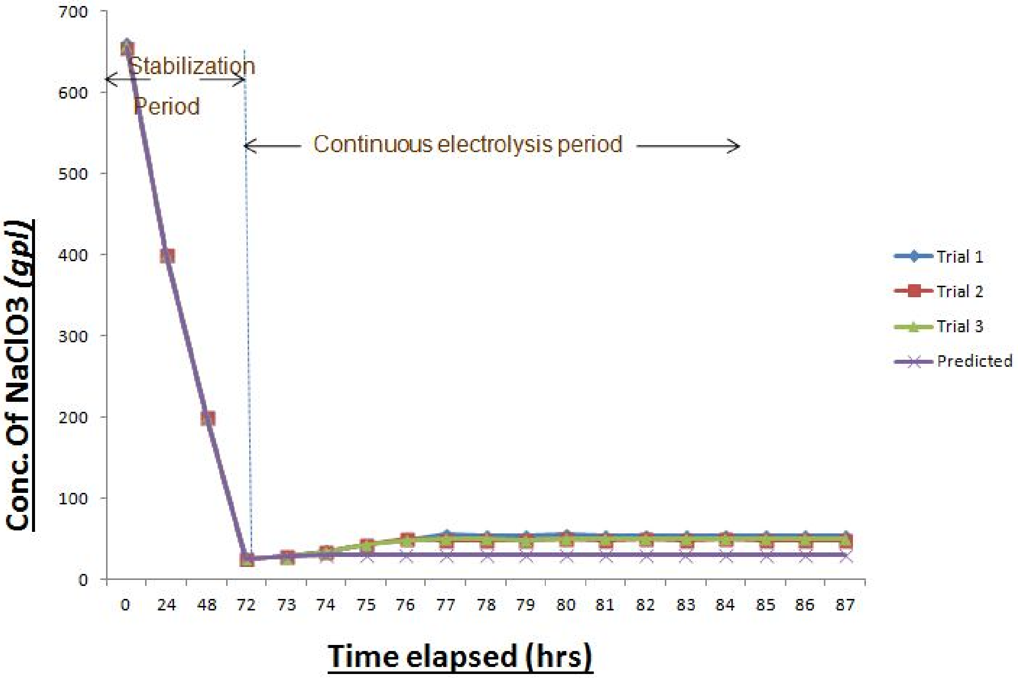

Fig.4.26 Transient behavior in $NaClO_3$ conc. in product SPC during continuous electrolysis

From the above graph, its clear that there is a significant rise in concentration of $NaClO_3$ in the product solution after elapsing definite time period, in comparison with the predicted one. This emphasizes the incompletion of reaction even after traversing through all the cells arranged in series. In otherwords, rate of conversion at which chlorate ions getting completely oxidized to perhclorate ions, was slower with respect to the rate at which chlorate ions were fed to the system. Recirculation of cooled electrolytes to individual cells causing the flow disturbances, also adds to the problems.

4.4.1 Modifications/ Improvements carried out

The above issues were resolved by introducing line condensers between each cells and modifying orientation of cells as depicted in Fig.4.27 and Fig.4.28. Introduction of line condensers for electrolyte cooling avoids the necessity of having independent electrolyte circulation streams to each cells. Rigorous back mixing inside cells, offered by recirculation loop, primarily disturbs the flow dynamics resulting in poor conversion. Line condensers between cells removes the ohmic heat of electrolyte as well as smoothens the electrolyte flow through bed thereby tantamounting to plug flow mode. From Fig.4.28, it is clear that 4th cell was disconnected from the cascade and introduced as a ‘polishing cell’. This cell needs to deal only the end stage electrolyte (preferably <100 gpl sodium chlorate in electrolyte) have only lean concentration of sodium chlorate overflowing from the product cooler. It is known from experience that significant drop in current efficiency is noticed when concentration of reactant radicals (here sodium chlorate) goes below 100 gpl. This could be the potential reason behind the poor performance of the previous configuration as depicted in Fig. 4.26. To a greater extend, this performance can be improved by providing enough residence time for the electrolyte specifically in its end stages. Introduction of polishing cell thus provides ample residence time for electrolyte overflown from the intermediate cooler which is approaching its final stage conversion. Improvement in performance of the system could be captured from Fig.4.29.

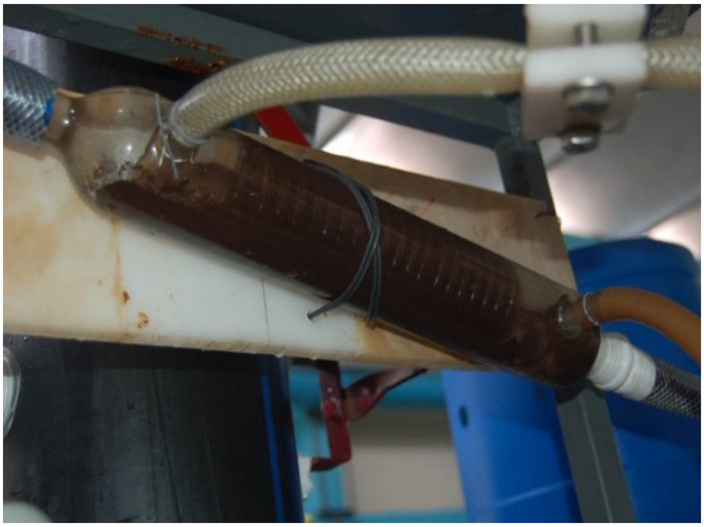

Fig.4.27 Line condensers inserted between cells

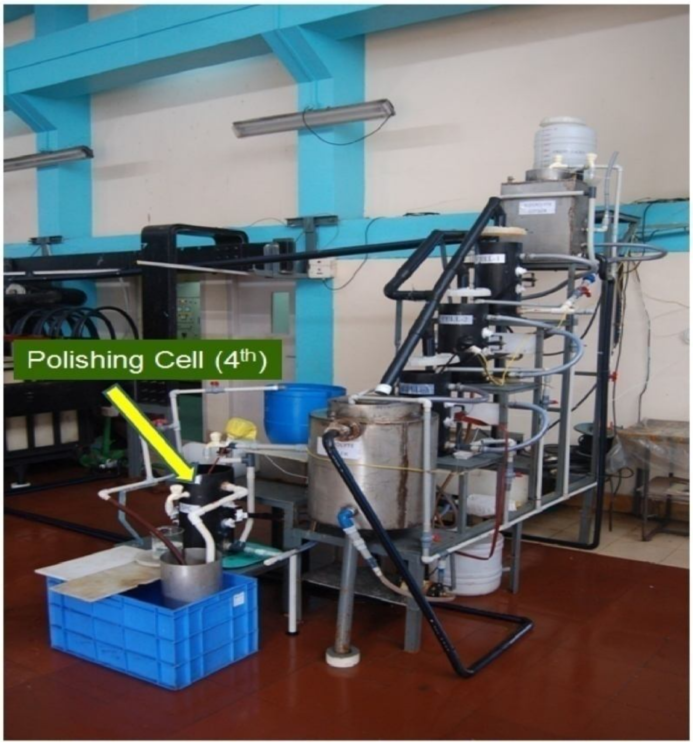

Fig.4.28 Modified orientation of 4th cell (“Polishing cell”)

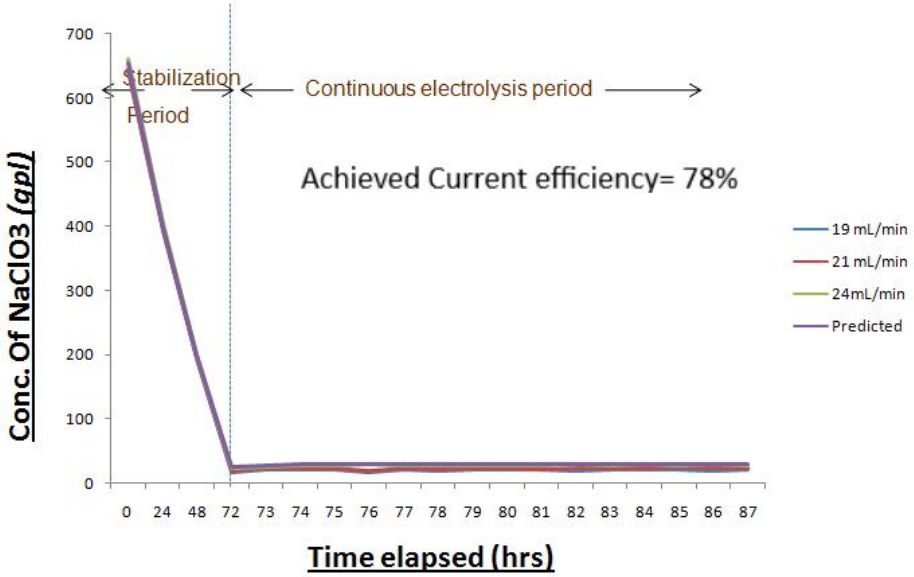

Fig.4.29 Transient behavior in $NaClO_3$ conc. in product SPC during continuous electrolysis

An average current efficiency of 78% could be achieved in continuous mode which is much higher than conventional system (55-60%).

4.5 MODELLING RESIDENCE TIME DISTRIBUTION (RTD) BEHAVIOUR IN A COMPACT/PACKED BED ELECTROCHEMICAL REACTOR (PBER)

4.5.1 Theory

A. Open Dispersion Model

This model predicts that electrolyte flow in the PBER is undisturbed at the inlet and outlet. Fundamental mathematical form is

$$\frac{\partial C}{\partial \theta} = \left(\frac{D}{uL}\right) . \frac{\partial^2 C}{\partial z^2} - \frac{\partial C}{\partial z} \tag{4.5}$$

Boundary conditions from are as follows.

For open system, at entrance, $F_T(0^-,t) = F_T(0^+,t)$.

$$\text{i.e} -D\left(\frac{\partial C_T}{\partial z}\right)_{z=0^-} + UC_T(0^-,t) = -D\left(\frac{\partial C_T}{\partial z}\right)_{z=0^+} + UC_T(0^+,t) \tag{4.6}$$

Or, $C_T(0^-,t) = C_T(0^+,t)$

At the exit,

$C_T(0^-,t) = C_T(0^+,t)$

$$-D\left(\frac{\partial C_T}{\partial z}\right)_{z=L^-} + UC_T(L^-,t) = -D\left(\frac{\partial C_T}{\partial z}\right)_{z=L^+} + UC_T(L^+,t) \tag{4.7}$$

Analytical solution of 4.7 is as follows.

$$E(\theta) = C/C_d = \frac{1}{\sqrt{4\pi(\frac{D}{uL})}} . e^{(-(1-\theta^2)u.L/4\theta.D)} \tag{4.8}$$

B. Model predicting small extent of dispersion (Small dispersion)

For small extent of dispersion, the spreading tracer curve does not change its shape as it passes the measuring point. This yields a symmetric curve and analytical solution is as follows.

$$E(\theta) = C/C_d = \frac{1}{\sqrt{4\pi(\frac{D}{uL})}} . e^{(-(1-\theta^2)u.L/4D)} \tag{4.9}$$

C. Tanks in Series Model

This model predicts that electrolyte flow in PBER is discretised into equal sized hypothetical CSTR's. The number of tanks in series n_T describes the dispersion with $n_T = 1$ representing infinite dispersion and being equivalent to Pe= 0. Analytical solution which is also the definition of Erlang distribution is as follows.

$$E(\theta) = C/C_d = n_T^{n_T}/(n_T-1)!\theta^{(n_T-1)}e^{-n_T\theta} \qquad (4.10)$$

Peclet No: (Pe) assumes greater significance in this context. It is defined as the ratio of transport by convection to the transport by diffusion or dispersion. Pe=0 indicates that dispersion coefficient is maximum and system behaves as a backmix reactor whereas on the other hand Pe tending to infinity indicates that system behaves like a plugflow reactor. Thus, determining dispersion coefficient in a particular flow behavior permits to determine the reaction behavior inside a system.

4.5.2. Residence Time Distribution (RTD) curves at various flow rates

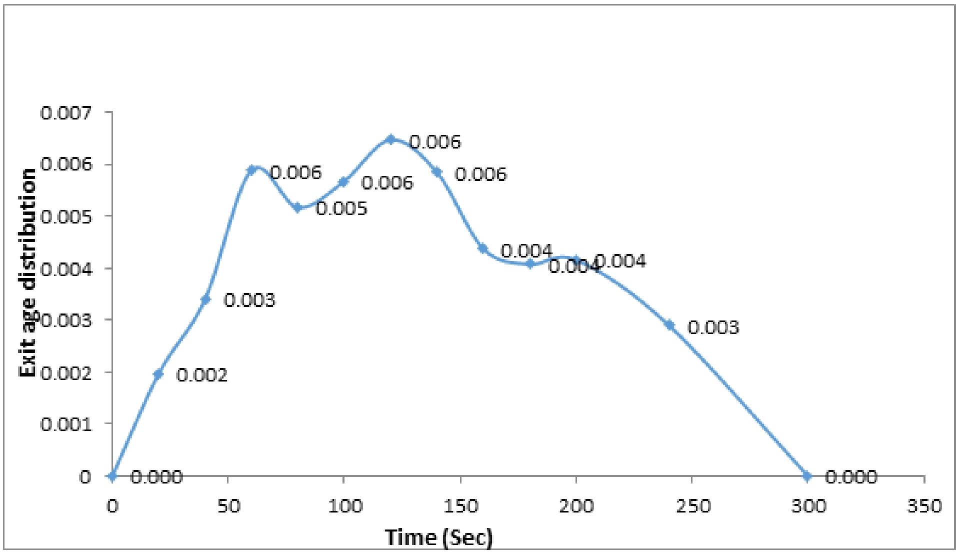

Fig.4.30 (a) – RTD behaviour at 3.33 x10^{-5} m^3/sec

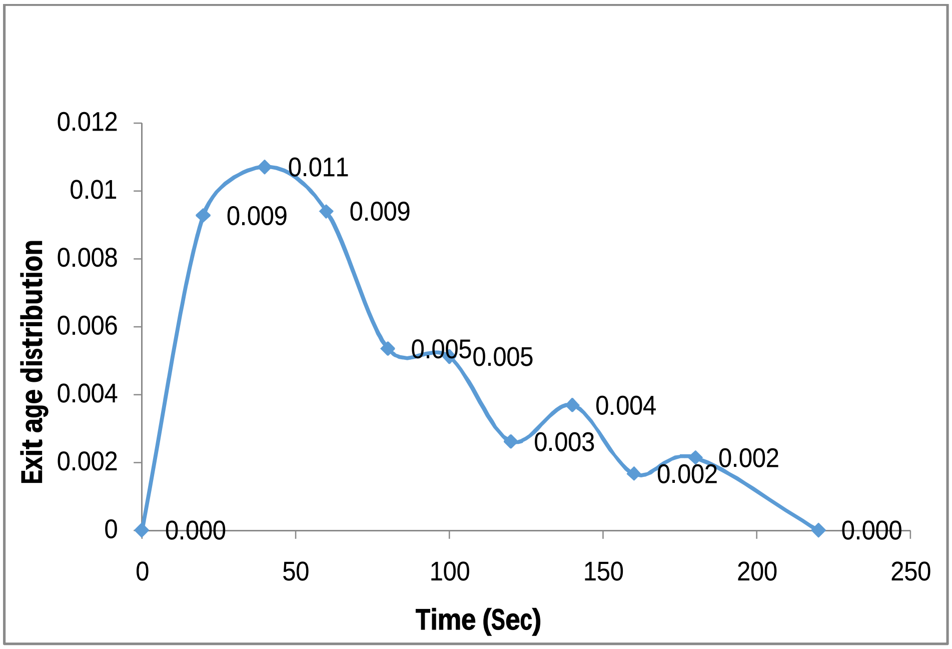

Fig.4.30 (b) – RTD behaviour at 6.67 x 10^{-5} m^3/sec

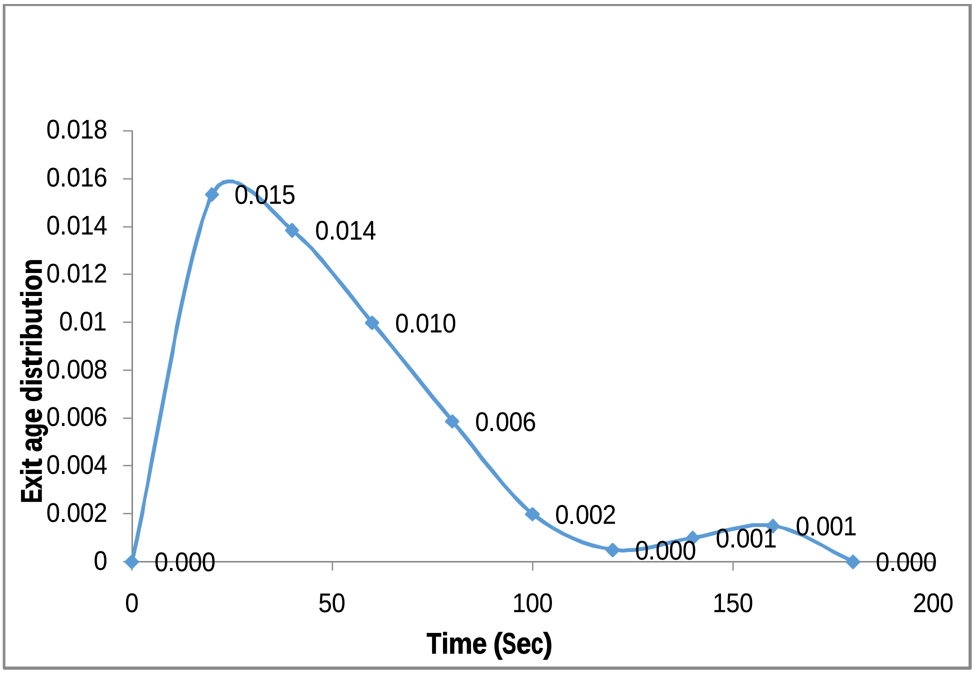

Fig. 4.30 (c) – RTD behaviour At 1 x$10^{-4}$$m^3$/sec

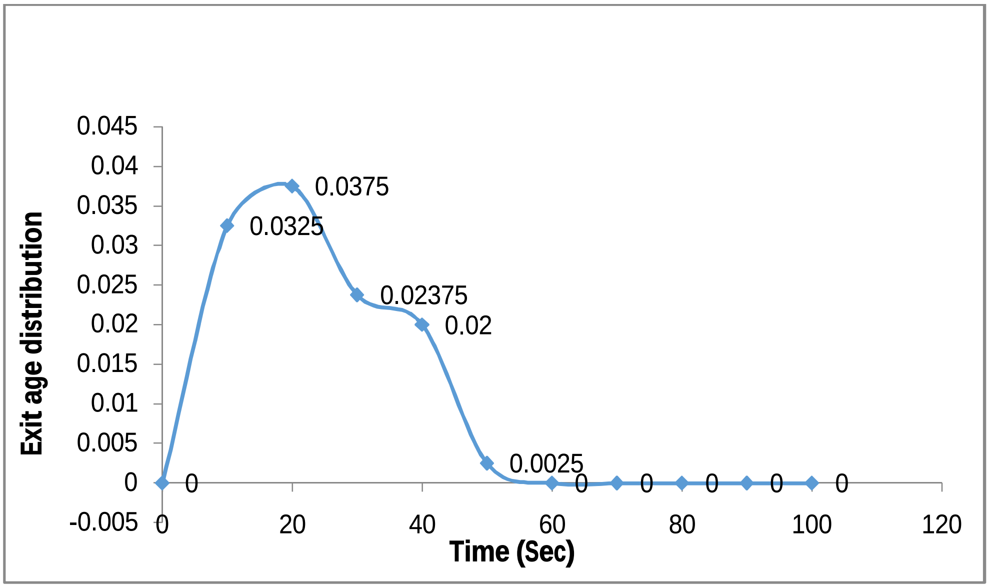

Fig.4.30 (d) – RTD behavior At 1.33 x 10^{-4} m^3/sec

Fig.4.30- RTD behaviour under various electrolyte flow rates under non electroysing mode

Table 4.1 Moments at various flow rates

Sl No	**Flow rate** **(m^3/sec)**	**1st moment (sec)** $t_{mean}= \int_0^\infty t.\ E(t)\ dt$	**2nd moment about mean (sec^2)** $\sigma^2 = \int_0^\infty (t-t_{mean})^2\ E(t)\ dt$
1	3.33 x 10^{-5}	141.48	3257
2	6.67 x 10^{-5}	65.05	2339.5
3	1 x10^{-4}	41.32	1109
4	1.33 x 10^{-4}	22.35	153.33

RTD behaviors of PBER under various electrolyte flows are depicted in Fig.4.30 (a to d). Table 4.1 shows the calculated 1st and 2nd moment about mean. Reasonably good flow was observed through the reactor at 3.33 x 10^{-5} m^3/sec, as the mean time interval falls at the right place. As the flow rate is increased, the curve shifts towards the left indicating the presence of early time mean. This observation along with long tail indicates the presence of stagnant backwaters. This can be ascertained by comparing the space time under each flow rates with the observed mean from graph. Following table 4.2 indicates that % difference predominantly increases at higher flows substantiating the presence of stagnant regions.

Table 4.2 Difference between space time and observed mean

Sl No:	**Flow rate (m^3/sec)**	**Space time (τ) (sec)**	**t_{mean} (observed from figure 4.30) (sec)**	**Difference (τ-t_{mean}) in %**
1	3.33 x 10^{-5}	150	141.48	6
2	6.67 x 10^{-5}	75	65.05	10.64
3	1 x10^{-4}	50	41.32	21
4	1.33 x 10^{-4}	37.5	22.35	67.78

4.5.3 Modeling RTD behaviour

Let Q_R be the flow of electrolyte through the bed and V_R be the volume of PBER. Then tank residence time, $T_R = V_R/Q_R$. All time domains were converted to dimensionless θ mode, where $\theta = t/T_R$. From the respective exit age distribution curves, σ^2 and t_{mean} is estimated.

Then, $\sigma^2_\theta = \sigma^2/ t_{mean}^2$ (4.11)

Peclet no: is found out using the following equation;

$\sigma^2_\theta = 2 \times D/(u.L) - 2 \times (D/(u.L))^2 \times (1-e^{(-uL/D)})$ (4.12)

Above parameters were inserted in respective modeling equations mentioned in equation 4.8 and 4.9 to get the predicted E_θ values using open dispersion model and model predicting small extent of dispersion respectively. For tank in series model, following equations were used.

$Pe = 2(n_T -1)$ (4.13)

$E_\theta = (n_T^{nT})/(n_T-1)! \,.\, \theta^{(n_T-1)}.\, e^{-nT.\theta}$ (4.14)

where n_T represents number of tanks in series.

Using these parameters and respective model equations, E_θ was analytically determined under various flow rates. Following is the graphical representation of these models.

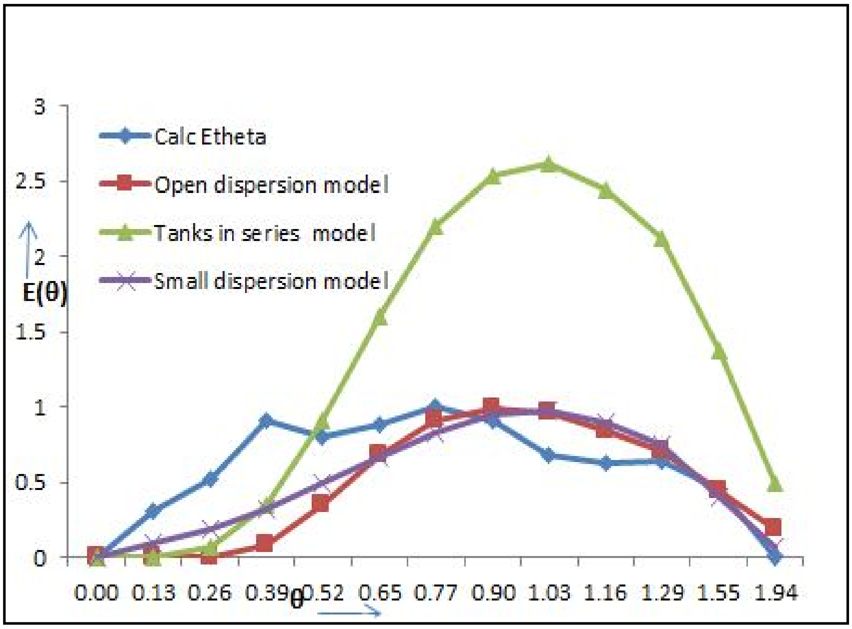

Fig.4.31 (a) – RTD behaviour at 3.33 x10^{-5} m^3/sec

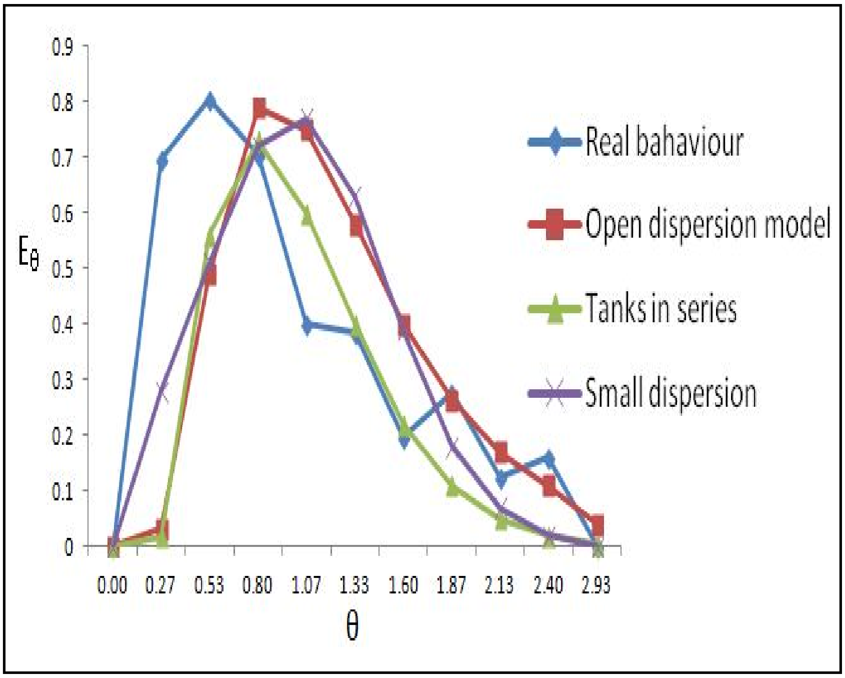

Fig. 4.31 (b) – RTD behaviour at 6.67 x 10^{-5} m^3/sec

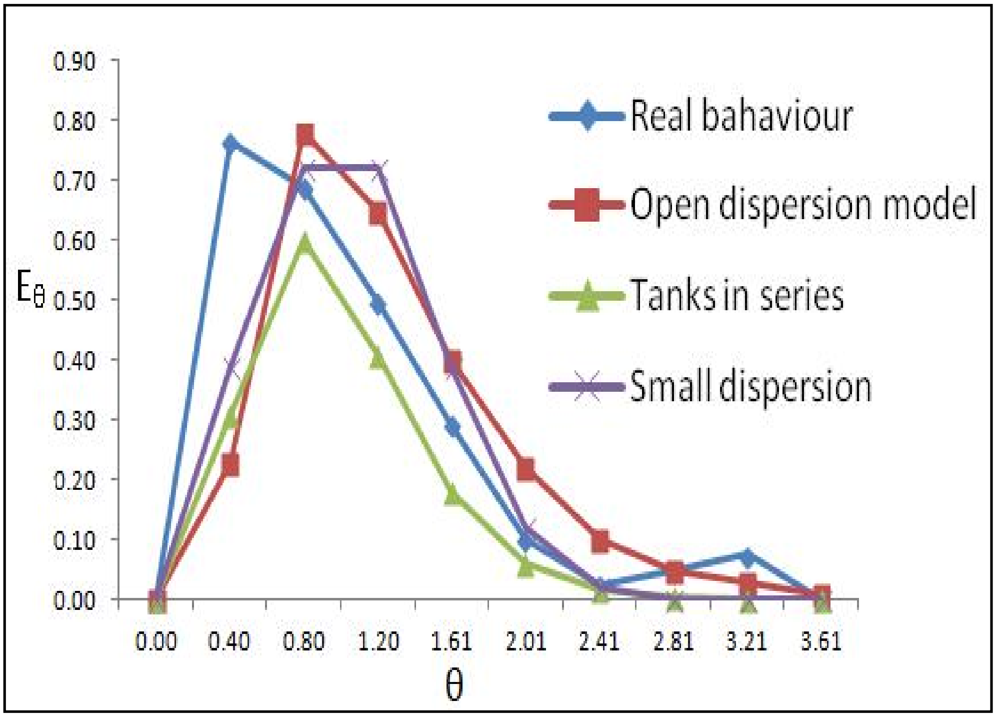

Fig.4.31 (c) – RTD behaviour at 1 x$10^{-4}$$m^3$/sec

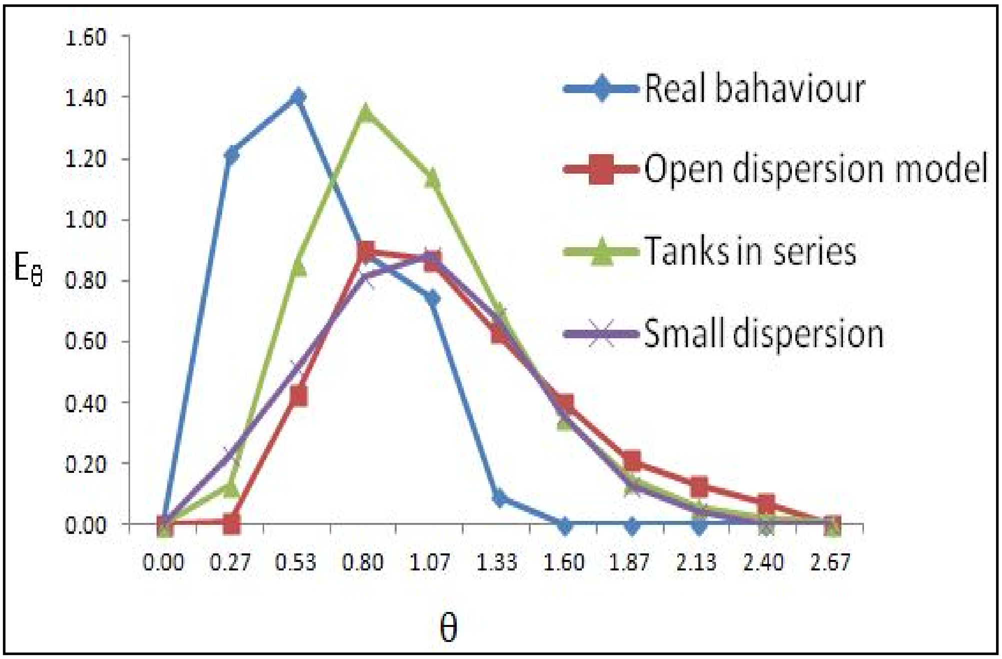

Fig. 4.31 (d) – RTD behaviour at 1.33 x 10^{-4} m^3/sec

Fig.4.31- Modelling RTD behavior under various electrolyte flow rates under non electrolyzing mode

From Fig.4.31 (a to d), it's quite explicit that RTD behavior of PBER can be well approximated by open dispersion model and model predicting small extent of dispersion. Though tank in Series model could predict at higher flow rates, significant disparities could be seen at lower flows. In order to estimate the extent of dispersion, vessel Dispersion number (D/uL) was determined from equation 4.12 and the same was plotted under various flow rates in Fig.4.32. Table 4.3 shows the calculated values of D/u.L. It is observed that D/u.L values increases till the flow reaches 6 LPM and beyond which it decreases. It shows that axial dispersion coefficients become less prominent as the flow rate increases owing to predominant backmixing. This is the definitive reason for decrease in D/u.L values under high flow rates.

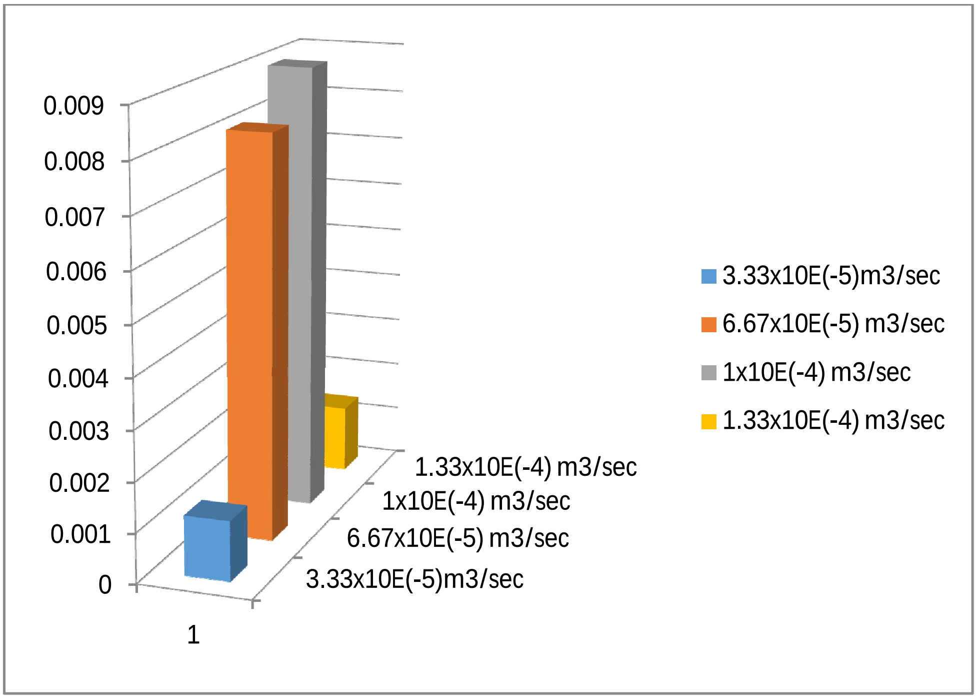

Fig.4.32 Plot of D/u.L for various flow rates under non electrolyzing mode

Table 4.3 Calculated values of D/u.L

Sl No:	Flow rate (m^3/sec)	σ^2_θ (from graph)	D/uL
1	3.33×10^{-5}	0.0024	0.0012
2	6.67×10^{-5}	0.016	0.0081
3	1×10^{-4}	0.0178	0.009
4	1.33×10^{-4}	0.0027	0.00136

4.5.4 RTD curves under electrolyzing conditions

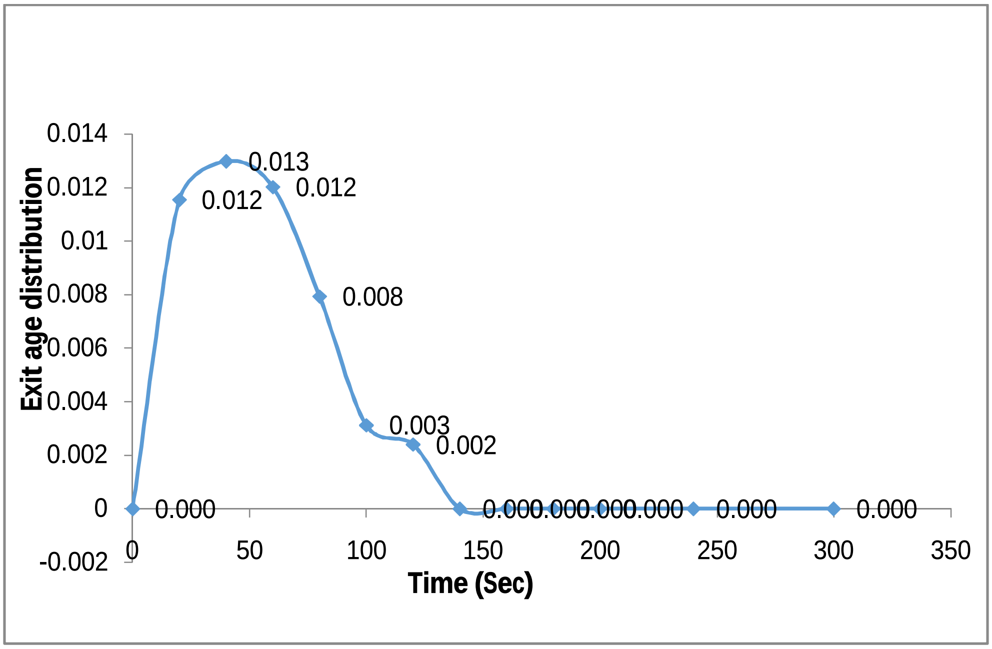

Fig.4.33(a) – RTD behaviour at 3.33 $x10^{-5}$ m^3/sec

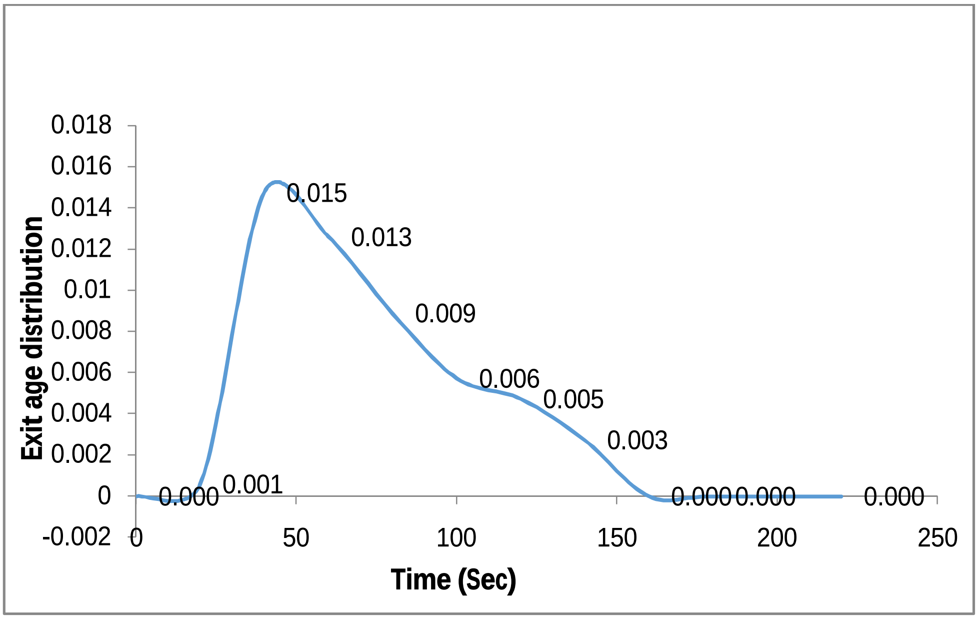

Fig.4.33(b) – RTD behaviour at 6.67 x 10^{-5} m^3/sec

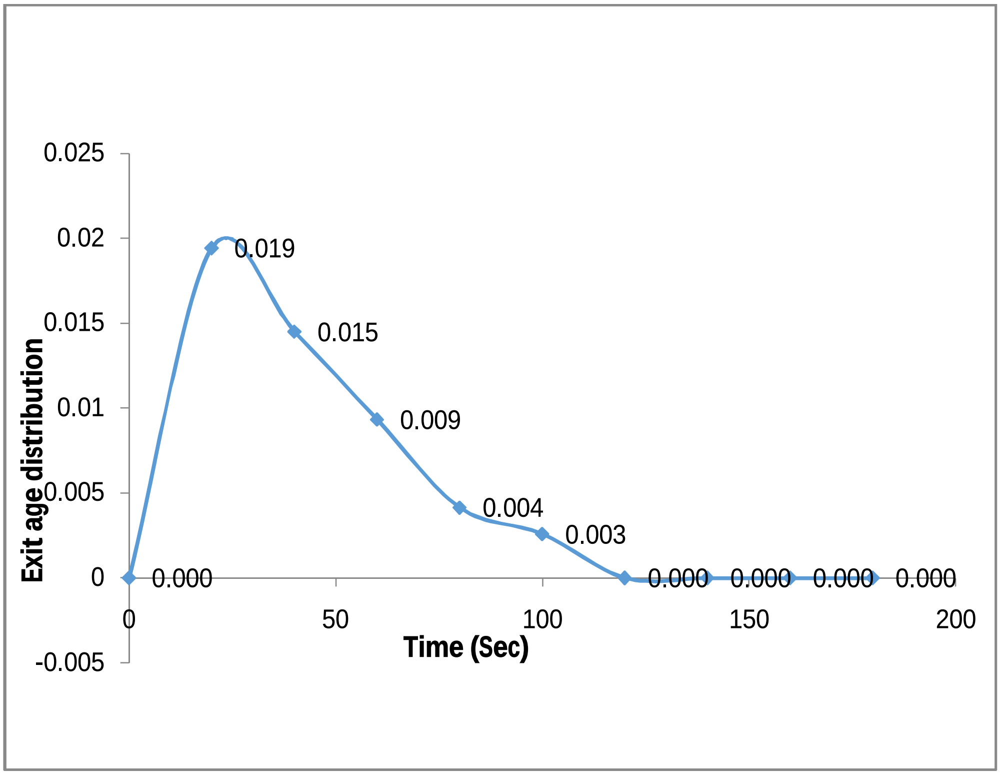

Fig.4.33(c) – RTD behaviour at 1 x$10^{-4}$$m^3$/sec

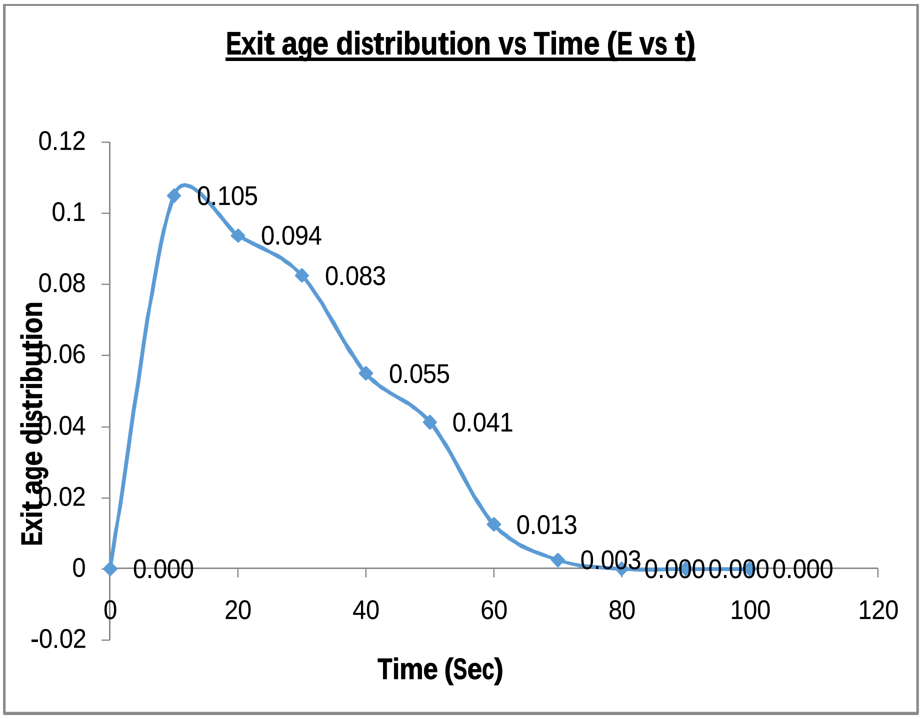

Fig.4.33(d) – RTD behaviour at 1.33 x 10^{-4} m^3/sec

Fig.4.33- RTD behavior under electrolyzing mode

Table 4.4 Moments at various flow rates under electrolyzing mode

Sl No:	**Flow rate** (m^3/sec)	**1^{st} moment (sec)** $t_{mean} = \int_0^\infty t.\ E(t)\ dt$	**2^{nd} moment about mean (sec^2)** $\sigma^2 = \int_0^\infty (t-t_{mean})^2\ E(t)\ dt$
1	3.33 x 10^{-5}	64.13	775.71
2	6.67 x 10^{-5}	59.2	741
3	1 x10^{-4}	42.38	544
4	1.33 x 10^{-4}	27	217

Fig.4.33 shows RTD behavior under electrolyzing conditions at various flow rates. Table 4.4 shows the calculated 1st and 2nd moment about mean. In general, an axial dispersion effect gets diminished under electrolysing mode at intermediate flow rates. This is primarily because non ideal axial flow currents gets disturbed by the back flow currents generated by gases which are inevitably produced at the electrode surface under electrolysing conditions. Recirculation, channeling and short circuit flows observed under certain flow conditions got totally eliminated under electrolyzing mode which may obviously be due to adequate backmixing of electrolyte between the particles, contributed by the gases generated around these electrode particles.

4.5.5 Modified Dispersed Plug Flow Model (MDPFM) under electrolyzing conditions

(Please refer Appendix A1 for detailed analytical treatment)

This model assumes that a fraction of recirculation flow (α) generated due to gaseous evolution around the electrodes, flows back to the conventional platform of dispersed plug flow. It is pictorially denoted in Fig.4.34.

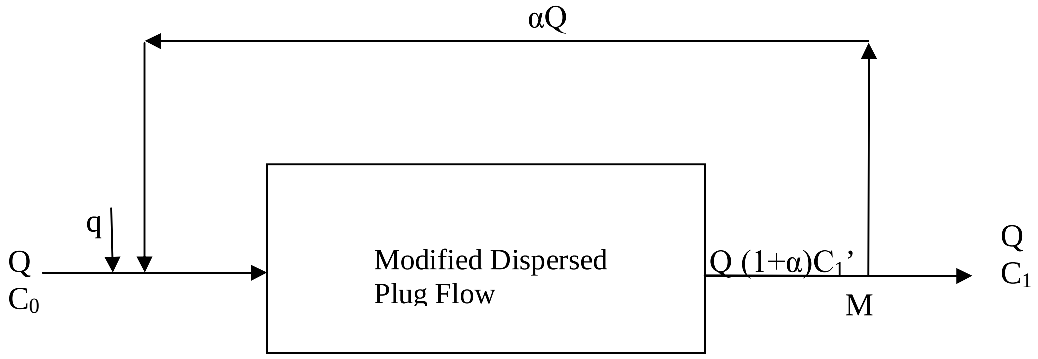

Fig.4.34- MDPFM conceptual block diagram

Exit age distribution (E_θ) as per dispersed plug flow model,

$$E(\theta) = \frac{1}{\sqrt{4\pi(Pe^{-1})}} \cdot e^{(-(1-\theta)^2 \mathrm{Pe}/4)} \qquad \backslash \qquad (4.15)$$

Thus, as per above model,

$$\frac{C_1'(\mathrm{t})}{C_0} = \frac{1}{\sqrt{4\pi(Pe^{-1})}} \cdot e^{(-(1-\frac{t}{T_R})^2 \mathrm{Pe}/4)} \qquad (4.16)$$

$$\mathrm{C_1'(t)} = \frac{C_0}{\sqrt{4\pi(Pe^{-1})}} \cdot e^{(-(1-\frac{t}{T_R})^2 \mathrm{Pe}/4)} \qquad (4.17)$$

Taking material balances

$Q + \alpha Q = Q\,(1+\alpha)$

At Junction point M,

$Q(1+\alpha)C_1' = Q.C_1 + \alpha q.\delta(t=0)$ (4.18)

Taking Laplace transform across (4.18),

$Q.C_1(s) + \alpha q = Q(1+\alpha)\,C_1'(s)$ (4.19)

We Know, $C_1'(s) = \int_0^\infty e^{-st}\, C_1(t)\, dt$

Using standard results from integration,

$$C_1(s) = (1+\alpha).\frac{C_0}{\sqrt{4\pi Pe^{-1}}}.\mathrm{T_R}\,.\,\sqrt{\pi}\mathrm{Pe}^{-1}.\ \mathrm{erfc}\,(\sqrt{\pi}\mathrm{Pe}^{-1}\,.\,\mathrm{T_R}\,(s+0.5\frac{Pe}{\mathrm{T_R}}).\, e^{[(\frac{1}{pe}).T_R{}^2\,(s^2 + s.\mathrm{Pe}/\mathrm{T_R})]} - \alpha q/Q$$

(4.20)

To find $C_1(t)$ by taking inverse Laplace Transform of $C_1(s)$

Comparing from the standard form of results for inverse Laplace transform for product form of exponential and error function,

$L^{-1}\,[\,e^{k2.s2}\ \mathrm{x\ erfc}\,(ks)]\,,\ k>0 = 1/(k\sqrt{\pi}).\ e^{(-t2/4k2)}$

$$C_1(t) = (1+\alpha).\frac{C_0}{\sqrt{4\pi Pe^{-1}}}.\mathrm{T_R}.\ \sqrt{(\pi \mathrm{Pe}^{-1})}.\ \frac{1}{k\sqrt{\pi}}.e^{-Pe}\,.\,e^{(-t^2/4k^2)}e^{(-Pe/2T_R)t} - \alpha q/Q \qquad (4.21)$$

Further simplifying and putting residence time distribution function as E(θ) = $C_1(t)/C_0$ (from equation A9)

$$E(\theta) = (1+\alpha).\frac{e^{-Pe}}{\sqrt{4\pi Pe^{-1}}}.e^{-0.5\,Pe\,(\theta+\theta^2)} - \alpha q / QC_0 \qquad (4.22)$$

4.5.6 Validation of MDPFM

By putting α=0.5, equation 4.22 was used to predict the values of E(θ) under various flow rates. Fig.4.35 represents the comparison with the actual behavior.

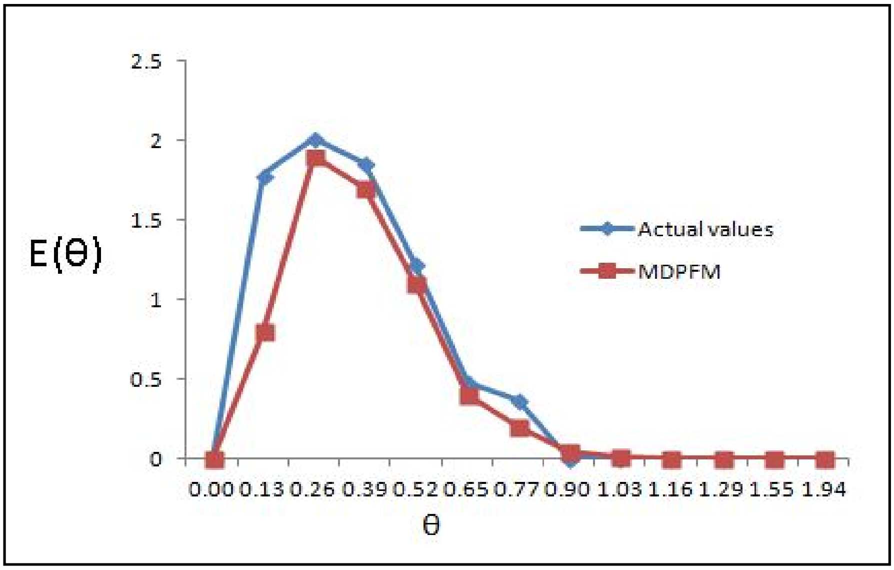

Fig.4.35 (a) – E(θ) at 3.33 x10^{-5} m^3/sec

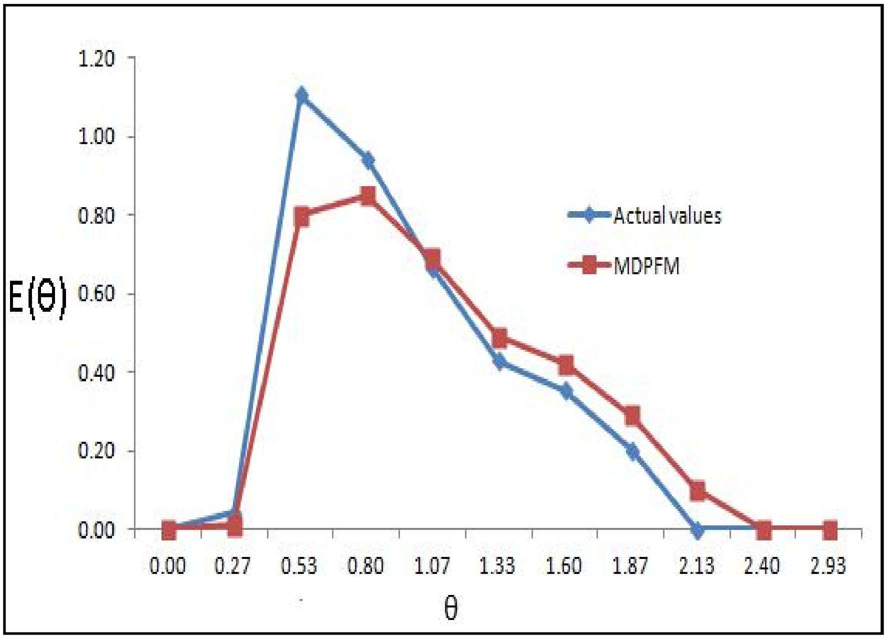

Fig.4.35 (b) – E(θ) at 6.67 x 10^{-5} m^3/sec

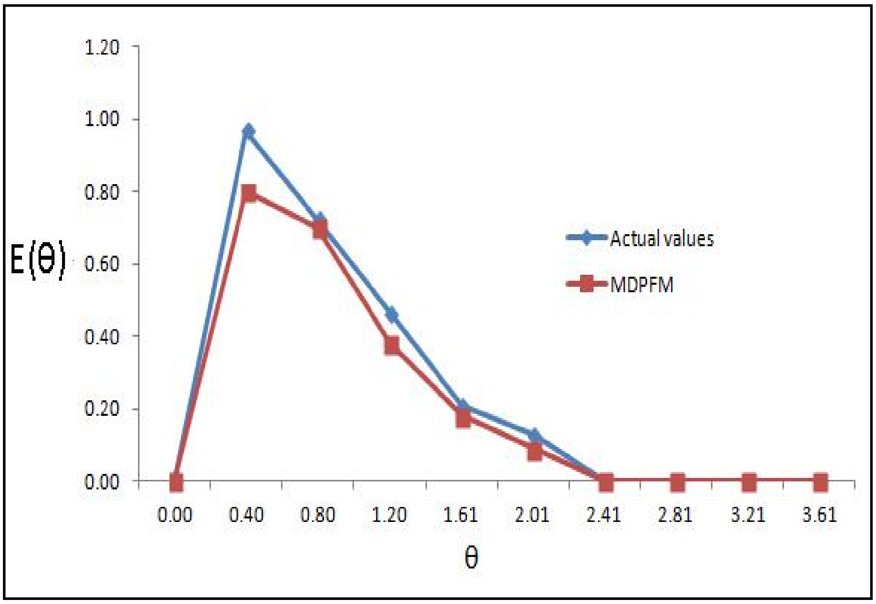

Fig.4.35(c) – E(θ) at 1 x$10^{-4}$$m^3$/sec

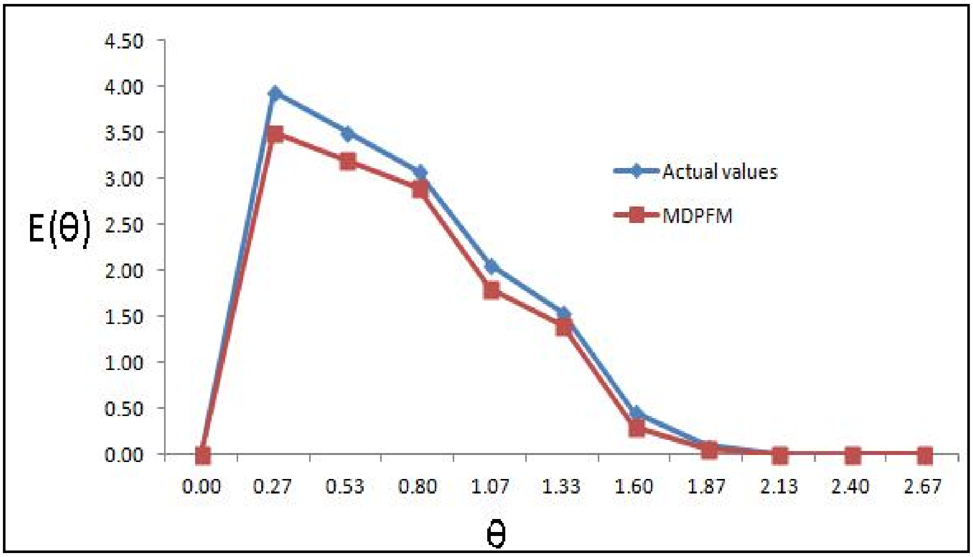

Fig.4.35 (d) – E(θ) at 1.33 x 10^{-4} m^3/sec

Fig.4.35- Prediction of E(θ) using MDPFM

Equation4.22 represents the complimentary influences of two important terms $e^{-0.5Pe\ (\theta\ +\ \theta 2/2)}$ and $\alpha q/QC_0$. I term being the dispersion effects due to non-idealities in flow dynamics and II term shows the back flow effects owing to the liquid recirculation aided by gas evolution under electrolyzing mode. Understandably, from above graphs, it is zoomed out that non idealities in flow currents gets diminished by the back flow currents generated by gases which are inevitably produced at the electrode surface under electrolysing conditions. From Fig.4.35 (a to d), it is clear that MDPFM predicts RTD behavior of PBER under electrolyzing conditions.

4.6 EFFECT OF MODIFIED LEAD DIOXIDE ANODES IN CONVENTIONAL PERCHLORATE CELLS

4.6.1 SEM Characterization.

Fig.4.36 (a) shows that Normal (or unchanged) anodes have asymmetrical surface growths due to dearth in control of crystal size of PbO_2 during coating operation. In contrast, existence of foreign agents like surfactants in the conventional electrolyte impede the bumpy development of PbO_2crystals, ensuing a uniform surface texture (Fig.4.36 (b to d)). Finer crystal habitat warrants restrained packing generating micropores thereby improving specific surface area of PbO_2. Amongst the improved samples, crystalline features in samples representing Fig.4.36 (b) and (d) are effectively enriched with tips and more distinct edges whereas similar features are not observed in Fig. 4.36 (c). This can be due to the loss of crystallinity of PbO_2 when Teepol is present in the coating solution thereby making it less chosen for this application.

It is presumed that these foreign agents may adsorb on the PbO_2surface forming a layer. This facilitates the surface diffusion of adsorbed atoms subduing the formation of excess new nuclei. These occurrences give not only a more uniform distribution of the current at the electrode/electrolyte interface, but also permits phenomenon to happen in a sluggish manner facilitating the adsorbed species to find the most appropriate locations in the deposit configuration. Consequently, deposits with thickly packed structure, smooth surface and lesser macropores could be attained. Further, this facilitates high mechanical strength and stronger adhesion of deposits to the substrate (Fig.4.36 (b to d)). Merging both additives (fluoride and cerium) and surfactants in identical ratio had revealed their influence on Lead dioxide structure (Figure 4.37 (a) to (c)). Despite the fact that, entire 3 combinations ensued a compactly packed and smooth surface, combination of sodium fluoride and cetyl tri methyl ammonium bromide (CTAB) in identical proportions had given an ideal coating with lesser macropores.

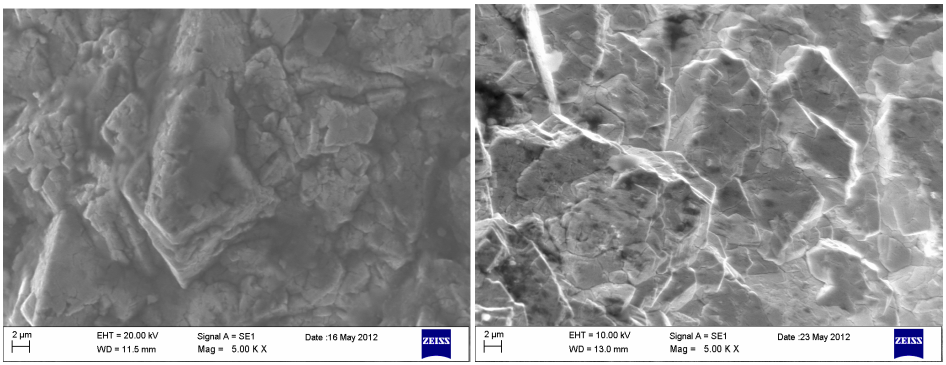
2 µm
EHT = 20.00 kV
WD = 11.5 mm
Signal A = SE1
Mag = 5.00 K X
Date :16 May 2012
ZEISS
2 µm
EHT = 10.00 kV
WD = 13.0 mm
Signal A = SE1
Mag = 5.00 K X
Date :23 May 2012
ZEISS

a) LA/Normal b) LA/CTAB

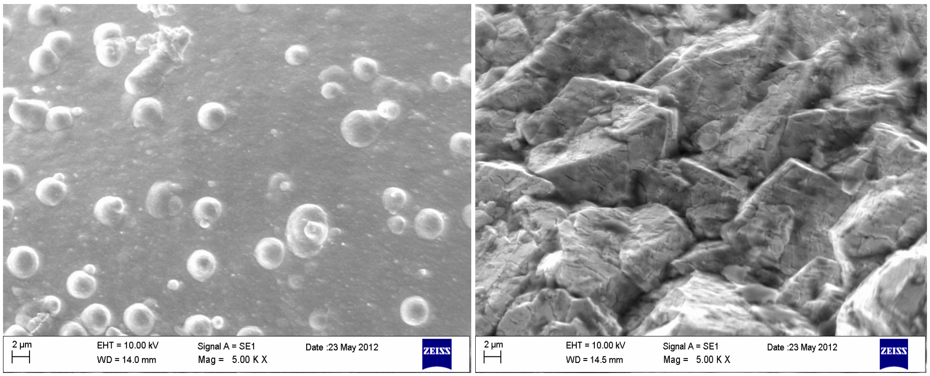
2 µm
EHT = 10.00 kV
WD = 14.0 mm
Signal A = SE1
Mag = 5.00 K X
Date :23 May 2012
ZEISS
2 µm
EHT = 10.00 kV
WD = 14.5 mm
Signal A = SE1
Mag = 5.00 K X
Date :23 May 2012
ZEISS

c) LA/Teepol d) LA/Triton X-100

Fig.4.36 SEM images of anodes modified using surfactants.

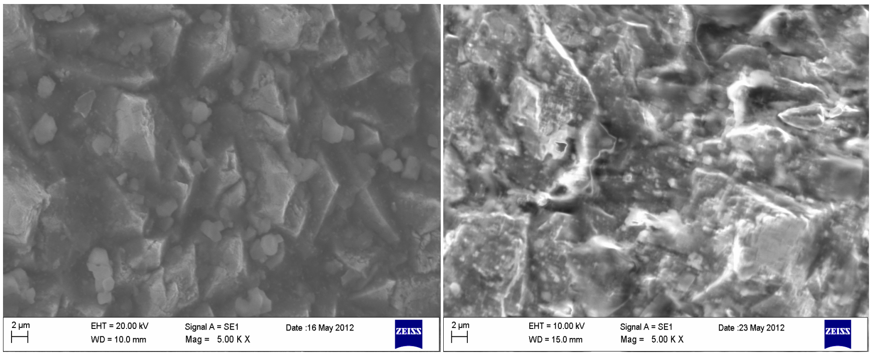
2 µm
EHT = 20.00 kV
WD = 10.0 mm
Signal A = SE1
Mag = 5.00 K X
Date :16 May 2012
ZEISS
2 µm
EHT = 10.00 kV
WD = 15.0 mm
Signal A = SE1
Mag = 5.00 K X
Date :23 May 2012
ZEISS

a) LA/NaF+ CTAB b) LA/Cerium Nitrate + Triton X

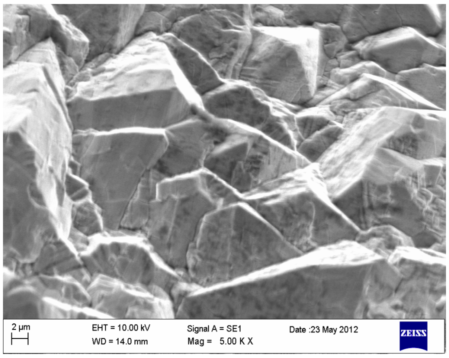

c) LA/NaF + TritonX

Fig. 4.37 SEM images of Modified Anodes with combination

4.6.2 X-ray Diffraction

Fig 4.38 and Fig. 4.39 reveals that when compared with un modified samples, the XRD patterns implies an obvious diminution in peak width of the diffraction lines and an exactly opposite trend in the intensity of peaks in improved Lead dioxide samples. Table 4.5 specifies that the magnitude of lattice spacing is reduced in modified samples. The lengthening of diffraction lines is the outcome of two interrelated phenomena: a reduction of crystallites and an upsurge in the range of microscopic stresses. Widening of diffraction lines is in accordance with the physical bonding between the coating and Ti substrate. Thus, the more crystalline is the sample, the sturdier is its gripping with Ti substrate.

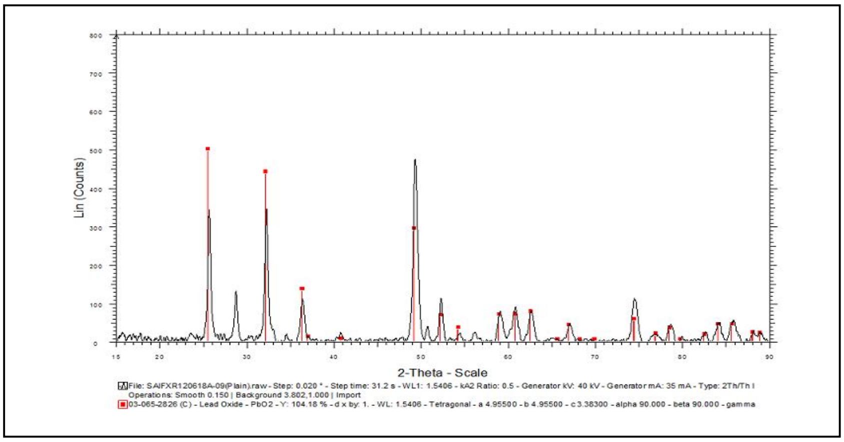

a) LA/Normal

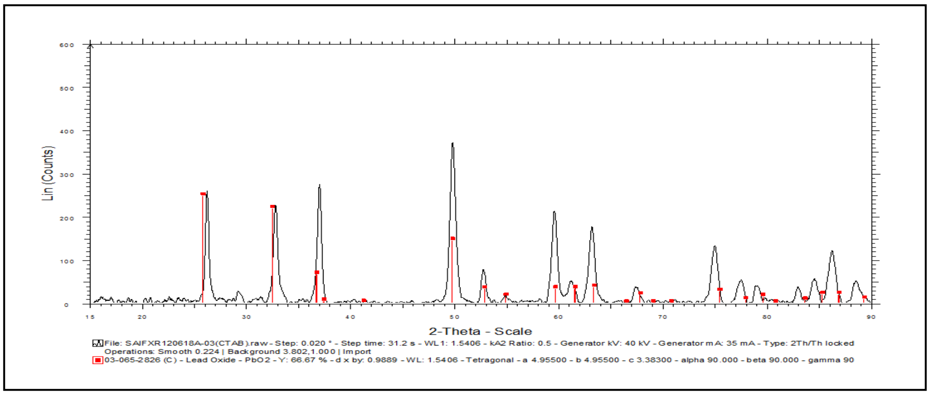

b) LA/CTAB

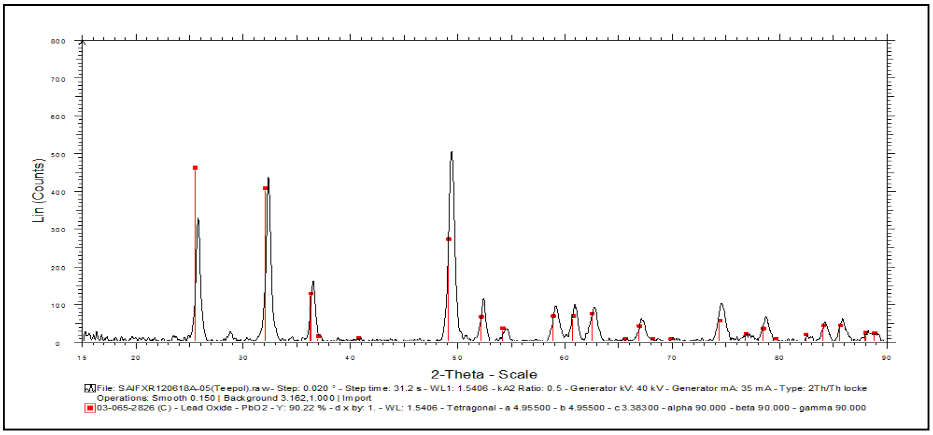

c) LA/Teepol

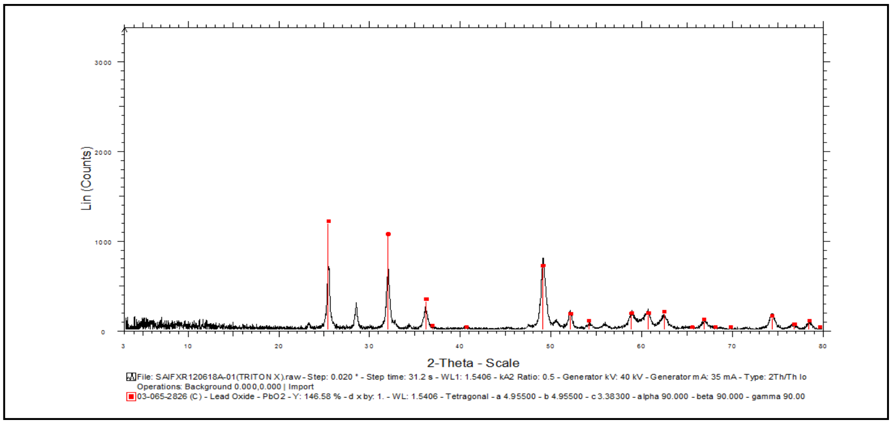

d) LA/Triton X

Fig.4.38 XRD of anodes modified using surfactants

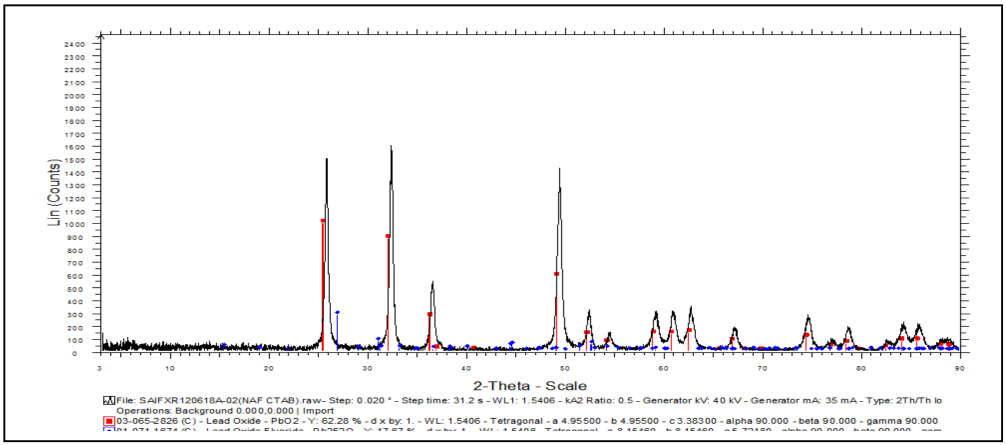

a) LA/NaF + CTAB

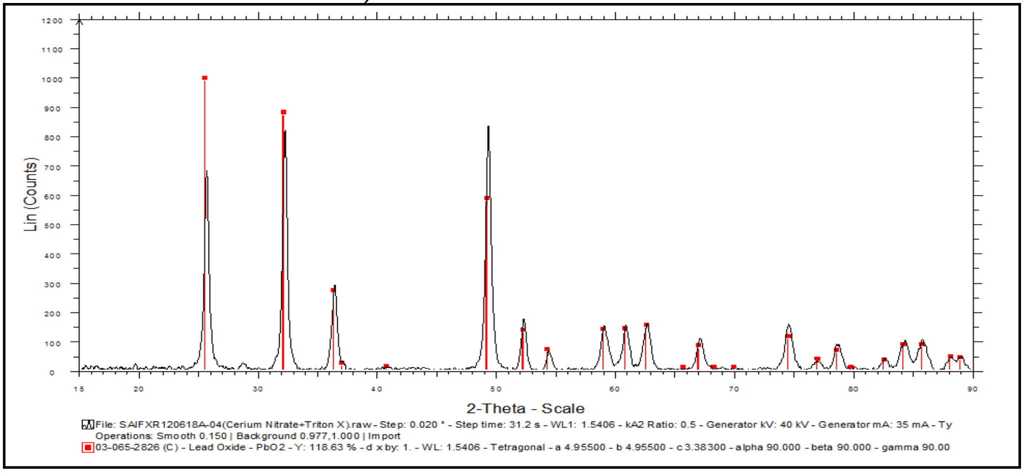

b) LA/Cerium Nitrate + Triton X

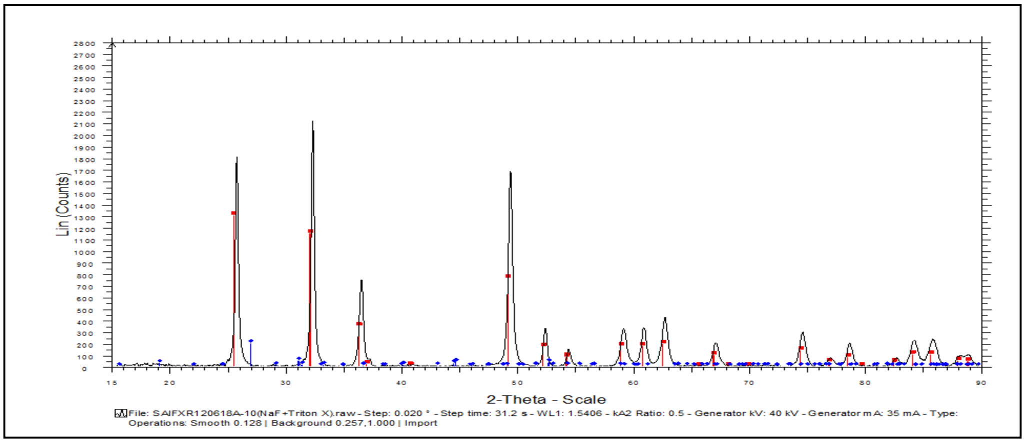

c) LA/NaF + CTAB

Fig.4.39 XRD of anodes modified by combinations of surfactants and additives

4.6.2.1 Evaluation of % α-PbO_2 in β-PbO_2 samples

α-PbO_2 and β -PbO_2 are the two polymorphic forms of lead dioxide. β -PbO_2 is more preferred for this application than the alpha form because it has relatively low resistivity, good corrosion resistance even in low-pH medium, and a high overvoltage for the evolution of oxygen in sulfuric acid and nitric acid based electrolytes. Fraction of α-PbO_2 (W_α) in beta form can be calculated from following relation given by Munichandraiah *et al*(1988) based on XRD data.

$$W_\alpha = 2\,x\,\frac{J\alpha'}{K * (J_{\beta1}' + J_{\beta2'})} \qquad (4.23)$$

where *K* is a constant. The β-PbO_2 form may be recognized from its most prominent lines (110, at $25.4^{\circ}2\theta$) and (101, at $32.05^{\circ}2\theta$), and α form from its (111, at $28.5^{\circ}2\theta$) line. The comparative intensities of these lines are designated as $J_{\beta1'}$, $J_{\beta2'}$ and $J_{\alpha'}$, respectively. Parameters from XRD are shown in table 4.5. Results shown in table 4.6specify that for undoped normal sample, the value is about 0.388 while in other improved samples, the value is much lesser. % ofα-PbO_2 in samples improved using sodium fluoride and CTAB is found to be much lesser by about one tenth, implying that those samples are enriched in beta form.

Table 4.5 Parameters from X-ray Diffractogram

Samples	25.4^0 2θ		28.5^0 2θ	32.05^0 2θ	
	Wide (A^0)	Height (A^0)	Height(A^0)	Wide(A^0)	Height(A^0)
LA/Normal	3.478	340	132	2.78	340
LA/CTAB	3.409	276	14.3	2.735	245

LA/Teepol	3.462	330	26.4	2.756	332
LA/Triton X (TX)	3.5	690	269	2.792	700
LA/NaF + CTAB	3.450	1444	38.4	2.763	1529
LA/Cerium Nitrate+ TX	3.477	679	23	2.78	819
LA/NaF + TX	3.467	1746	13.3	2.774	2066

Table 4.6 Fraction of calculated α-PbO_2 in prepared β-PbO_2 samples.

Sl No	Sample Description	$J_{\alpha'}(A^0)$	$J_{\beta1'}(A^0)$	$J_{\beta2'}(A^0)$	$[W_\alpha = 2 * J_{\alpha'} / (K * (J_{\beta1'} + J_{\beta2'})]$
1	LA/Normal	132	340	340	0.388
2	LA/ CTAB	14.3	276	245	0.055
3	LA/Teepol	26.4	330	438	0.068
4	LA/TX	269	690	700	0.387
5	LA/NaF+ CTAB	38.4	1444	1529	0.025
6	LA/Cerium Nitrate+TX	23	673	819	0.031
7	LA/NaF+T X	20.3	500	1066	0.026

4.6.3 Electrochemical Impedance Spectroscopy (EIS) analytical results

EIS plots indicate that that by adding foreign agent like surfactants, electro catalytic features of attained lead dioxide changes quite effectively. Assessment of Nyquist plots of both normal and other modified anodes from Fig. 4.40 clearly illustrates that addition of surfactants in the coating electrolyte made a substantial bearing on the kinetic features of the reaction. Experimental conditions for EIS studies are mentioned in table 4.6. Impedance values for anode samples improved using CTAB are about 5 times higher than that for normal type. This is evidently due to enormously higher charge transfer resistance offered by those modified anodes. It may be probably because of poor charge transfer owing to trimethyl functional group present in CTAB. As H_2SO_4 was used as the electrolyte for EIS studies, the only reaction predictable at the surface of working electrode is O_2 evolution.

It may be noted that decisive steps for crystal growth are diffusion processes and incorporation of adsorbed atoms at lattice sites in the micropores of active mass and in electrolyte. As per this mechanism, the rate of growth of lead dioxide particulates may be governed by the quantity of midway product $Pb(OH)_2$ generated at the electrode surface. Existence of surfactants in coating solution is recognized to slow down creation of hydroxyl radicals than surface diffusion of deposited species. This postulation is hinged on the fact that generation of hydrophobic layers of surfactants makes the exchanges at the electrode/electrolyte interface more cumbersome. The diminution of the anodic generation of O_2 may also be ascribed to possible interactions of surfactants with the hydroxyl radicals, as intermediate for O_2 evolution. Samples prepared by combining both surfactants and additives also demonstrate an analogous trend (Fig.4.41). Charge transfer resistance (R_{ct}) for oxygen evolution (under the existing conditions) vary as

LA/NaF+CTAB (12.5Ω) > LA/NaF +Triton X (11Ω) >LA/Cerium Nitrate + Triton X (4.5Ω) >LA/ Plain (0.8Ω). High Charge transfer resistance indicates that kinetics of the undesired oxygen evolution reaction is ominously affected.

Table 4.7 EIS Experimental Conditions

Working Electrode	Lead dioxide
Counter Electrode	Platinum/Iridium mesh
Reference Electrode	Calomel Electrode
Electrolyte	1 M H_2SO_4
Frequency	100 KHz to 10 mHz
Amplitude	5 mV

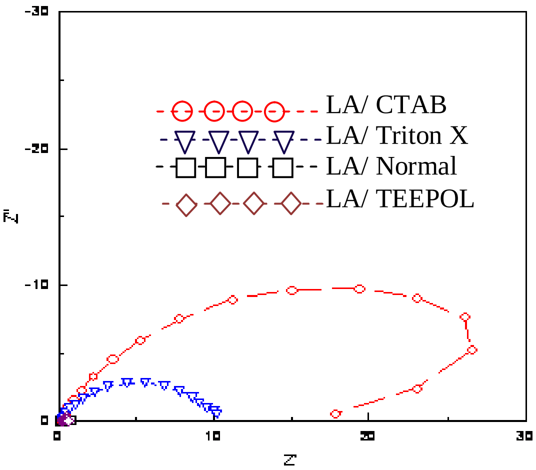

Fig.4.40 EIS plots of anodes modified with surfactants

(Units of Z' and Z'' are in Ω (ohms)

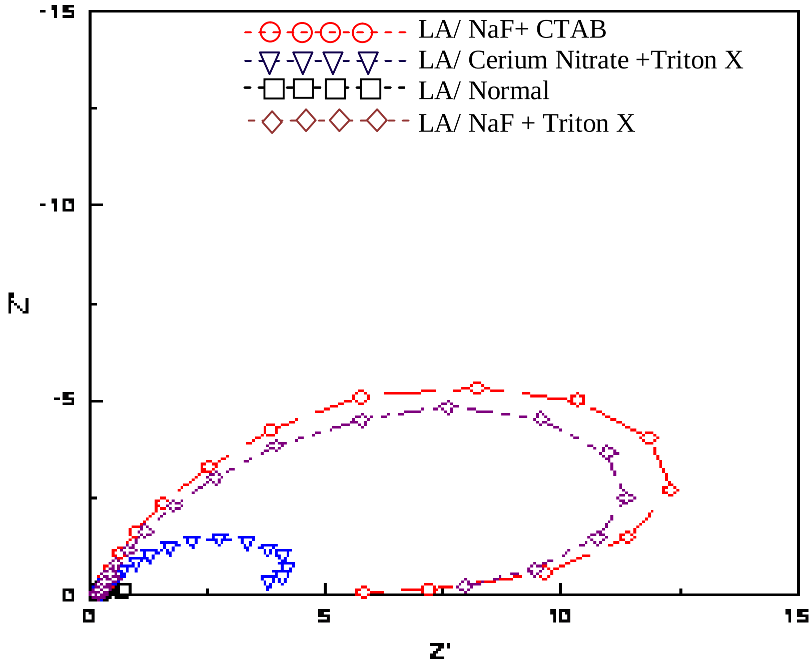

Fig.4.41 EIS plots of anodes modified with combination of surfactants &additives (Units of Z' and Z'' are in Ω (ohms)

4.6.4 Potentio Dynamic Response (PDR) Results

Fig 4.42 shows PDR plot as obtained from Corrview^{R} Software. Since the objective is to understand the phenomena in positive (anodic) region, data from these regions were retrieved and the same was plotted with Log I on Y axis and Overpotential in X axis.

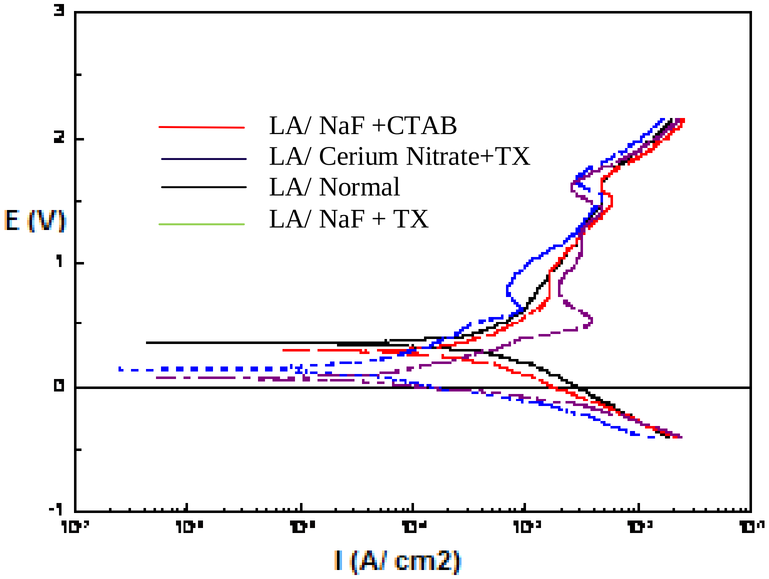

(a) PDR plots for full range of potential

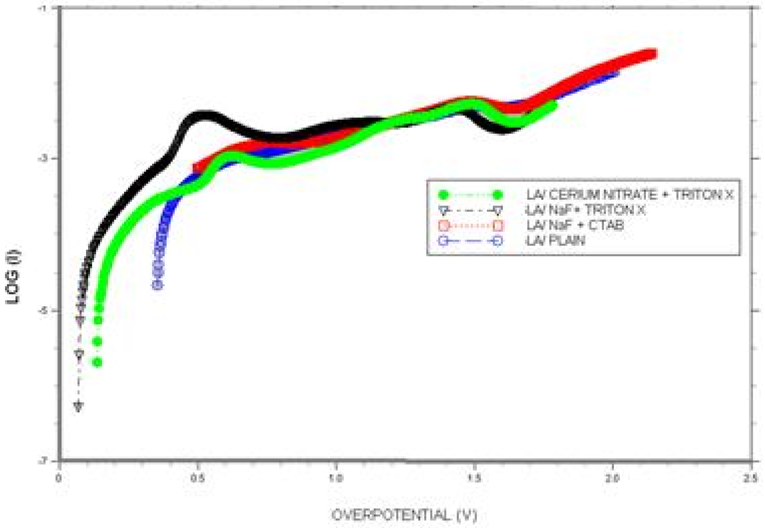

b) PDR plots of anodes for desired range

Fig. 4.42 PDR plots of anodes modified with surfactants and additives

Exchange current density $i_0$was obtained from the above graphs (from the intercepts on Y axis) and shown in Fig. 4.43. By closely analyzing, it is clear that i_0 values are highest for LA/ NaF+CTAB and LA/ CTAB.

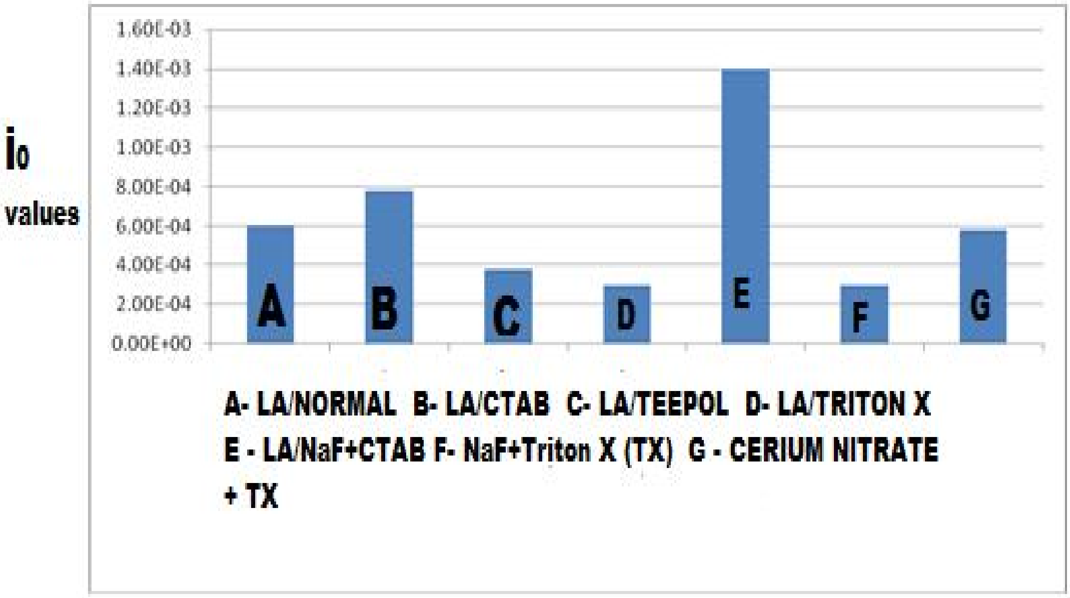

Fig. 4.43 Exchange current density (i_0) values in Amps/cm^2

4.6.5 Validation in perchlorate cell

Experiments were carried out in 200 L cell for 3 individual batches using LA/ Normal, LA/CTAB and LA/NaF+CTAB to understand their performance in perchlorate cell. Calculated current efficiency details are given in Figure4.44. Significant increase in current efficiency was noticed for the modified anodes. This confirms the interpretations regarding the improvements in kinetic activity of this anode for perchlorate reaction as shown by EIS and PDR studies.

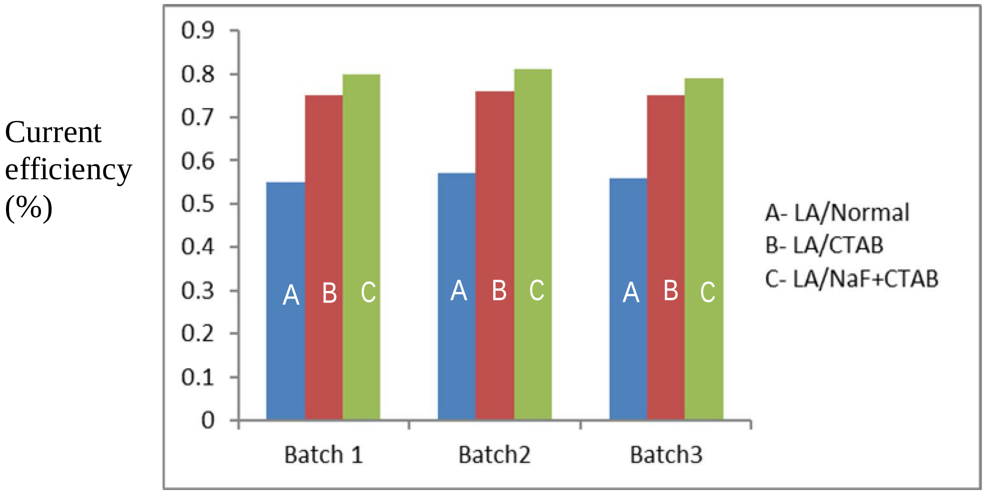

Fig.4.44 Calculated Current Efficiencies for perchlorate formation

After the completion of 3 batches, anodes were taken out and physical inspection was carried out. All the above mentioned anodes were intact without any peel out of lead dioxide which ensures an assured long service life of these modified anodes. These findings were in close agreement with the indication given by Amadelli (1999), Shiyun Ai (2001) and Amjad (2010).

4.7 QUANTIFICATION OF INTERFACIAL ADSORPTIVE CHARACTERISTICS OVER LEADDIOXIDE ELECTRODES

4.7.1 Theory

In contrast to measurement of interfacial tension for liquids, the direct measurement of interfacial tension for solids can be considered an impossible task. However, it is possible to apply indirect measurements to obtain electrocapillary curves for solid electrodes and therefore the information from these curves. Here, methodology adopted for determining charge density of electrodes was by plotting current transients. i.e by measuring the current, I passing through the circuit as a function of time when the potential is changed from a value where adsorption of electroactive species does not occur to a value where adsorption occurs (at various fractions) at a given concentration of species in solution. Charge of the electrode can then be obtained by integrating these curves according to the equation,

$$\int_{(q_{\mathrm{M}})_0}^{(q_{\mathrm{M}})_\theta}(dq_{\mathrm{M}}) = \int_0^t I\,dt \text{ or } \Delta q_{\mathrm{M}} = \int_0^t I\,dt \qquad (4.24)$$

where $\Delta\ q_M$ is defined by the equation :

$\Delta\ q_M = (q_M)_\theta - (q_M)_0$. In this equation $(q_M)_\theta$ is the charge density of the electrode at a potential where the electrode is covered by 'θ' fraction of adsorbate and $(q_M)_0$ in the absence of adsorbate.

4.7.1.1 Plotting of electrocapillary curves of electrodes

The interfacial tension at the electrode-electrolyte interface depends on the forces arising from the particles present in the interface region. If the composition of interface (i.e arrangement of particles at the interphase) is altered by varying the potential difference across the interface, then forces at the interface should change and thus a change in interfacial tension. Hence, it is expected that interfacial tension of the electrode-electrolyte interface should vary with the potential difference supplied by the external source. What is more informative is the type of variation of electrocapillary curves (interfacial tension Vs potential difference) for various electrode modifications which gives a clear understanding of the structure of interface.By applying basic thermodynamic principles at the electrode-electrolyte interface, following fundamental equation for polarizable interface can be obtained.

$$d\gamma = -q_{\mathrm{M}}dV - \frac{q_{\mathrm{M}}}{z_{\mathrm{j}}F}d\mu_{\mathrm{j}} - \sum z_{\mathrm{i}}\,d\mu_{\mathrm{i}} \qquad (4.25)$$

where γ- interfacial tension, q_M - charge density, j- particular species involved in the leakage of charge across the non polarizable interface, Γ_i – surface excess of species ‘i’ of interest; here Chlorate ions, μ – Chemical potential.

Since, during experimental conditions, composition of electrolyte is fixed, here 100gpl of aq: solution of $NaClO_3$, $\sum \Gamma_i \, d\mu_i = 0$ and $d\mu_j = 0$. Hence equation 4.25 is modified as

$$\left(\frac{\partial\gamma}{\partial V}\right)_{\text{const. composition}} = -q_M \tag{4.26}$$

This equation is known as Lipmann equation. Having known the values of q_M from equation 4.25, interfacial tension at various potentials can be obtained from equation4.26. The potentials at which interfacial tension is maximum is known as electrocapillary maximum.

4.7.1.2 Differential double layer capacity

An electrified interface can be considered a system capable of storing charge, considering that it is a region where charges are accumulated or depleted relative to the bulk of the electrolyte. Unlike an electric capacitor, constancy of capacity may not be the case with electrified interfaces and in order to be prepared for this eventuality, it is best to define a differential capacity, C thus,

$$C = \left(\frac{\partial q_M}{\partial V}\right)_{\text{const. composition}} = -\left(\frac{\partial^2\gamma}{\partial V^2}\right)_{\text{const. composition}} \tag{4.27}$$

Hence, by differentiating curve q_M Vs V at various potentials, a relation between differential capacity and potential difference can be obtained.

4.7.2 Determination of charge density of electrodesamples

Fig 4.45 shows the current transients for various samples under potentials ranging from 0.01V to 2.1V (Vs Ref). Fig 4.46 shows the respective charge transients obtained by integrating the above curve.

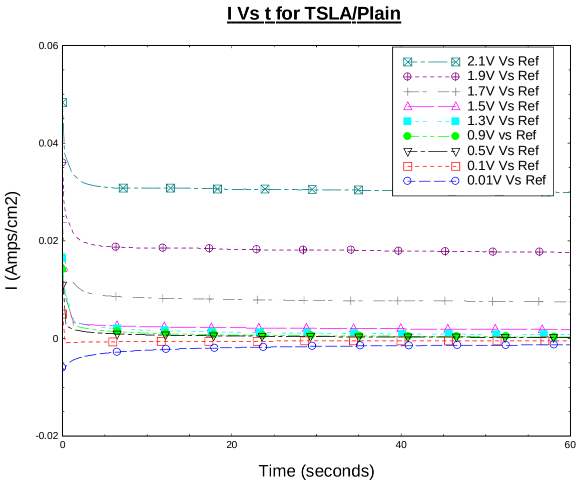

(a)

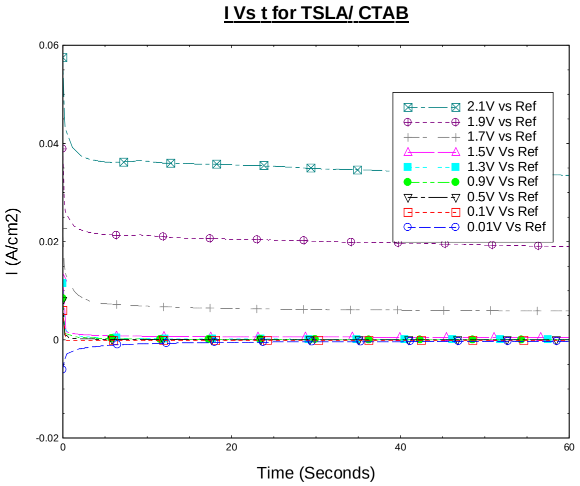

(b)

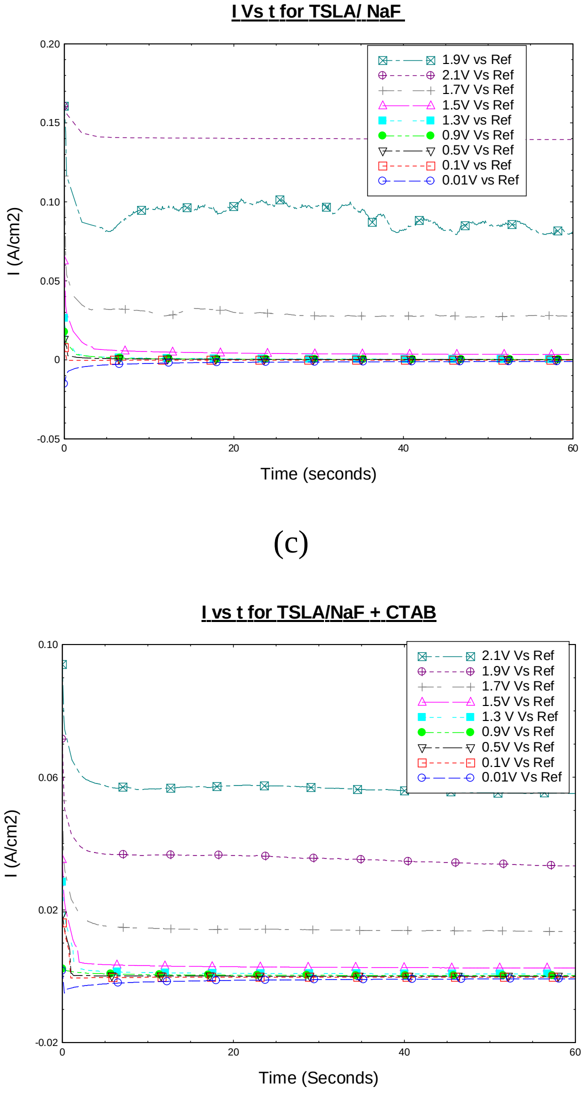

(c)

(d)

Fig.4.45 Current transients for various samples (a) LA/Plain/Normal (b) LA/CTAB (c)LA/NaF (d)LA/NaF+CTAB

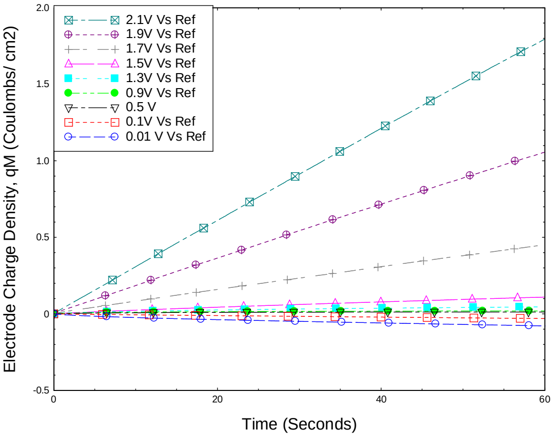

Electrode Charge Density (q_M) vs Time (t) for TSLA/ Plain

(a)

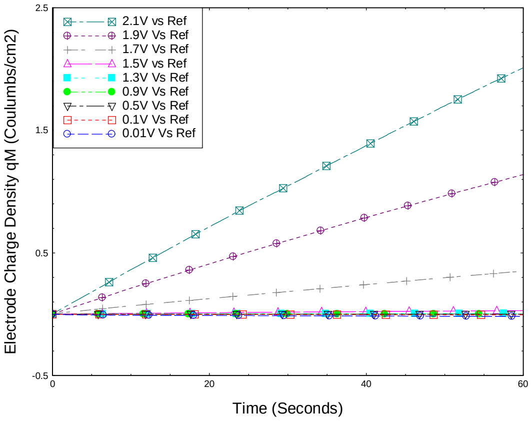

Electrode Charge Density (qM) Vs Time (t) for TSLA/ CTAB

(b)

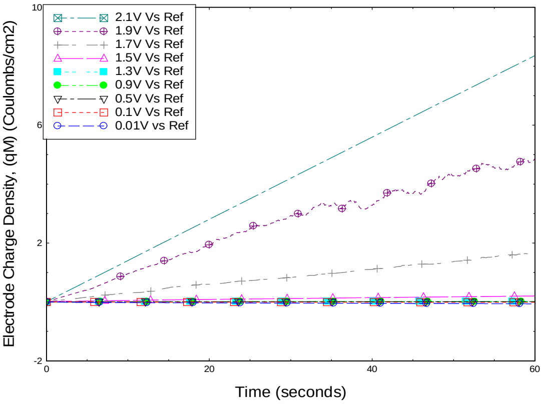

Electrode Charge Density (qM) Vs Time (t) for TSLA/NaF

(c)

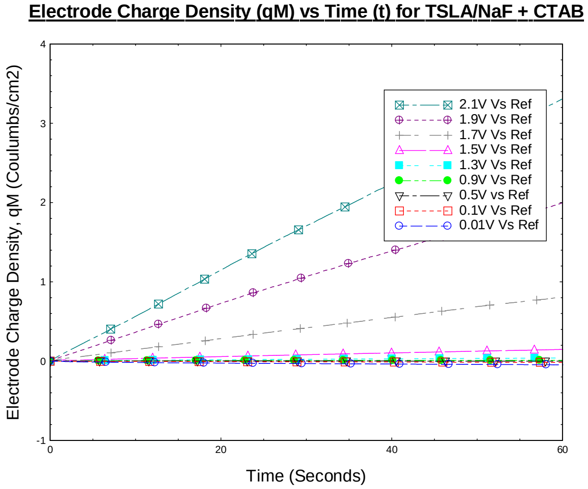

(d)

Fig.4.46 Charge transients for various samples
(a) LA/Normal (b) LA/CTAB (c)LA/NaF
(d) LA/NaF+CTAB

As it is seen from current transients, the curves are initially nonlinear indicating any non Faraday reactions occurring at the electrode surface. Since our interests were to unravel information across electrochemical double layer, current transients were replotted to highlight the characteristics during the initial period, say initial 5sec. Modified plots are shown in Fig 4.47. If we look closer at all the above curves, it is clear that charge rise during lower potential step (0.01V Vs Ref) is lesser than 0.001C/cm^2. This is due to lack of adsorption of reactive species (here Chlorate ions) on the electrode surface at this potential. Hence the transient values at this potential can be conveniently considered as potential at which no adsorption takes place.

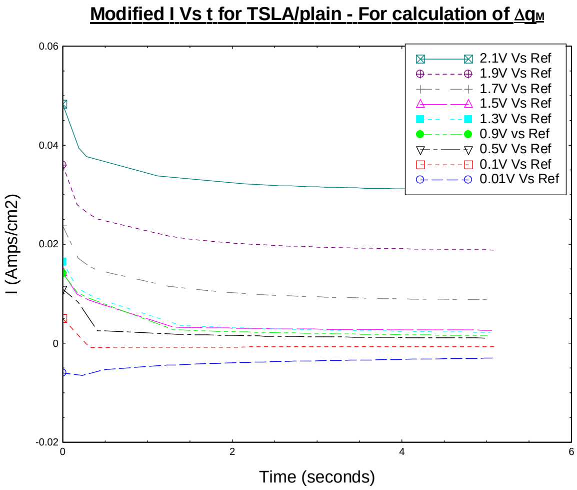
Modified I Vs t for TSLA/plain - For calculation of ΔqM
2.1V Vs Ref
1.9V Vs Ref
1.7V Vs Ref
1.5V Vs Ref
1.3V Vs Ref
0.9V vs Ref
0.5V Vs Ref
0.1V Vs Ref
0.01V Vs Ref
I (Amps/cm2)
0.06
0.04
0.02
0
-0.02
0
2
4
6
Time (seconds)

(a)

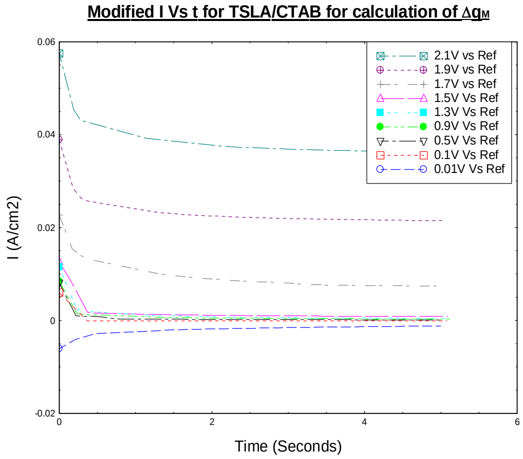
Modified I Vs t for TSLA/CTAB for calculation of ΔqM
2.1V vs Ref
1.9V vs Ref
1.7V vs Ref
1.5V Vs Ref
1.3V Vs Ref
0.9V Vs Ref
0.5V Vs Ref
0.1V Vs Ref
0.01V Vs Ref
I (A/cm2)
0.06
0.04
0.02
0
-0.02
0
2
4
6
Time (Seconds)

(b)

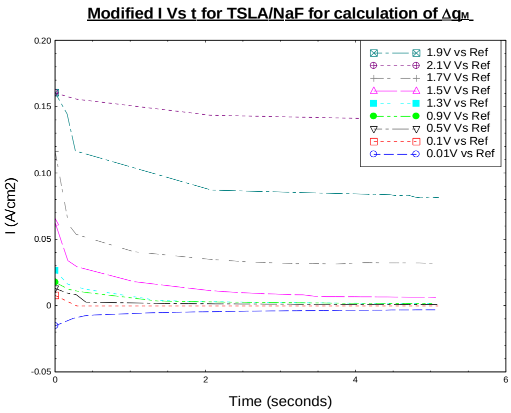
Modified I Vs t for TSLA/NaF for calculation of ΔqM
1.9V vs Ref
2.1V Vs Ref
1.7V Vs Ref
1.5V Vs Ref
1.3V vs Ref
0.9V Vs Ref
0.5V Vs Ref
0.1V vs Ref
0.01V vs Ref
I (A/cm2)
0.20
0.15
0.10
0.05
0
-0.05
0
2
4
6
Time (seconds)

(c)

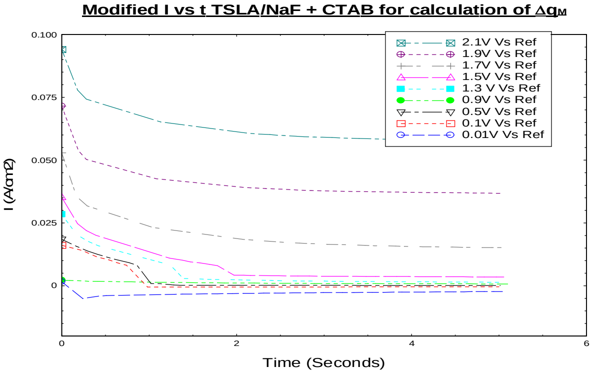

(d)

Fig. 4.47 Modified Current transients for various samples

a) LA/Plain (b) LA/CTAB

c)LA/NaF(d)LA/NaF+CTAB

Electrode charge density, Δ q_M was calculated by integrating above curve Fig 4.47. Since $(q_M)_0$ corresponds to the charge density at 0.01V Vs Ref, values of $(q_M)_\theta$ for all electrode samples were calculated at various potentials using the relation,Δ $q_M = (q_M)_\theta - (q_M)_0$ and the same is tabulated in Table 4.8.

Table 4.8 Calculated values of $(q_M)_\theta$

E (Vs Ref) in Volts	$(q_M)_\theta$ – plain (C/m^2)	$(q_M)_\theta$ – CTAB (C/m^2)	$(q_M)_\theta$ – NaF (C/m^2)	$(q_M)_\theta$ – NaF+CTAB (C/m^2)
0.01	-0.0450	-0.0204	-0.052	-0.0344
0.1	-0.0270	-0.0108	-0.0277	0.0013
0.5	-0.0123	-0.0085	-0.015	0.0014
0.9	-0.0055	-0.0071	-0.007	0.0028
1.3	-0.0025	-0.0052	-0.003	0.0088
1.5	-0.0015	-0.0022	0.044	0.0238
1.7	0.0385	0.0428	0.189	0.0948
1.9	0.0985	0.1238	0.508	0.2188
2.1	0.1705	0.2158	0.817	0.3478

4.7.3 Electrocapillary curves

Fig. 4.48 shows the variation of electrode charge density ($(q_M)_\theta$) Vs Potential (E) for all samples.

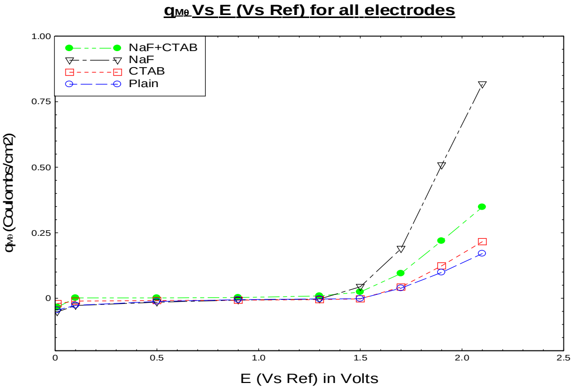

Fig.4.48 Variation of $(q_M)_\theta$ with Potential (E vs Ref) for various samples

Interfacial tension at various potentials for all electrode samples was calculated using Lipmann equation. (i.e by integrating Fig. 4.48). Electrocapillary curves for various samples were made as shown in Fig 4.49. Electrocapillary maximum for all samples were tabulated in Table 4.9

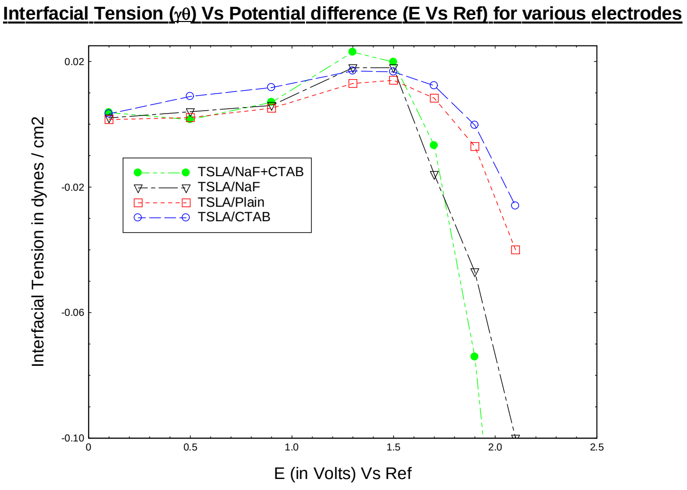

Fig.4.49 Electrocapillary curves for various samples

Table 4.9 Electrocapillary maximum for various anode samples

Type of anodes	Maximum value of γ_θ (dynes/cm^2)	Electrocapillary maximum (Volts)
LA/Normal	0.014	1.5
LA/CTAB	0.0167	1.4
LA/NaF	0.018	1.4
LA/NaF+CTAB	0.0198	1.3

As shown in Fig. 4.49, electrocapillary curves were not true parabolas but a distorted one. This is due to the deviation from an ideal parallel plate model suggested by Perrin and Helmholtz. This is expected in an electrochemical interface where there will be both fixed and mobile charges with fixed one in contact with the electrode and mobile charges scattered in the solution, as explained by Guoy-Chapman and Stern in their respective interface models. This results in variation of double layer capacity with potential causing a deviation from a normal parabolic shape of electrocapillary cuve.For modified samples, especially for LA/ NaF+CTAB $(\gamma_\theta)_{max}$ is found to be higher than the normal electrode. Similarly $(\gamma_\theta)_{max}$ occurs at a lower potential than the unmodified ones. Combining NaF and CTAB in equal ratio had given the best results due to their combined influence in modifying the surface. Above surface modifications gave rise to a conducive surface for the preferential adsorption of Chlorate/ hydroxyl ions over the electrode surface resulting in higher values of interfacial tension at lesser potential driving force. Since adsorption of electroactive species is the rate determining step in perchlorate formation, the increase in interfacial tension can inadvertently electrocatalyse the reaction.

4.7.4 Determination of differential double layer capacity

By differentiating Fig.4.47 differential double layer capacity (C) for all the electrode samples were obtained. Fig.4.50 shows its variation with potential.

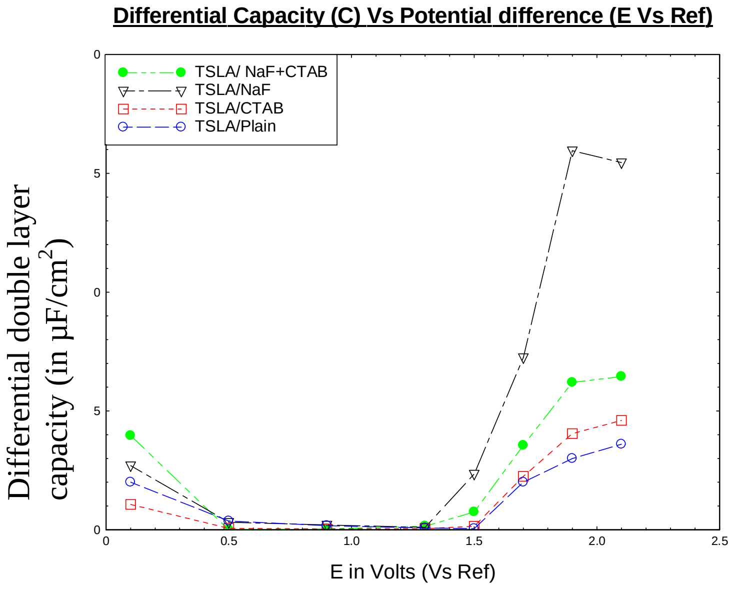

Fig. 4.50 Variation of Differential Capacity(C) for various samples

CHAPTER 5

SUMMARY AND CONCLUSIONS

5.1 STUDIES RELATED WITH SINGLE BED PACKED BED ELECTROCHEMICAL REACTOR (PBER)

- An optimized flow- through packed bed electrochemical reactor using discarded Lead dioxide particles was made for energy efficient production of Sodium perchlorate.
- Systematic studies were conducted to understand the influence of various critical parameters like current, temperature and flow rate on the performance of electrochemical reactor. This electrolyser outperforms the conventional parallel plate design owing to higher contact surface available.
- Another added feature of above design is the complete elimination of expensive inert substrate and noble metal oxide under- coating required in parallel plate design.
- Being most cost effective and energy efficient, this electrolyser outperforms the conventional parallel plate design.
- Though not recorded in the study, the service life of these particulate electrodes will be extensively higher, since the life of TSLA's (Titanium Substrate Lead dioxide coated anode) is defined till lead dioxide gets adhered to the substrate. Thus it excludes the necessity of labour intensive repeated lead dioxide coating procedures adopted in several electrochemical industries.
- Another promising element regarding this design is the flexibility in leveraging its application in other industries where electrochemical oxidation is preferred like oxidation of effluents containing traces of organics like phenol etc,.

5.2 STUDIES RELATED WITH DUAL BED PACKED BEDELECTROCHEMICAL REACTOR (PBER)

- Sharp voltage rise in a single bed reactor could be drastically brought down using a dual bed reactor.
- A demonstration of continuous production of sodium perchlorate could be carried out by arranging these dual bed reactors after resolving problems connected with incomplete conversion.

5.3 FLOW MODELLING USING RTD STUDIES

- RTD behavior of PBER was studied in various flow rates with and without electrolysis.
- Conventional dispersion models could explain the RTD behavior when PBER is operated without electrolysis. (D/u.L) values were determined by fitting in the dispersion model to assess the quantum of axial dispersion inside the packed bed.
- Modified Dispersion Plug Flow Model (MDPFM) was developed to predict the residence time distribution function ($E(\theta)$) under electrolyzing conditions.
- Finally, the model was validated in RTD studies using PBER operated under electrolyzing mode at various flow rates.

5.4 EFFECT OF MODIFIED LEAD DIOXIDE ANODES IN CONVENTIONAL PERCHLORATE CELLS

- Morphology of samples prepared by altering coating electrolytes shows considerable distinction when viewed under SEM.
- Existence of surfactants is likely to reduce the roughness of the deposits.SEM studies demonstrate that a combination of sodium fluoride and CTAB in coating solution imparts highly even and finer deposits of Lead dioxide.
- XRD results specified that existence of fluoride ions in coating electrolyte appreciably dwindles the presence of α $-PbO_2$ in the preparation of β-PbO_2 and hence highly suitable for perchlorate formation.
- EIS studies signify that anodes tailored using NaF and CTAB provides higher charge transfer resistance for oxygen evolution and thereby restrains it and hence favoring desired perchlorate reaction.
- Values of $i_0$determined from PDR of various anodes once again pointed out that kinetic activity of these anodes get varied for Perchlorate formation.
- An increase of 10-15% in CE was observed for Perchlorate generation in a pilot level cell using LA/NaF+CTAB over LA/ Normal. This underlines the enhancement in kinetic activity of this anode for perchlorate reaction as shown by EIS and PDR studies.

5.5 QUANTIFICATION OF INTERFACIAL ADSORPTIVE CHARACTERISTICS OVER LEADDIOXIDE ELECTRODES

- Adsorption of electroactive species on Lead dioxide electrode during electrochemical oxidation of Sodium Chlorate to Sodium perchlorate was indirectly quantified using electrocapillary studies.

- It was observed that Lead dioxide electrode modified using a combination of CTAB and NaF had shown maximum variation in interfacial tension values at the electrode surface. This is due to the modifications on the electrode surface giving rise to a conducive surface for the preferential adsorption of Chlorate/ hydroxyl ions over the electrode surface.
- Values of electrocapillary maximum for this modified electrode were also found to be lower indicating its better performance in conversion.

5.6 SCOPE OF FUTURE RESEARCH

- Effect of particle size distribution of peeled off lead dioxide in the performance of packed bed electrochemical reactor.
- Further options in reducing the voltage consumption of cell by adopting other options like mode of packing, etc.
- Further flow modelling studies adopting CFD techniques.
- Prediction of charge transfer resistance for the electrodes by developing a suitable equivalent circuit model via EIS techniques.

REFERENCES

1. **Xiaohong Li, Derek Pletcher and Frank C. Walsh** (2011) Electrodeposited Lead dioxide coatings. *Chem. Soc. Rev.,* **40**, 3879-3894.

2. **J.P. Carr and N.A. Hampson** (1972) Lead dioxide electrode, *Chem. Rev.,* **72**, 679-703.

3. **Onwughara** (2013) Focus on potential environmental issues on plastic world towards a sustainable plastic recycling in developing countries, *Int. J.of Ind. Chemistry.,* **4**, 34-37.

4. **John. S. Newman and Charles. W. Tobias** (1962) Theoretical Analysis of Current Distribution in Porous Electrodes. *Journal of Electrochemical Society,* **109**, 1183-1191.

5. **Y. Volkman** (1978) Analysis of the performance of packed-bed electrochemical reactors. *Journal of Applied Electrochemistry,* **8**, 347-352.

6. **T. Doherty, J. G. Sunderland, E. P. L. Roberts and D. J. Pickett** (1996) An improved model of potential and current distribution within a flow-through porous electrode. *Electrochimic Acta* , **41**, 519-526.

7. **N.M.S. Kaminari** (2005) Study of the operational parameters involved in designing a particle bed reactor for the removal of lead from industrial wastewater—central composite design methodology.*Chemical engineering Journal,* **105**, 111–115.

8. **R. Saravanathamizhan, R. Paranthaman, N. Balasubramanian and C. Ahmed Basha** (2008) Residence time distribution in continuous stirred tank electrochemical reactor. *Chemical Engineering Journal*, **142**, 209-216.

9. **T.Atmakidis** (2015) Numerical analysis of mass transfer in packed bed reactor with irregular particle arrangements. *Chem.Prod.Process Model*, **10**, 17-26.

10. **Zheng Zou, Yuan long Zhao, Hu Zhao and Hing Zhang Li** (2017) Numerical analysis of residence time distribution of solids in a bubbling fluidized bed based on the modified structure based drag model. *Particulogy*, **32**, 30-38.

11. **Ouassila Benhabiles** (2012) Determination of Residence time distribution in CPC reactor type. *Energy Procedia*, **18**, 368-376

12. **A.D. Martin** (2000) Interpretation of Residence time distribution data. *Chemical Engineering science*, **55**, 5907-5917

13. **Munichandriah, N. and Satyanarayana, S** (1987)Kinetics and mechanism of anodic oxidation of chlorate ion to perchlorate ion on Lead dioxide anodes.*J. Appl. Electrochem*., **17**.

14. **Ghaemi, M, Ghafouri, E, Neshati, J** (2006) Influence of the nonionic surfactant TritonX-100 on electrocrystallization and electrochemical performance of lead dioxide Electrode. *Journal of Power Sources*, **157**, 550-662.

15. **Bockris John O'M, Reddy Amulya, Maria Gamboa- Aldeco** (2000) *Modern Electrochemistry 2A* (2ndedition), Springer International Edition.

16. **Douglas N. Bennion and John .S. Newman** (1972) Electrochemical removal of copper ions from very dilute solutions. *Journal of Applied Electrochemistry*, **2**, 113-122.

17. **R.W. Houghton and A.T. Kuhn** (1974) Antimony removal form dilute solutions using a restrained bed electrochemical reactor. *J .Appl.Electrochem.* **4**, 173-180

18. **J. Newman and W. Tiedeman** (1975) Porous electrode theory with battery applications, *Amer. Inst. Chem.. Engineers*, 27, 25-41

19. **R.E.Sioda (1971)** Distribution of potential in a porous electrode under conditions of flow electrolysis. *Electrochimic Acta* , **16,** 1569-1576.

20. **A. Gaunand, D. Hutin and F. Coeuret** (1977) Potential distribution in flow-through porous electrodes under limiting current conditions. *Electrochimica Acta*, **22**, 93-97.

21. **James A. Trainham and John Newman** (1977) A Flow-Through Porous Electrode Model: Application to Metal-Ion Removal from Dilute Streams.*Journal of Electrochemical Society*, **124**, 1528-1540.

22. **M Matlosz and J.Newman** (1986) Experimental investigation of a porous carbon electrode for the removal of mercury from contaminated brine. *J. Electrochem. Soc.*, **133**, 1850-1858

23. **M.S.El-Deab** (1999) Electrochemical removal of Lead ions in flowing electrolytes using packed bed electrodes. *J. Electrochemical Society*, **146**, 208-213.

24. **Mahmoud M Saleh** (2004) On the effectiveness factor of flow through porous electrodes. *J. Phys. Chem. B*, **108**, 13419-13426

25. **R. Alkire and R. Gould** (1976) Analysis of multiple reaction sequences in flow through porous electrodes. *ibid*, **123**, 1842-1850

26. **G. Kreysa and E. Heitz** (1976) *Chem-Ing.–Tech.*, **48**, 852-860

27. **R.D. Armstrong, O.R. Brown, R.O. Giles and J.A. Harrison** (1968), *Nature*, **219**, 94-100.

28. **R. Alkire and B. Gracon** (1975) Through porous electrodes. *ibid*, **122**, 1594-1600.

29. **B.G. Ateya** (1977) Kinetics of multiple electron transfer reactions at porpos electrodes under stationary and flow conditions. *J. Electroanal. Chem.*, **76**, 315-325.

30. **G. Kreysa and C. Reynvann** (1982) Optimal design of packed bed cells for high conversion. *Journal of Applied Electrochemistry*,**12**, 241-251.

31. **Anthony G. Dixon**(2001) CFD as a Design Tool for Fixed-Bed Reactors.*Ind. Eng. Chem. Res.***,** **40**, 5246-5254.

32. **J.L. Nava** (2009) Mass transport and potential studies in a flow through porous electrode reactor. *Electrochimic acta*, **27**, 381-396.

33. **Chu** (1974) Packed bed electrodes. I. The electrochemical extraction of Copper ions from dilute aqueous solutions. *Journal of Applied Electrochemistry*, **4**, 323-330

34. **Richard Alkire and Patrick K. Ng** (1974) Two-Dimensional Current Distribution within a Packed-Bed Electrochemical Flow Reactor. *J. Electrochemical Society*, **121**, 95-103.

35. **P.Fedkiw and J. Newman** (1979)**,** Entrance region mass transfer coefficients in packed bed reactors. *AIChE J.* ,**25**, 1077-1080

36. **Stephen E Lyke and Stanely H Langer** (1991) Internal ohmic drop limits on effectiveness of packed bed electrodes obeying Tafel Kinetics .*J. Electrochemical Society*, **13**, 2327-2330.

37. **B.E. El-Anadoulli and B.G. Ateya** (1992) Effect of gas bubbles on the current and potential profiles within porous flow through electrodes. *J Appl. Electrochem*.**, 22,** 277-284.

38. **Katsuki Kusakabe** (1986) Simultaneous electrochemical removal of copper and chemical oxygen demand using a packed-bed electrode cell. *Journal of Applied Electrochemistry*, **16**, 121-126.

39. **R.E. Sioda** (1968) Electrolysis with flowing solution. *Electrochim. Acta*, **15**, 375-382

40. **R.E. Sioda** (1975) The ece mechanism in flow electrolysis in porous electrodes under conditions of limiting current. *Electrochim. Acta*, **20**, 457-461

41. **F.Coeuret** (1976), A first investigation of flow through orous electrodes. *Electrochim. Acta*, 21, 185-193

42. **D.J. Pickett** (1977), *Electrochemical Reactor design* (1st Edition), Elsevier publishing Co., New York.

43. **F.C. Walsh** (1993) A first course in electrochemical engineering, the electrochemical consultancy. *ibid*, **38**, 465-472.

44. **Colin Oloman and Park Reilly** (1987), Modelling and parameter estimation of a Fixed bed electrochemical reactor. *J. Electrochemical Society*, **134**, 859-866.

45. **K. Scott and E.M. Paton** (1993), An analysis of metal recovery by electrodeposition from mixed metal ion solutions-part II. electrodeposition of cadmium from process solutions. *Electrochim. Acta*, **38**, 2191-2198.

46. **A. T. S. Walker and A. A. Wuagg** (1977) The modelling of concentration-time relationships in recirculating electrochemical reactor systems.*Electrochimic Acta* ,**22,** 1129-1134.

47. **E.A. Soltan, S.A. Nosier, A.Y. Salem, I.A.S. Mansour and, G.H. Sedahmed** (2003) Mass transfer behaviour of a flow-by fixed bed

electrochemical reactor under different hydrodynamic conditions. *Chemical Engineering Journal*, **91**, 33–41.

48. **Yan-Ping Sun and Keith Scott** (2004) An analysis of the influence of mass transfer on porous electrode performance. *Chemical Engineering Journal,***102**, 83–91

49. **B. Delanghe, S. Tellier and M. Astruc** (1990) Mass transfer to a carbon or Graphite felt electrode**.***Electrochimica Acta***,** **35**, 1369-1376.

50. **Faisal Larachi** (2003) Heat and mass transfer in concurrent gas-liquid beds. Analysis, recommendations and new correlations.*Ind. Eng. Chem. Res*, **42**, 222-242

51. **Camino Fernandez** (2014) Application of a Packed Bed Reactor for the Production of Hydrogen From Cheese Whey Permeate: Effect of Organic Loading Rate. *J Environ Sci Health A Tox Hazard Subst Environ Eng*, **49,** 210-217.

52. **Cuixian Yang** (2018) Catalytic hydrogenation of *N*-4-nitrophenyl nicotinamide in a micro-packed bed reactor. *J Green Chemistry*, **4,** 50-56.

53. **Subbalaxmi Selvaraj & Ramachandra Murty Vytla** (2018) Solid state fermentation of *Bacillus gottheilii* M2S2 in laboratory-scale packed bed reactor for tannase production. *Preparative biooochemmmistry 7 biotechnology*, **48,** 201-207.

54. **V. D. Stankovic** (1995) Pressure drop behaviour in a three-dimensional packed bed cell during copper deposition and hydrogen evolution.*Journal of Applied Electrochemistry*,**25**, 864-868.

55. **Daniel Simonsson** (1984) A flow-by packed-bed electrode for removal of metal ions from waste waters. *Journal of Applied Electrochemistry,* **14**, 595-604.

56. **M. V. Mikelsons and T. C. Pinkerton** (1986) A Carbon Particulate, Packed Bed Electrolysis Flow Cell for the Production of Technetium Complexes.*Appl. Radiat. Isot*.,**37**, 991-994.

57. **Somsaluay Suwanprasop** (2005) Scale-up and Modelling of Fixed-Bed Reactors for Catalytic Phenol Oxidation over Adsorptive Active Carbon. *Ind. Eng. Chem. Res*.**,** **44**, 9513-9523.

58. **Rossano Amadelli and. Velichenko A. B** Lead dioxide electrodes for high potential anodic processes, *Conference proceedings from Ukranian Chemical Technology*, 22 August 2001.

59. **Amadelli R , Armelao L, Velichenko A. B and Nikolenko N. V** Oxygen and ozone evolution at fluoride modified lead dioxide electrodes, Proceedings from Ukranian Chemical Technology, 15 November 1999.

60. **Shiyun Ai, Mengnan Gao, Wen Zhang, Zhengdong Sun and Litong Jin (2001)** Preparation of Fluorine-Doped Lead Dioxide Modified Electrodes for Electroanalytical Applications. *Journal of Fluorine Chemistry*, **1**, 100–110.

61. **Boggio A,. Maja M and Penazzi N** (2001) Effects of antimony on the electrochemical behaviour of lead dioxide in sulphuric acid, *Proceedings from Int conference on electrochemistry* , 30 July 2001.

62. **M. Amjad and Toqeer Ahmed** (2010) Electrochemical behaviour of cerium oxide incorporated lead dioxide electrodes electrodeposited from Ce^{+3} containing Pb^{++} electrolytes, *Pakistan Journal of Science* ,**62**, 100-110

63. **Jianren Feng** (2002) Anodic oxygen-transfer electrocatalysis at iron-doped lead dioxide electrodes, *Journal of Power Sources***,** **2**, 45-50.

64. **I.A. Khattab, M.F. Shaffei, N.A. Shaaban, H.S. Hussein, S.S. and Abd El-Rehim**(2013)Electrochemical removal of copper ions from dilute solutions using packed bed electrode. Part I.*Egyptian Journal of Petroleum* **22***,* 199–203

65. **Richard Alkire and Patrick K**(1977) Studies on Flow-by porous electrodes having perpendicular directions of current and electrolyte flow.*J. Electrochemical Society*,**124**, 1220-1227.

66. **H. Sharifian and D. W. Kirk** (1986) Electrochemical Oxidation of Phenol.*J. Electrochemical Society*, **133**, 921-924.

67. **Yuanxin Wu** (1996) Comparison of Upflow and Downflow Two-Phase Flow Packed-Bed Reactors with and without Fines: Experimental Observations. *Ind. Eng. Chem. Res.*,**35**, 397-405.

68. **J. O'M. Bockris and J. Kim** (1997) Effect of contact resistance between particles on the current distribution in a packed bed electrode. *Journal of Applied Electrochemistry*,**27**,890 – 901.

69. **T. Huh** (1992) Further studies of a zinc-air cell employing a packed bed anode Part II: Regeneration of zinc particles and electrolyte by fluidized bed electrodeposition.*Journal of Applied Electrochemistry*,**22,** 916-921.

70. **J.M.Bisang** (1996) Theoretical and experimental studies of the effect of side reactions in copper deposition from dilute solutions on packed-bed electrodes.*Journal of Applied Electrochemistry*,**26**, 135-142.

71. **Frank Walsh and Gavin Reade** (1994) Design and Performance of Electrochemical Reactors for Efficient Synthesis and Environmental Treatment Part 1. Electrode Geometry and Figures of Merit.*Analyst*, **119**, 791-796.

72. **Jingping Wang,Xiang Li, Linghua Guo and Xiangjun Luo** (2010) Effect of surface morphology of ead dioxide particles on their ozone generating performance.*Environ. Sci. Technology*, **44**,1751–1753.

73. **Guohua Zhao, Yonggang Zhang, Yanzhu lei, Baoying Lv, Junxia Gao, Yanan Zhang and Dongming Li** (2010) Fabrication and Electrochemical Treatment Application of A Novel Lead Dioxide Anode with Superhydrophobic Surfaces, High Oxygen Evolution Potential, and Oxidation Capability.*Environ. Sci. Technology.*, **44**, 1754–1759.

74. **Gnanasekaran K.S. A, Narasimham K.C. and Udupa H.V. K** (1970) Stress measurements in electrodeposited Lead dioxide. *Electrochimica Acta*, **15**,1867-1876.

75. **Pei Kang Shen and Xiao Lan Wei** (2003) Morphologic study of electrochemically formed Lead dioxide.*Chem. Soc. Rev***.**, **1**, 2500-2515.

76. **Robinson R.S** (1990) Scanning tunneling microscopy of Lead dioxide. *Journal of Applied Electrochemistry*., **3**, 1515-1525.

77. **Masashi Shiota, Yoshiaki Yamaguchi, Yasuhide Nakayama, Kazuyuki Adachi, Shunji Taniguchi, Nobumitsu Hirai and Shigeta Hara** (2001)In situ observation of morphology change in lead dioxide surface for Lead-acid battery.*Journal of Power Sources*,**20**, 101-107.

78. **Konrad Thürmer,Ellen Williams and Janice Reutt-Robey** (2003)Autocatalytic Oxidation of Lead Crystallite Surfaces.*Journal of Power Sources,***8**,111-117.

79. **David J. Payne , Russell G. Egdell ,Wang Hao , John S. Foord , Aron Walsh and Graeme. W. Watson** (2005) Why is lead dioxide metallic?.*Chemical Physics Letters*,**411**, 181–185.

80. **González-García. J, Sánchez-Cano G, A. Aldaz and Montiel V** (2006) Surface analysis of titanium electrodes.*Journal of Power Sources*, **5**,98-102.

81. **Randle, T.H and Kuhn, A.T** (2011)A Kinetic Study of the Electrolytic Oxidation of Cerium(III) and Manganese(II) in Sulfuric Acid at the Lead Dioxide Electrode. *Australian Journal of Chemistry*,**42**, 229 – 242.

82. **Randle, T.H and Kuhn, A.T** (2011) The Kinetics and Participation of the Lead Dioxide Electrode in Electrochemical Oxidation Reactions in Sulfuric Acid.*Australian Journal of Chemistry***,42**, 243-245.

83. **Janssen L, J. J and Van der heyden, D. L** (1995)Mechanism of anodic oxidation of chlorate to perchlorate on platinum electrodes.*Journal of Applied Electrochemistry*,**25**, 126-136.

84. **Chen Bu-ming, Guo Zhong-cheng, Yang Xian-wan and Cao Yuan-dong** (1999) Morphology of alpha-lead dioxide electrodeposited on aluminum substrate electrode.*Journal of Applied Electrochemistry,* **3**, 199-202.

85. **Claudine Hamela, Thierry Brousseb, Daniel Bélangerc, and Daniel Guaya(2004)**Effect of Ball-milling on Physical and Electrochemical properties of Lead Dioxide.*Journal of Power Sources*, 65-70.

86. **Narasimham, K. C., Sundararajan, S., and Udupa H, V. K** (1961) Lead Dioxide Anode in the Preparation of Perchlorates.*J. Electrochem. Soc*.**, 108**, 798-805.

87. **Narasimham K.C and Udupa H.V.K** (1970) Preparation and Applications of Graphite Substrate LeadDioxide(GSLD)Anode.*Electrochimica Acta*,**15**, 45-50.

88. **Sun Feng-mei, Pan Jian-yue and Luo Qi-fu** (2011)Lead Dioxide Anode with Platinum Intermediate Layer.*Environ. Sci. Technology.*, **24**, 1644–1650.

89. **Hassan Karami and Mahboodeh Alipour** (2009) Synthesis of Lead dioxide Nanoparticles by the Pulsed Current Electrochemical Method.*Int. J. Electrochem. Sci.*, **4**,1511-1527.

90. **Narasimham, K.C, Narayanaswami, A & Dey, B.B** (1957) Electrolytic Preparation of Perchlorates.*Journal of Scientific & Industrial Research*, **16A**.

91. **Takashi Osuga, Shojiro Fujii, Kiichiro Sugino and Taro Sekine** (2001) Electrolytic Production of Perchlorate by Lead Dioxide Anodes.*Journal of Applied Electrochemistry*,**15**, 143-150

92. **Jose′ González-García, Jesús Iniesta, Antonio Aldaz and Vicente Montiel** (1998)Effects of ultrasound on the electrodeposition of lead dioxide on glassy carbon electrodes.*New J. Chem*,**22**, 343-349.

93. **Nina Zakharchuk, Stefan Meyer, Britta Lange, and Fritz Scholz** (1989)AComparative Study of Lead Oxide Modified Graphite Paste Electrodes and Solid Graphite Electrodes with Mechanically Immobilized Lead Oxides.*Journal of Applied Electrochemistry*, **12**, 111-123.

94. **Velayutham, D and Noel, M** (1990)The influence of electrolyte media on the deposition-dissolution behaviour of lead dioxide on glassy carbon electrode.*Electrochimica Acta*,**11**, 65-72.

95. **Philippe Perret, Thierry Brousse, Daniel Bélanger, and Daniel Guay** (2009) Electrochemical Template Synthesis of Ordered Lead Dioxide Nanowires.*J. Electrochem. Soc.*, **156**, A645-A651.

97. **Ali Mehdinia, Mir Fazllolah Mousavi,and Mojtaba Shamsipur** (1999)Nano-structured Lead dioxide as a novel stationary phase for solid-phase microextraction**.***Journal of Power Sources*, **12**, 50-54.

98. **Joseph, C. Schumacher, David, R. Stern, and Paul, R. Graham** (1958)Electrolytic Production of Sodium Perchlorate Using Lead Dioxide Anodes.*J. Electrochem. Soc.*, **105**, 151-155.

99. **Takashi Osuga and Shojiro Fujii, Kiichiro Sugino and Taro Sekine** (1969) Electrolytic Production of Perchlorate by Lead Dioxide Anodes.*J. Electrochem. Soc.*, **116**, 203-207.

100. **Vasundara,S, Narasimham, K. C. and Udupa, H V. K** (1987)Effect of addition of lead acetate during the deposition of lead dioxide from the nitrate bath.*Journal of Scientific & Industrial Research*, 100-110

101. **Mehdinia, A, Mousavi, MF and Shamsipur,M** (2006)Nano-structured lead dioxide as a novel stationary phase for solid-phase microextraction.*J Chromatography*, **17**, 24-31.

102. **Shiyun Ai, Mengnan Gao, Wen Zhang, Zhengdong Sun and Litong Jin** (2001) Preparation of Fluorine-Doped Lead Dioxide Modified Electrodes for Electroanalytical Applications. *Journal of Fluorine Chemistry*, **1**, 100–110.

103. **Landfors, J, Simonsson, D and White, R. E** (2012) Discharge behaviour of tubular lead dioxide electrodes Part III: Two-dimensional current density distribution. *Journal of Applied Electrochemistry*,**25**, 315-325.

104. **Wang and Jing** (2002) Effect of Lead dioxide particles on the anodic electrode performance for ozone generation. *Environ. Sci. Technology*, **11**, 1223–1235.

105. **Mohd, Yusairie and Pletcher, Derek** (1952) Fabrication of lead dioxide layers on a titanium substrate.*Electrochimica Acta***,** **3**, 786-793.

APPENDICES

APPENDIX-A.1 Derivation of MDPFM (RTD Model)

Exit age distribution (E_θ) as per dispersed plug flow model,

$$E(\theta) = \frac{1}{\sqrt{4\pi(Pe^{-1})}} . e^{(-(1-\theta)^2 \mathrm{Pe}/4)} \tag{A.1}$$

Thus, as per above model,

$$\frac{C_1^{'}(\mathrm{t})}{C_0} = \frac{1}{\sqrt{4\pi(Pe^{-1})}} . e^{(-(1-\frac{t}{T_\mathrm{R}})^2 \mathrm{Pe}/4)} \tag{A.2}$$

$$\mathrm{C_1'(t)} = \frac{C_0}{\sqrt{4\pi(Pe^{-1})}} . e^{(-(1-\frac{t}{T_\mathrm{R}})^2 \mathrm{Pe}/4)} \tag{A.3}$$

Taking material balances

$Q + \alpha Q = Q\,(1+\alpha)$

At Junction point M,

$$Q(1+\alpha)C_1' = Q.C_1 + \alpha q.\delta(t=0) \tag{A.4}$$

Taking Laplace transform across (A.4),

$$Q.C_1(s) + \alpha q = Q(1+\alpha)\, C_1'(s) \tag{A.5}$$

We Know, $\mathrm{C_1^{'}(s)} = \int_0^\infty e^{-st}\, C_1^{'}(\mathrm{t})\, \mathrm{dt}$

Using standard results from integration,

i.e, $\mathrm{C_1^{'}(s)} = \int_0^\infty e^{-st} \frac{C_0}{\sqrt{4\pi(Pe^{-1})}} . e^{(-(1-\frac{t}{T_\mathrm{R}})^2 \mathrm{Pe}/4)}\, \mathrm{dt}$

From the standard form of integration results for exponential function,

$$\int_0^\infty e^{-(ax^2+bx+c)}\,\mathrm{d}x = \frac{1}{2} \cdot \sqrt{\frac{\pi}{a}} \cdot e^{(b^2-4ac)/4a} \cdot erfc\left(\frac{b}{2\sqrt{a}}\right) \tag{A.6}$$

Where $a = Pe/4.T_R^2$, $b = s + (Pe/2T_R)$, $c = Pe/4$.

By appropriately inserting values for variables and simplifying $C_1'(s)$ is obtained. From A.5,

$$C_1(s) = (1+\alpha).\frac{C_0}{\sqrt{4\pi Pe^{-1}}}.T_R . \sqrt{\pi}Pe^{-1}. \mathrm{erfc}\left(\sqrt{\pi}Pe^{-1} . T_R \left(s+0.5\frac{Pe}{T_R}\right)\right). e^{\left[\left(\frac{1}{pe}\right).T_R^2 (s^2 + s.Pe/T_R)\right]} - \alpha q/Q \tag{A.7}$$

To find $C_1(t)$ by taking inverse Laplace Transform of $C_1(s)$

Comparing from the standard form of results for inverse Laplace transform for product form of exponential and error function,

L^{-1} [$e^{k2.s2}$ x erfc (ks)] , k>0 = $1/(k\sqrt{\pi})$. $e^{(-t2/4k2)}$

$$C_1(t) = (1+\alpha).\frac{C_0}{\sqrt{4\pi Pe^{-1}}}.T_R. \sqrt{(\pi Pe^{-1})}. \frac{1}{k\sqrt{\pi}}. e^{-Pe} . e^{(-t^2/4k^2)} e^{(-Pe/2T_R)t} - \alpha q/Q \tag{A. 8}$$

Further simplifying and putting residence time distribution function as E(θ) =

$$C_1(t)/C_0 E(\theta) = (1+\alpha).\frac{e^{-Pe}}{\sqrt{4\pi Pe^{-1}}}. e^{-0.5\,Pe\,(\theta+\theta^2)} - \alpha q/QC_0 \tag{A.9}$$

LIST OF PUBLICATIONS

REFEREED JOURNALS

1. **Sananth H Menon, Madhu G, Mohamed Sadhik, Shaneeth M, Raghu R and Jojo Mathew** (2015) Design and Development of Packed Bed Electrochemical Reactors (PBER's) using scrap Lead Dioxide as Novel Electrodes.*J. Chem. Eng. Process Technol*,**6**.
2. **Sananth H Menon, G. Madhu and Jojo Mathew** (2019) Modeling Residence Time Distribution (RTD) behaviour in a Packed Bed Electrochemical Reactor (PBER).*Int. J. Chem. Engg.*(https://doi.org/10.1155/2019/7856340)
3. **Sananth H Menon, G. Madhu and Jojo Mathew** (2019)Compact flow-through electrochemical cell - a novel perspective in industrial manufacture of perchlorates, *The Open Chem. Engg.Journal,* **13.**

PRESENTATION IN INTERNATIONAL CONFERENCES

1) **Sananth H. Menon, Mohamed Sadhik A, Shaneeth M, Raghu R, Jojo Mathew and G. Madhu.** Quantification of Interfacial Adsorptive Characteristics over Lead dioxide Electrodes.*9th International High Energy Materials Conference & Exhibits HEMCE 2014*, Thiruvananthapuram, Kerala,13-15 February,2014.
2) **Sananth H. Menon, Mohamed Sadhik A, Shaneeth M, Raghu R, Jojo Mathew and G. Madhu**. Impact of Modified Lead dioxide Anodes in Perchlorate Cells.*International Conference on Advances in Chemical Engineering & Technology (ICACE TKMCE'14) Elsevier Procedia,* TKM College of Engineering, Kollam, Kerala, , 16-18 October, 2014.

CURRICULUM VITAE

Name	:	SANANTH H MENON
Date of Birth	:	16/08/1981

EDUCATIONAL QUALIFICATIONS

- November 1999- June 2003
  B-Tech in Chemical Engineering
  Government Engineering College, Thrissur, Kerala, India
- October 2009- June 2012
  M.Tech (PT) in Chemical Engineering (Process Engineering)
  Cochin University of Science & Technology, Kerala, India
- October 2012- Present
  Doctor of Philosophy
  Faculty of Engineering, SOE, CUSAT
  Reg. Date – 10/10/2013

EXPERIENCE

- June 2003-May 2005
  Shift Production Officer,
  Gharda Chemicals, Pvt Ltd, Ratnagiri, Maharashtra, India
- June 2005- March 2006
  Scientist/ Engineer-SC,
  Sathish Dhawan Space Centre (SHAR)
  Indian Space Research Organisation (ISRO), Andhra Pradesh, India
- March 2006-Present
  Scientist/ Engineer- SF,
  Manager, Electrolysis and Strontium Perchlorate Plant,
  Ammonium Perchlorate Experimental Plant, Aluva
  Vikram Sarabhai Space Centre (VSSC), ISRO, India